INVESTIGATION THE EFFECT OF TRIBOLOGICAL COATINGS: WC/a-C:H AND BLACK OXIDE ON MICROPITTING BEHAVIOR OF SAE52100 BEARING STEEL

A Dissertation

Presented to

The Graduate Faculty of The University of Akron

In Partial Fulfillment of

the Requirements for the Degree

Doctor of Philosophy

Behzad Mahmoudi

December, 2015

INVESTIGATION THE EFFECT OF TRIBOLOGICAL COATINGS: WC/a-C:H AND BLACK OXIDE ON MICROPITTING BEHAVIOR OF SAE52100 BEARING STEEL

Behzad Mahmoudi

Dissertation

Approved:	Accepted:
Advisor Dr. Gary L. Doll	Department Chair Dr. Wieslaw K. Binienda
Committee Member Dr. Wieslaw K. Binienda	Interim Dean of the College Dr. Mario R. Garzia
Committee Member Dr. Craig C. Menzemer	Interim Dean of the Graduate School Dr. Chand Midha
Committee Member Dr. Yalin Dong	Date
Committee Member Dr. Erol Sancaktar	
Committee Member Dr. Ryan D. Evans	

ABSTRACT

Spherical roller bearings (SRBs) utilized in the gearboxes of wind turbine generators are known to be especially susceptible to premature failure due to low cycle micropitting of the raceways. Micropitting in rolling element bearings is believed to arise from significant roller/raceway sliding in thin film lubrication conditions. Roller/raceway sliding occurs in SRBs as a consequence of their geometry, and almost all the bearings in wind turbine gearboxes operate in thin film (or low lambda) lubrication conditions. There is currently no accepted solution to mitigate micropitting in wind turbine gearboxes that are equipped with SRBs. Since WC/a-C:H coatings on rolling elements have been effectively used to solve wear issues encountered by SRBs in other industrial applications, these coatings have been offered as a solution to low cycle micropitting in wind turbine gearbox SRBs.

This research plan has been developed to test the hypothesis that a WC/a-C:H coating will mitigate or eliminate micropitting such as that experienced by SRBs in wind turbine gearboxes. The laboratory tool that is used to create micropitting on test specimens is the PCS Instruments Micropitting Rig (PCS MPR). The MPR is a three-contact disc machine in which there are three rings of equal diameter positioned at 120 degrees apart with a smaller diameter roller located in the middle and in contact with all the rings. This arrangement allows the test roller to be subjected to a large number of rolling contact cycles in a short period of time and hence significantly reduces testing time. At a typical entrainment speed of 3.5m/s, the central test roller will experience

approximately one million contact cycles per hour. Since the controls of the PCS MPR allow the speed, slide-roll ratio, temperature, and load to be automatically and independently controlled, the thin film lubrication and slide/roll ratio conditions that generate micropitting on SRBs can be reproduced in the laboratory. Most wind turbine gearboxes operate with a synthetic ISO-320 lubricating oil with anti-wear and extreme pressure additives. However, to ensure thin film lubrication conditions necessary for micropitting experiments were performed on the MPR using an ISO-10 base oil.

Baseline tribological testing were performed using untreated SAE 52100 rings and the roller. The targeted surface finish on the rings and the rollers varied from about 0.2 to about 0.6 micrometer Ra, and the entire surface topography was quantified using a Zygo 7300 3D optical profilometer. The sets of roller and rings were tested on the MPR using a range of slide/roll ratios from 0.0 to +/- 10% at contact stresses up to about 3 GPa. The number of cycles needed to generate the onset of micropitting was recorded and some tests were repeated up to three times. Results of micropitting tests on steel/steel, steel/WC/a-C:H and WC/a-C:H/steel contacts were compared with a tribological conversion coating; black oxide. Black oxide is a surface treatment that converts the surface of ferrous alloys to magnetite (Fe_3O_4). It has been utilized to reduce wear and corrosion of rolling element bearings and gears, and its use has become especially widespread on roller bearings used in the gearboxes of modular wind turbines. It has been reported that black oxide might have a lower friction coefficient than steel, which may reduce shear stresses due to friction, dampen vibrations, or possibly prevent the diffusion of hydrogen.

ACKNOWLEDGEMENTS

I would like to express my gratefulness to everyone who contributed in some way to this project.

First and foremost, I would like to thank my supervisor, Professor Gary Doll for his smile, parties, level of energy, patience, understanding, moral and financial support. His guidance throughout my research and write-up was invaluable. His constant encouragement gave me a boost of confidence and stimulation. Without his support this PhD would not have been possible.

I wish to thank Dr. Ryan Evans for all the support in various occasions, and providing this opportunity. I also owe a debt of gratitude to Dr. Carl Hager for many technical discussions and helpful comments on this research. Thanks also to the members of Timken Surface Engineered laboratories; Dr. Paul Schiller, Rich Fowler and Barbara Tury. Special thanks to my colleagues; Alireza Saatchi, Harpal Singh, Kalyan Muchala, Jonathan Fauts, Haifang Chen who are more than friend and support me through this project.

I wish to thank my parents in Iran who have been very supportive throughout all the stages of my work, and for understanding my absence in some moments when they needed me. This thesis is dedicated to them.

The final acknowledgement goes to those who funded this work. My studies were supported by the Timken Bearing Company and University of Akron. Special thanks to Dr. Doll for the financial support during the last stage of this project and my study.

TABLE OF CONTENTS

Page

LIST OF FIGURES

LIST OF TABLES

Table Page

NOMENCLATURE AND SUBSCRIPTS

a, b	=	semi-axes of the contact ellipse
B_{Mi}	=	the thermal contact coefficient of contact i
C	=	Specific heat capacity (J/kg.K)
d	=	the approach of distant points (m)
E	=	Elastic modulus (Pa)
E^*	=	is effective young modulus $\frac{1}{E^*} = \frac{1}{E_1} + \frac{1}{E_2}$ (MPa)
F	=	Contact force (N)
G	=	Dimensionless materials parameter
H	=	Hardness (GPa)
h	=	Lubricant film thickness (m)
h_{cen}	=	Dimensionless central film thickness
h_{min}	=	Dimensionless minimum film thickness
Hd-Hr	=	Hardness of disc minus Hardness of Roller (GPa)
k	=	Specific heat conductivity (W/m.K)
L	=	Contact length
P	=	the Hertzian contact stress (MPa)
P_e	=	Peclec Number ($Pe = \frac{Vb}{2K}$)
P_{max}	=	Maximum Hertzian contact pressure (Pa)
q,Q	=	Heat
R	=	Radius of asperity
R^*	=	educed contact radius $\frac{1}{R^*} = \frac{1}{R_1} + \frac{1}{R_2}$ (m)
$R_a^{\wedge}$	=	Arithmetic average of the absolute values of the profile height deviations from the mean line of the surface (μm)

$R_{sk}^{\wedge}$	=	Indication of the asymmetry of the amplitude density curve.
$R_{ku}^{\wedge}$	=	Kurtosis is a measure of the distribution of spikes above and below the mean line.
$R_{p}^{\wedge}$ $R_{v}^{\wedge}$	=	Maximum profile peak height and Maximum profile valley depth are the distances from the mean line/surface to the highest/lowest point in the evaluation length/area.
R_i	=	Radius in the i direction (m)
R_e	=	effective radius of curvature (m)
$R_{z}^{\wedge}$	=	The Average maximum profile of the ten greatest peak-to-valley separations in the evaluation area.
SRR	=	Slide to roll ratio (%)
T	=	Temperature (˚C)
U	=	the local sliding velocity (m/s)
V	=	Entrainment velocity of a contact (m/s)
α	=	pressure-viscosity coefficient
α	=	Heat partitioning factor
u	=	Mean entrainment velocity (m/s)
W	=	dimensionless load parameter
α	=	pressure-viscosity coefficient(Pa^{-1})
λ	=	Relative film thickness parameter ($\lambda=h/R_a$)
η	=	Lubricant viscosity (Pa s)
ψ	=	Plasticity Index
σ (r.m.s)	=	Root Mean Square of a surfaces measured microscopic peaks and valleys
κ	=	Thermal diffusivity ($K = \frac{k}{\rho C}$)
μ	=	the coefficient of friction
ρ	=	Density (kg/m^3)
ν_θ	=	Kinematic viscosity of oil at temperature θ (mm^2/s)
η_θ	=	Dynamic viscosity of oil at temperature θ ($N.s/m^2$)
MPR	=	Micropitting rig

D	=	Disc
R	=	Roller
uD/uR-R	=	Uncoated Discs/uncoated Roller-Disc's surfaces are Rough
uD/uR-S	=	Uncoated Discs/uncoated Roller-Disc's surfaces are Smooth
cD/uR-R	=	WC/a-C:H Coated Discs/uncoated Roller − Disc's surfaces are Rough
cD/uR-S	=	WC/a-C:H Coated Discs/uncoated Roller − Disc's surfaces are Smooth
uD/cR-R	=	Uncoated Discs/ WC/a-C:H Coated Roller − Roller's surface is Rough
uD/cR-S	=	Uncoated Discs/ WC/a-C:H Coated Roller − Roller's surface is Smooth
WC/a-C:H	=	Tungsten carbide-containing diamond-like carbon
PAO	=	Poly alpha olefin
EP	=	Extreme pressure additive
AW	=	Anti-wear additive

CHAPTER I

INTRODUCTION

1.1. Overview

Micropitting is a surface contact fatigue phenomenon that occurs in rolling/sliding contacts. The British Standard Institution describes micropitting as "a form of surface fatigue phenomena, which consists of degradation of gear tooth working surfaces under lubrication conditions where the film is too thin for the load" [1]. ISO TR 15144 defines micropitting as “a phenomenon that occurs in Hertzian types of rolling and sliding contact that operates in elastohydrodynamic (EHL) or boundary lubrication regimes” [2]. ISO TR 15144 is an ISO standard technical report on the calculation of micropitting load capacity of cylindrical spur and helical gears.

Gears and bearings are of the most common mechanical components that can suffer from rolling contact fatigue and micropitting. Many research and studies have been conducted on the understanding of the initiation and propagation behavior of micropitting [3, 4, 5, 6, 7, 8, 9] as well as the prevention, control and prediction of micropitting [10, 11, 12, 13, 2].

1.2. History of research on micropitting

It is not clear when research first started on micropitting however, S. Way in 1935 was one of the first who studied surface distress in lubricated contacts [14]. He observed that polishing of contacting discs increased their resistance to surface distress

substantially. Nowadays, there is no doubt that surface roughness and high stress between contacting asperities have a contribution to the rate of micropitting.

1.3. Failure modes in rolling contact

In 1967, Tallian published a paper on competing failure modes in rolling contact. Tallian has categorized rolling contact failures into four classes of wear, plastic flow, fatigue and bulk failures. Table 1-1 shows four classes of failure modes in rolling contacts.

Table 1-1: Failure modes of rolling contacts [15]

Mode	Manifestation
1. Wear type failure	1.1. Surface removal
	1.1.1. Removal of loose particles ("wear")
	1.1.2. Chemical or electrical surface removal
	1.2. Cumulative material transfer between surfaces ("Smearing")
2. Plastic flow	2.1. Loss of contact geometry due to cold flow
	2.2. Destruction by material softening due to the overheating
3. Contact fatigue	3.1. Spalling
	3.2. Surface distress
4. Bulk failures	4.1. Overload cracking
	4.2. Overheat cracking
	4.3. Bulk fatigue
	4.4. Fretting of fit surfaces
	4.5. Permanent dimensional changes

Wear is further subdivided into mild wear (which is loose particle removal) and smearing (which involves material transfer). All solid surfaces in moving contacts

undergo wear unless totally separated by a lubricant [15]. Smearing failures appear to be limited to contacts that have undergone considerable sliding.

Plastic flow could be due to overload or high contact temperatures. Plastic flow forms Brinnel marks and defines the static local capacity for rolling bearings. Plastic flow can be distinguished from pitting by observing the edge of a deformed surface or pit. If the material is pushed above the edge of the depression (or pit), then most likely plastic flow happened due to debris dent. In contrast, straight line around the pit could be a sign of fatigue cracking and micropitting [15].

Fatigue is related to micropitting. Fatigue can be considered as a life limiting failure of a bearing if installation is performed correctly. Fatigue failure is divided into two categories of spalling and surface distress. Spalling is defined as a subsurface fatigue failure associated with maximum Hertzian shear stress located about 150 microns below the surface. Micropitting is a type of surface distress due to asperity interactions. In micropiting, it is believed that the initial stage of surface distress arises from the plastic deformation of asperities [15], and it may end or progress, depending upon the working condition. If it progresses, micropits can form that which can roughen the surface and lead to macropitting and spallation. Tallian believed surface distress is a type of surface fatigue without much material removal, involving cracking and pitting. Moreover, its formation is gradual with increasing cycles, when generally several hundred thousand or a few million cycles are required for generation of micropitting or surface distress. An important discussion by Tallian is the distinction between surface distress and smearing. He believed smearing arises from a high degree of sliding, whereas, surface fatigue

occurs in practically pure rolling and in fact does not seem to occur when high sliding is present [15].

Tallian mentioned "of the four main groups of failure modes listed in Table 1-1, the first three are confined, at least initially, to the material volume subject to contact stress" [15]. This statement might be important since there is a size difference between the roller and discs in the micropiting experiments conducted on the MPR.

In 1982, Takuda et al. published a paper with a title of "Observations of the peeling mode of failure and surface-originated flaking from a ring-to-ring rolling contact fatigue test rig"[1]. They observed a relation between peeling and flaking. They also studied these two failures in several oils and greases with two rigs each with two rings running against each other. One rig was capable of measuring metal to metal contact by electrical discharge between the two rings and the other capable of applying high contact stresses. They observed peeling on the softer or smoother roller when it runs against a harder and rougher ring in lower contact stresses (2.3 GPa) in roughly 0.5 million cycles. However, peeling converts to flaking (defined as surface-initiated fatigue cracking and pitting) when the maximum Hertzian contact stress is about 3.9 GPa. The author considered the effects of viscosity, type of oil and surface roughness on the peeling. Interestingly, it has been observed there is relatively linear relationship between metallic contact ratio and peeling grade [16]. However, the remarkable result in this paper is that

[1] It should be noted at that time (1982), the term micropitting was not a common term for surface initiated fatigue features.

the peeling happens on the surface even when the λ ratio[1] is more than 6 (although the peeling ratio is just 10% compare to 30% for λ of below 0.2).

In 1988, K.L. Johnson presented a lecture at the Third Annual BP Tribology Symposium and spoke about the strength of surfaces in rolling contact. Although the lecture was presented in a non-technical form, it still has many interesting points in it.

Johnson deliberately compared the contact of a truck tire with a steel wheel on steel rail to clarify the tradeoff between rolling resistance and contact stress. Increasing the rigidity of the rolling surfaces (steel wheel/rail contact) reduces the rolling resistance but increases the contact stress. As a result, a truck tire has a high friction coefficient and mostly suffers from surface initiated failures such as wear or near surface spallation. On the other hand, in depth and sub-surface fatigue spallation is one of the main sources of failing in steel/steel contacts such as gears and bearings. Further, in rolling element bearings, an increase in conformity causes a reduction in contact stress and a gradual increase in rolling resistance as is shown in Figure 1-1. Increasing conformity between the rolling elements increases the eccentricity (b/a) of the ellipse of contact that reduces the contact stress, but only at the expense of increased spin loss [17]. Increase in rolling resistance may affect the wear, peeling and micropitting behavior of rolling contact elements.

Johnson mentioned rolling contact fatigue is the principal mode of failure of rolling surfaces and it governs the useful life of a component under a prescribed load [17]. Depending upon material properties and operating conditions, it manifests itself by

[1] λ is a film parameter; the ratio of lubricant film thickness over square root of contact surface roughnesses

the initiation and propagation of cracks in the near-surface layer until macroscopic pieces detach and form pits or spalls on the surface.

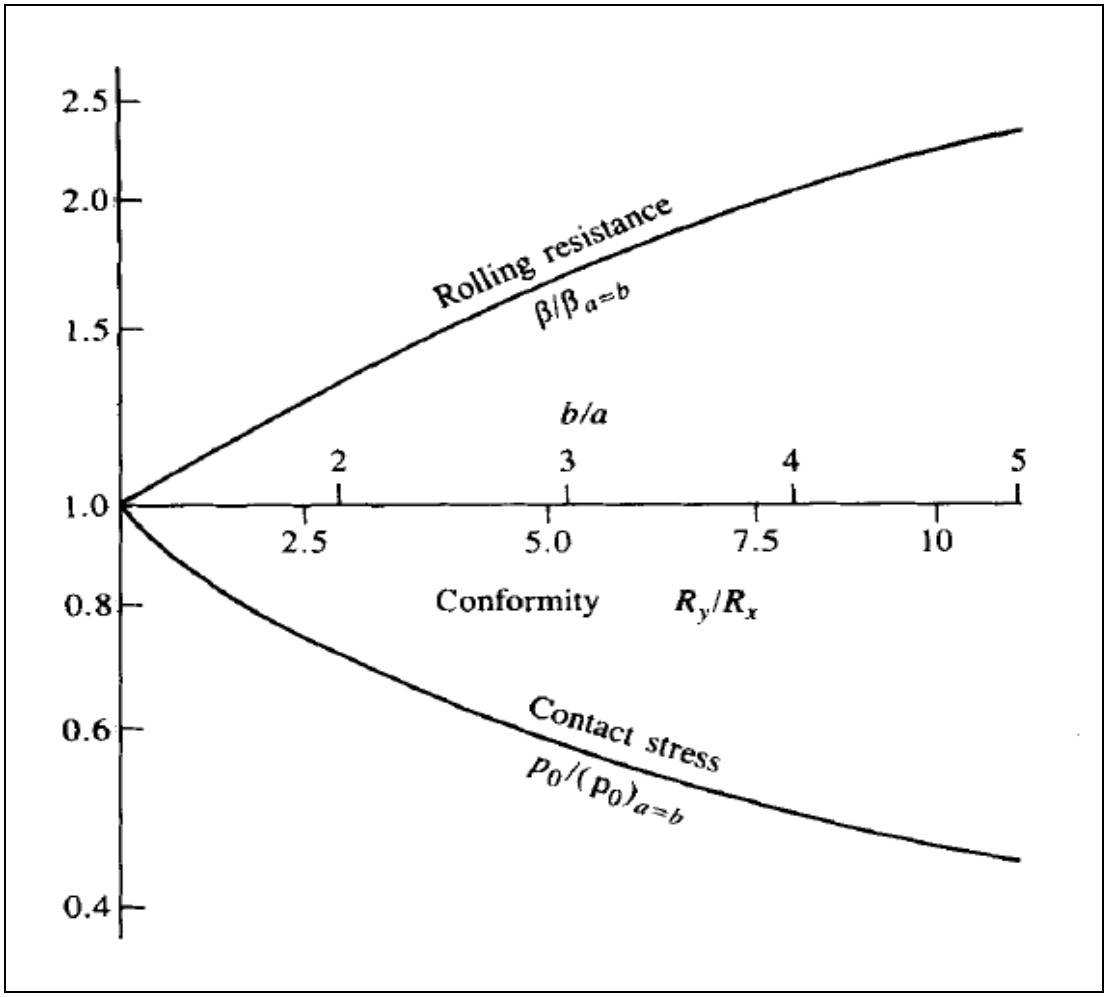

Figure 1-1: Loss factor β and contact stress P_0 in a friction drive as a function of conformity. R_y/R_x is the ratio of the transverse to longitudinal radii of curvature of surface [17].

Gear teeth behave differently than rolling element bearings since sliding is considerably higher. Higher sliding increases the plastic deformation of asperities and rate of cracks that initiate at the surface [17]. Cracks propagate into the substrate at an

acute angle (15˚-30˚) to the surface. Now, continuation of the propagation depends upon the material properties and the contact stress; medium hardened and soft gears show V-shaped individual microspalls while hard gears show large numbers of shallow micropits. Micropit depths are comparable with surface roughness, however, microspalls are deeper and their depth is roughly comparable with that of the maximum Hertzian shear stress. Some experiments have shown that the presence of the lubricant contributes to crack propagation. Crack propagation is confined to the slower moving surface, and in the direction of motion of the load [17]. Therefore, it can be said that the initiation of shear cracks is associated with the plastic deformation of sub-surface layer and asperity contact while propagation is associated with trapped lubricant inside the crack and whereby hydrostatic pressure of the trapped lubricant causes the crack to open. The application of fracture mechanics in this situation shows propagation would only be expected in a circumferential direction that has been observed in experiments [17].

In 1989, Y. Akamatsu from NTN Bearing published an article on peeling damage due to rolling contact fatigue. Akamatsu defines peeling as crowded minute cracks similar to shallow flaking which is a kind of rolling fatigue phenomena caused by an interference with surface asperities of the partner rolling element or a dust contaminated lubricant [18]. As previously mentioned, micropitting has been categorized as one type of peeling. Akamatsu studied the peeling grade of 52100 specimens using a twin disc machine. This machine is capable of measuring electrical contact between contacts. He tried to relate the peeling grade to the metallic contact ratio in several test conditions of contact stress, types of lubricant and lambda ratio. The primary results of this study are summarized below:

- There is a threshold contact stress for generation of peeling on the smoother surface.
- The rougher surface causes the smoother surface to suffer from peeling.
- There is linear relationship between the metallic contact ratio and the peeling grade, although the correlation coefficient is only 0.83.
- Micropitting occurs during the first few hundred thousand cycles and a decreasing amount of metallic contact results in a lower rate of peeling.
- Increase in lambda ratio (due to speed, temperature or viscosity of lubricant) decreases the peeling grade. Akamatsu mentioned that at high lambda values (>2) the peeling grade is nearly equal to 0% and for λ less than 1.2 (when the initial metallic contact ratio is nearly 88%)[1].

A typical metallic contact ratio from Akamatsu is presented in Figure 1-2. An interesting aspect of this article is the relationship between the peeling ratio and the directionality of asperities on the surface. Peeling tests were conducted on both longitudinally and transversely oriented surfaces. Results showed that the metallic contact ratio with the transversely ground driver roller is smaller than that of the longitudinally ground one and there was no peeling dent at the surface of the follower roller tested against the transversely ground driver roller [18].

[1] the rolling contact fatigue mode is the surface mode type (lambda was calculated based on the Cheng equation for lubricant film thickness and the r.m.s values of surface roughness

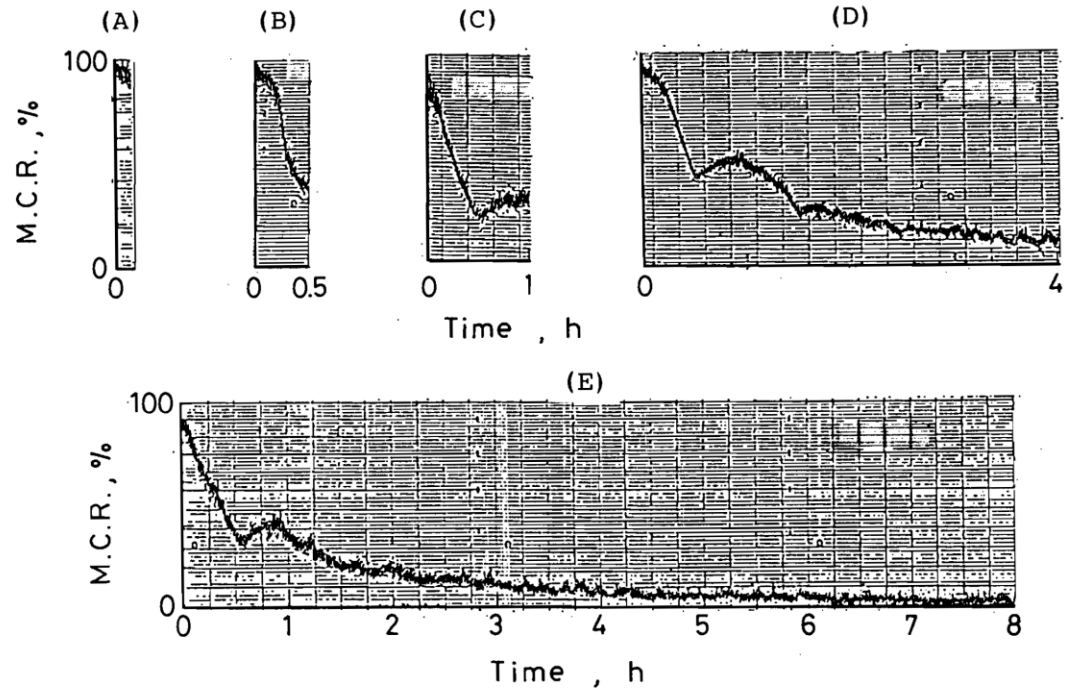

Figure 6 - Recording charts of the metallic contact ratio under tests with varied loading cycles.
(A) 20,000 cycles, (B) 60,000 cycles,(C)120,000 cycles,
(D)480,000 cycles, (E)960,000 cycles

Test conditions,

Pmax:	2.29 GPa
Speed of Rotation:	2,000 rpm
Surface Roughness:	D-roller 3.0 micron
	F-roller 0.2 micron
Lubricant:	turbine oil VG46

Figure 1-2: A graph of metallic contact ratio in Akamastsu's peeling measurements. Akamastsu believed the damage leading to peeling is started in the surface layer within 30 min (60,000 cycles) after the test [18].

In 1997, Fernandes published an article on "surface contact fatigue failures in gears". This is one of the papers that clearly emphasizes the occurrence of surface contact fatigue with and without sliding. Fernandes et al. address contact fatigue in terms of pure rolling and rolling-sliding contact. There are two unique characteristics of rolling contact fatigue pits that can be used to distinguish this type of damage from other forms of

pitting. Firstly, the formation of rolling contact fatigue pits occurs with no surface plastic deformation. This is contrary to pitting under sliding-rolling conditions [19, 20]. Secondly, in components with a case-hardened layer consisting of martensite with little or no retained austenite, rolling contact fatigue leads to the formation of a microstructural feature referred to as "butterfly wings". These are formed when the plastic deformation is constrained by the surrounding material, and is more common when shear stresses are extremely high [19].

Fernandes et al. also mentioned it is common that contact fatigue damage will first occur in the dedendum of the smaller gear which is usually the driving gear of a gear set. They explained this observation by the fact that the smaller gear will undergo more revolutions and larger number of stress cycles [19]. Therefore, making the smaller driving gear harder is a common solution.

In rolling-sliding surface contact damage, plastic deformation of the surface material can usually be detected using metallographic analysis. It can also be reduced effectively by proper lubrication. Moreover, surface hardness greater than 60 HRC is an effective approach to reducing surface fatigue [19].

In 1999, Nelias et al. published a paper on rolling contact fatigue categorized as surface versus sub-surface fatigue. They considered micropitting, peeling and surface distress as surface-initiated rolling contact fatigue. The aforementioned phenomena have the same origin and mechanism; however their appearance and features might be relatively different depending upon the geometry of contact and the level and profile of stress. They believe that a surface initiated fatigue crack is due to local friction and

interaction of the contact asperities while subsurface fatigue cracks are due to high shear stresses arises from residing inclusions near the maximum Hertzian contact stress. Inclusions act as stress raisers, leading to localized plastic deformation and crack nucleation, which will depend on the stress level and the number of cycles [21].

Regarding micropitting and surface initiated fatigue cracking, they believe that the role of surface roughness is of great importance and it can cause acceleration in the micropitting rate in two ways. First, during a run-in period, small wavelength asperities in contact can produce high stress concentration, even at low normal loads. Second, large wavelength produces normal pressure fluctuations and as a result can initiate near-surface cracks through high shear stresses [21].

Nelias et al. believe sliding to be the origin of the transverse micro-cracks due to an increase in local friction. However, surface topography and lubricant film thickness have contribution as well [21]. In their results, regardless of contact stress and sliding effect, surface damage occured whenever the λ ratio was below 1. What should be highlighted is that the number of cycles required for surface damage onset was on the order of 50 million cycles which is considerably higher for Tallian's revelation that surface distress occurs during the first few hundred thousand cycles. Therefore, Nelias et at. concluded asperity interaction and the level of roughness along with the contact pressure are the most important factors in the initiation of pits and cracks on the surface. Figure 1-3 illustrates the effect of surface roughness and applied load on the stress profile inside the contact [21].

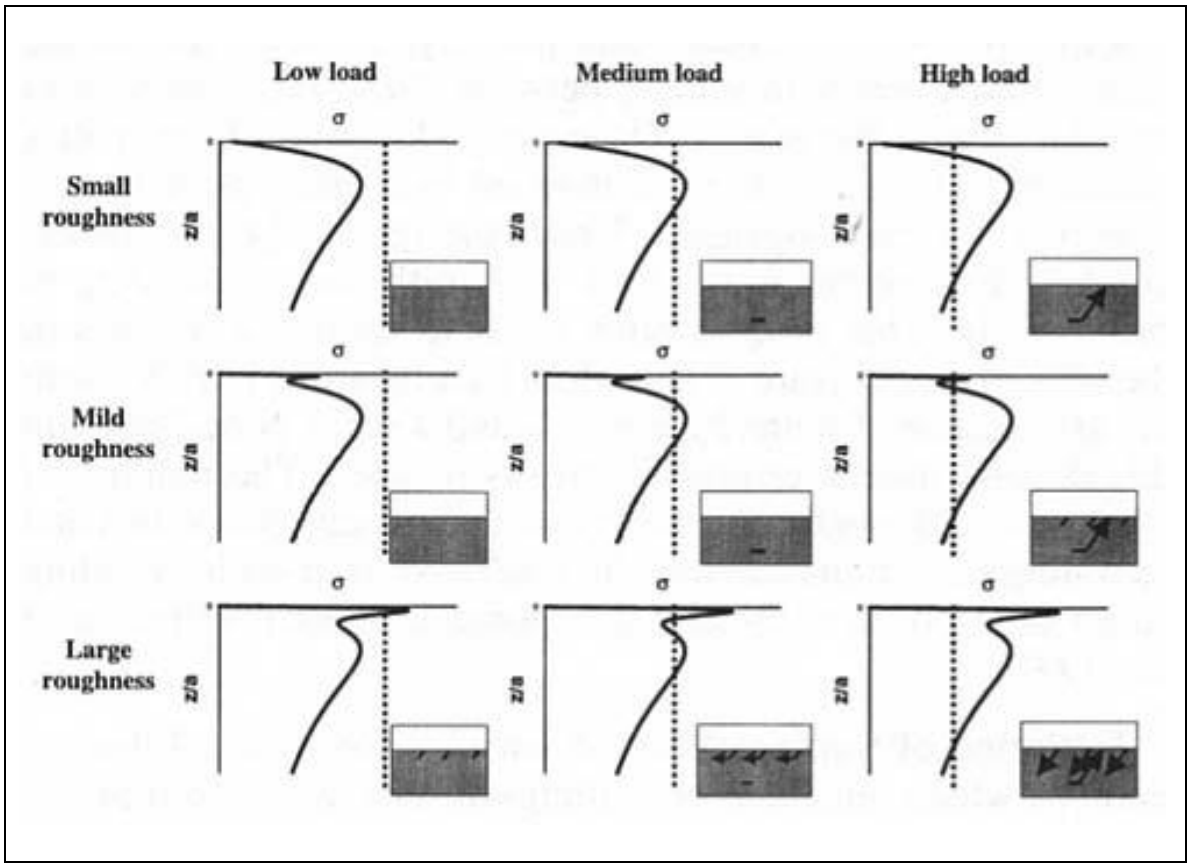

Figure 1-3: Competition between surface and subsurface crack growth for different loading and surface roughness. The full line represents the Tresca shear stress versus depth (normalized by the Hertzian pressure and the contact half-length a, respectively). The dash line represents the characteristic shear stress below which no crack initiation (straight lines) and propagation (arrow headlines) will occur. This limit takes into account the local inhomogeneities within the material [21].

1.4. Factors influencing micropitting

Micropitting is influenced by operating conditions such as load, speed, sliding and temperature, materials properties such as composition of counterparts, hardness, coatings and surface topography and finally lubricant conditions such as chemical composition of lubricant, additives and specific lubricant film thickness.

Oila and Bull studied the influence of seven factors on micropitting: material, surface finish, lubricant, load, temperature, speed and, slide-to-roll ratio. Their conclusion was that load has the largest effect on micropitting initiation whereas speed and slide-to-

roll ratio have the largest effects on micropitting propagation [5]. The effect of other variables that they measured is presented in Figure 1-4.

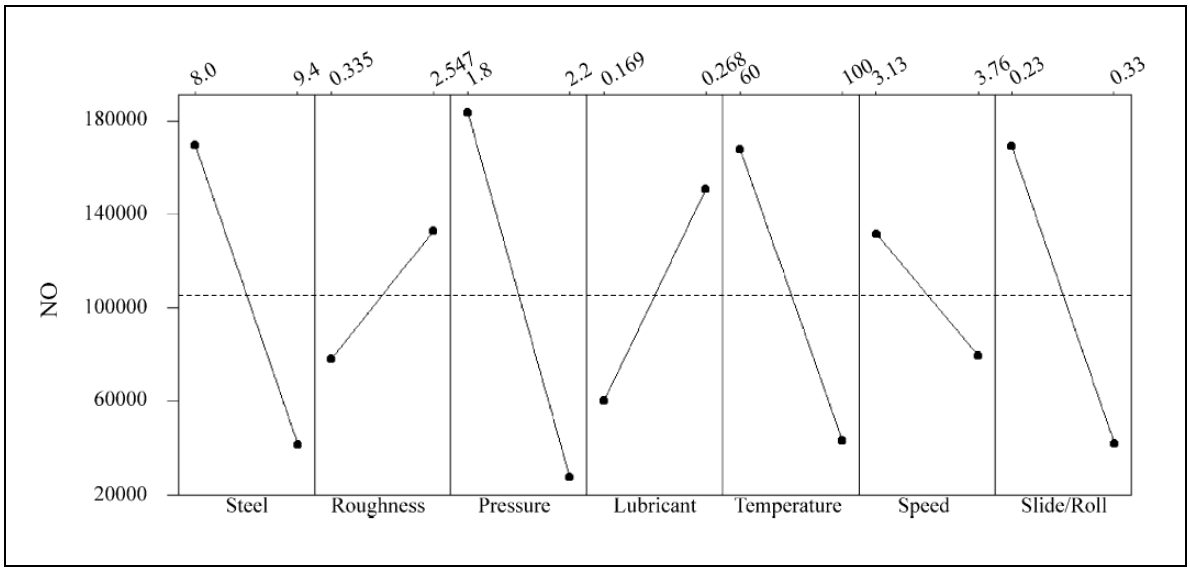

Figure 1-4: The main effects on micropitting initiation. N0 is the number of cycles after micropitting occupies 1.5% of the surface [5].

Slide to roll ratio is a challenging factor on micropitting. Oila [5], Graham [22] and Webster [23] et al. concluded that an increase in sliding increases the rate and probability of micropitting. They believe that an increase in sliding increases the frictional force that in turn generates a in higher shear stress on the surface and a greater chance of micropitting. This might be generally true for researchers who are trying to simulate micropitting phenomenon in gears, but researchers such as Morales-Espejel who are studying micropitting in bearings have another idea.

In a study by Morales-Espejel et al., they speculate that in rolling bearing conditions slip within 0.5 and 2% provides the highest risk of micropitting [24]. Instead, sliding more than 2% does not necessarily increase the risk of micropitting because the boundary friction coefficient is relatively constant for higher sliding ratio. In addition,

since the wear rate increases at higher sliding ratios, it is considered to be a competitor mechanism for micropitting and fatigue [24].

The factor of sliding in micropitting has been studied by many researchers since it has a great importance especially in gears [5, 24]. Morales-Espejel et al. believe the presence of slip and the associated boundary friction shear stress are required for the generation of micropitting [24]. However, Fernandes et al believe there are two types of micropitting: micropitting under pure rolling and under rolling/sliding conditions. They believe plastic deformation does not occur under pure rolling while it occurs on the surface under rolling/sliding conditions [20].

In 1980, Berthe et al. showed that both micropits and spalls occur during near pure rolling conditions [25]. They believe micropitting is initiated at the surface and related to asperity interaction. Spalling is related to maximum Hertzian shear stress in Hertzian depth.

Berthe et al. could not predict the rate of micropit formation; although it was found to depend upon running-in time. Results show that the rate of micropitting tends toward zero and fatigue life is increased when a running-in period takes place, i.e., when the pressure on asperity tips decreases to an elastic regime. They defined three stages on stress of the asperities based on hardness and lubricant film thickness: elastic, plastic and elastoplastic [25].

1.5. Mechanism of micropitting

Historically, nonmetallic inclusions have been the main source of spalling, phase change, and the creation of butterfly deffects in bearing steels. However, improved steel making productions have reduced size and number of inclusions dramatically. Therefore,

the load carrying capacity of bearing and gears has increased, which has led to increased power density through a reduction in the sizes of gears and bearings. Better and more homogenous steel microstructure reduced in-bulk failures leaving the surface as the most vulnerable part of components for failure. At this stage, micropitting and surface fatigue became a more important issue.. Understanding the mechanism of micropitting and surface fatigue could be a significant step in order to reduce surface failures.

Oila et al. proposed a mechanism for micropitting in 2005 [4]. They believed it is linked to phase transformations induced by the contact fatigue process. Plastic deformation of asperities on the surface due to Hertzian cyclic stress creates a considerably hard and highly dislocated phase on the surface known as the plastic deformation region (PDR). A dark etched region (DER) initiates at the prior austenite grain boundaries. Fatigue cracks initiate and propagate preferentially at the boundaries of the PDR and ultimately lead to the formation of micropits. Similar observations have been reported by Zhou et al. in 1989 who observed highly dislocated cells just one micron below a contact surface between martensite plates by TEM [26].

1.6. Hertzian contact theory

To gain a better understating of micropitting, it is important to analyze contact stress between mating parts. Hertz explains the stress and strain generated between the nom-conformal surfaces coming into contact. Hertzian theory uses deformation of an elastic half-space being acted upon by surface forces to solve the contact problem.

In the first step, a contact between a rigid sphere and an elastic half-space needs to be solved. A schematic of a contact between a rigid sphere and an elastic half-space is

shown in Figure 1-5. Displacement (d) between the original flat surface before contact and recession after the contact can be calculated using equation 1-1.

$$u_z = d - \frac{r^2}{2R} \tag{1-1}$$

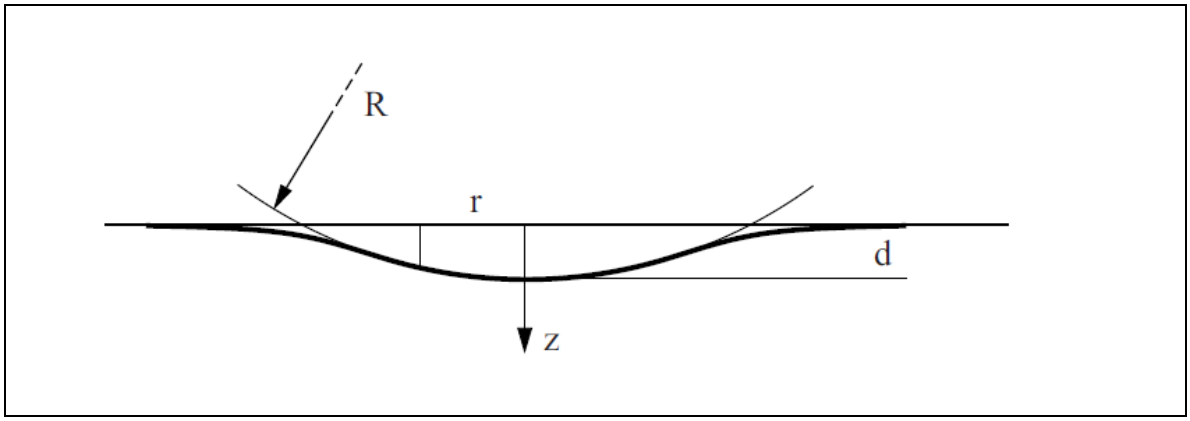

Figure 1-5: A rigid sphere in contact with an elastic half-space.

By applying elastic half-space theory equation, it is possible to calculate the contact radius (a) between the rigid sphere and half space. Therefore, a and d are related through equations 1-2 and 1-3.

$$a = \frac{\pi R P_0}{2E^*} \tag{1-2}$$

$$d = \frac{\pi a\, p_0}{2E^*} \tag{1-3}$$

It follows for the contact radius

$$a^2 = Rd \tag{1-4}$$

and for the maximum pressure

$$p_0 = \frac{2}{\pi} E^* \left(\frac{R}{d}\right)^{1/2} \tag{1-5}$$

Normal force can be calculated by equation 1-6

$$F = \frac{4}{3} E^* R^{1/2} d^{3/2} \quad (1\text{-}6)$$

Up to this point, all calculation is for a single sphere contacting an elastic half-space. In case of two bodies contacting each other; there are several assumptions that must be made to calculate the Hertzian contact between two bodies. The assumptions are:

- The surfaces are frictionless.
- The surfaces are continuous and non-conforming.
- The contact area is very small compared with the bulk volume of the two bodies.
- Subsequent strains are small.
- Each body can be regarded as an elastic half-space bounded by the plane z=0.

Considering the aforementioned assumptions, when two bodies approach each other, two recessions happen in each body $d = d_1 + d_2$ which is called the normal approach of interference.

Effective or composite radius of curvature and composite or reduced Young's modulus) are given by the equation 7 and 8 respectively:

$$\frac{1}{R_e} = \frac{1}{R_1} + \frac{1}{R_2} \quad (1\text{-}7)$$

$$\frac{1}{E^*} = \frac{1 - v_1^2}{E_1} + \frac{1 - v_2^2}{E_2} \quad (1\text{-}8)$$

1.6.1. Circular contact

An approach of two spheres generates a circular contact. The approach distance and contact radius can be calculated using equations 9 and 10:

$$d = \left(\frac{9\,P^2}{16E^{*2}\,R_e}\right)^{1/3} \quad (1\text{-}9)$$

$$a = \left(\frac{3\,PR_e}{4E^*}\right)^{1/3} \quad (1\text{-}10)$$

Here, R_1 and R_2 are the radii of curvature of the spheres, E_1 and E_2 are the moduli of elasticity and ν_1 and ν_2 the Poisson's ratios of both bodies. Figure 1-6 shows the schematic of contact between two spheres.

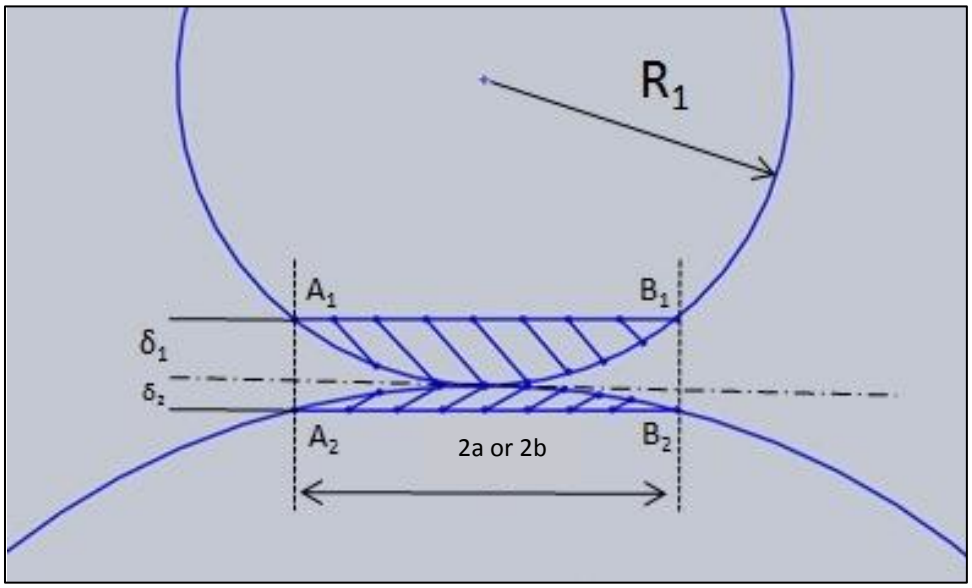

Figure 1-6: Schematic of contact between two spheres or two cylinders

1.6.2. Line contact

In case of contact between the two cylinders, a rectangular or line contact is created between the two bodies with one length equal to the cylinder length and the semi contact width can be calculated using equation 11:

$$b = \left(\frac{4\,P^*R_e}{\pi\,E^*}\right)^{1/2} \quad (1\text{-}11)$$

where P* is the force per unit length.

1.6.3. Elliptical contact

Elliptical contact falls between line, contact and circular contacts. To solve the approaching distance between two bodies which making an elliptical contact an equation for the composite radius is utilized. Therefore, two perpendicular planes can be defined as reference planes. The composite radius for each plane can be calculated from equation 7 and the final reduced radius can be approximated by equation 14. R_e is the equivalent radius of curvature.

$$\frac{1}{R'_e} = \frac{1}{R'_1} + \frac{1}{R'_2} \tag{1-12}$$

$$\frac{1}{R''_e} = \frac{1}{R''_1} + \frac{1}{R''_2} \tag{1-13}$$

$$R_e = \sqrt{R' \times R''} \tag{1-14}$$

The relation between a and b also called the ellipticity can be approximated with equation 15 and 16 respectively:

$$\frac{a}{b} \approx \left[\frac{R'}{R''}\right]^{2/3} \tag{1-15}$$

$$c = \sqrt{ab} = \left(\frac{3\,PR_e}{4E^*}\right)^{1/3} \tag{1-16}$$

Finally the approach of distant points can be achieved by equation 17:

$$d = \left(\frac{9\,P^2}{16E^{*2}\,R_e}\right)^{1/3} \tag{1-17}$$

All equations provided up to now are based on classical Hertzian contact theory and can be found in any contact mechanics reference book [27, 28].

The critical issue about any Hertzian contact problem is the recession in each body of contact. Johnson in “One hundred years of Hertzian contact” in the section “A simple treatment of the Hertz theory” explains the state of strain in each solid varies based on d/a and the state of stress in each solid, for a given value a, will vary in proportion to the mean contact pressure p:

$$\frac{d_1}{a}+\frac{d_2}{a}=\frac{a}{2}\left(\frac{1}{R_1}+\frac{1}{R_2}\right)=\frac{a}{2}\left(\frac{1}{R}\right) \quad (1\text{-}18)$$

Equation 18 has been derived for a circular contact. However, it should be considered that it is not possible to calculate d_1 and d_2 separately based on equation 17, this equation derived using the assumption that the contact occurs between the one rigid object and elastic half-space. Therefore, recession or elastic deformation is inherent in both objects. It is not generally concluded that there may be a difference between the recessions of contact bodies; although it could be a factor influencing the fatigue life of components.

In real applications, there is a need for an experimental measurement of deformation. Houpert applied Hertzian theory and experimental fitting curves to drive equations for transitions from point contact to line contact in rolling element bearings. Also Houpert provided an analytical approach for calculating the bearing load and moment, as well as a pressure distribution along the roller, as a function of roller/raceway deformation and misalignment [29, 30].

In addition, Hertzian theory was developed for smooth and perfect surfaces that do not exist on the surfaces of mechanical components. Machining and manufacturing of a bearing raceway or roller generates topographies characteristic of the machining

processes utilized. Surface roughness has many criteria and measurement methods. In the next section, a brief definition and explanation about surface roughness is presented.

1.7. Surface roughness

Surface roughness is a component of surface texture that is frequently shortened to roughness. It is possible to quantify the roughness by the deviations in the direction of the normal vector of a real surface from its ideal form. Although roughness is a relative term, when these deviations are large, the surface is rough and if they are small, the surface is smooth.

Roughness is one of the factors that determine how a surface will interact with its environment. Generally speaking, it is expected that rougher surfaces wear more quickly and have higher friction coefficients than smoother surfaces. Roughness determines the life of a mechanical component, as irregularities in the surface may form causing cracking or corrosion or wear.

Roughness is naturally considered to be the high-frequency, short-wavelength component of a measured surface. However, in practice it is necessary to know both the amplitude and frequency.

1.7.1. General terms for outlining roughness

Technical terms and definition of several concepts of surface roughness are:

- Roughness (nano- and micro- scale) is the change in the surface height characterized by hills or asperities (local maxima) and valleys (local minima). Asperities are generally referred to peaks and maxima.
- Waviness (macro-scale) is larger wavelength deviations of the surface height.

- Lay is the predominant direction of the surface pattern, normally introduced to surface due to manufacturing of the part.
- Arithmetical mean roughness (Râ): Arithmetical mean of the sums of all profile values. Râ is schematically is shown in top-section of Figure 1-7. The mean line is laid on a Cartesian coordinate system where in the mean line runs in the direction of the x-axis and magnification is the y-axis. The value obtained with the formula on the top of Figure 1-7 is expressed in micrometer (μm) when y = f(x) [31].
- Maximum peak (Rŷ): or maximum peak-valley distance is schematically is shown in mid-section of Figure 1-7. The distance between the peaks and valleys of the sampled line is measured in the y direction. The value is expressed in micrometer (μm) [31].
- Ten-point mean roughness (R$\hat{z}$): The average peak is obtained among 5 tallest peaks (Yp), as is the average valley between 5 lowest valleys (Yv). The sum of these two values is expressed in micrometer in bottom-section of Figure 1-7 [31].
- Standard deviation or variance or root mean square (σ, $R_q^{\wedge}$ or RMS) is the square root of the arithmetic mean of the square of the vertical deviation from the mean line.

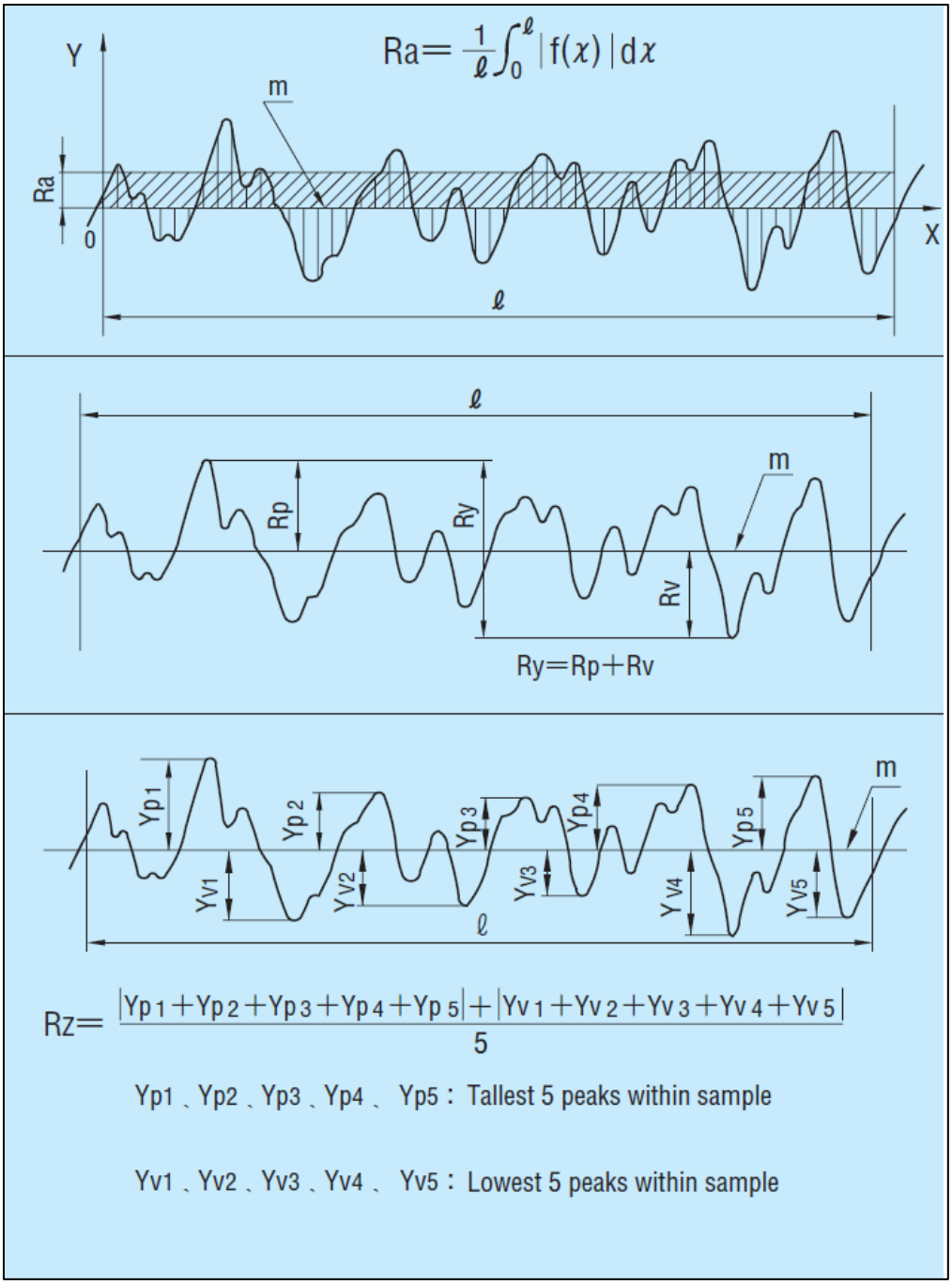

Figure 1-7: Typical ways for obtaining surface roughness [31].

1.7.2. Amplitude Probability Functions

The shape of the probability density function provides valuable information on the behavior of rolling element bearings. This shape can be clarified by Skewness, Kurtosis and Bearing Area Curve (BAC).

1.7.3. Skewness of the roughness profile ($R_{sk}^{\wedge}$)

This expresses the cubic mean of Z(x) in a sampling length rendered dimensionless as the cube of the root mean squared height, $R_{q}^{\wedge}$. It means the degree of skew, and expresses the symmetry of peaks and valleys using the average line as the center [32].

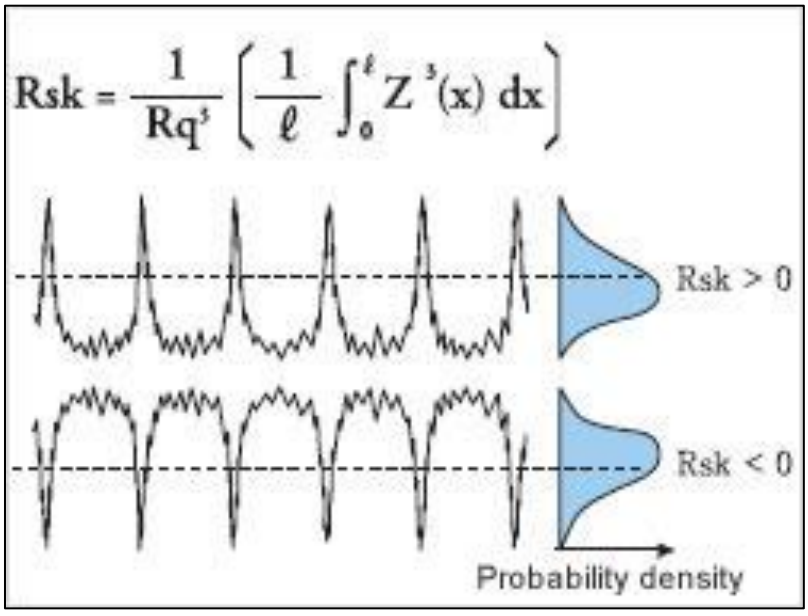

Figure 1-8: Schematic of Skewness of roughness profile [32]

1.7.4. Kurtosis of the roughness profile ($R_{ku}^{\wedge}$)

This expresses the biquadratic mean of Z(x) in a sampling length rendered dimensionless as the biquadratic of the root mean squared height $R_{q}^{\wedge}$. This means the kurtosis is a yardstick for the sharpness of a surface, and expresses the pointing (sharpness) of the height distribution [32].

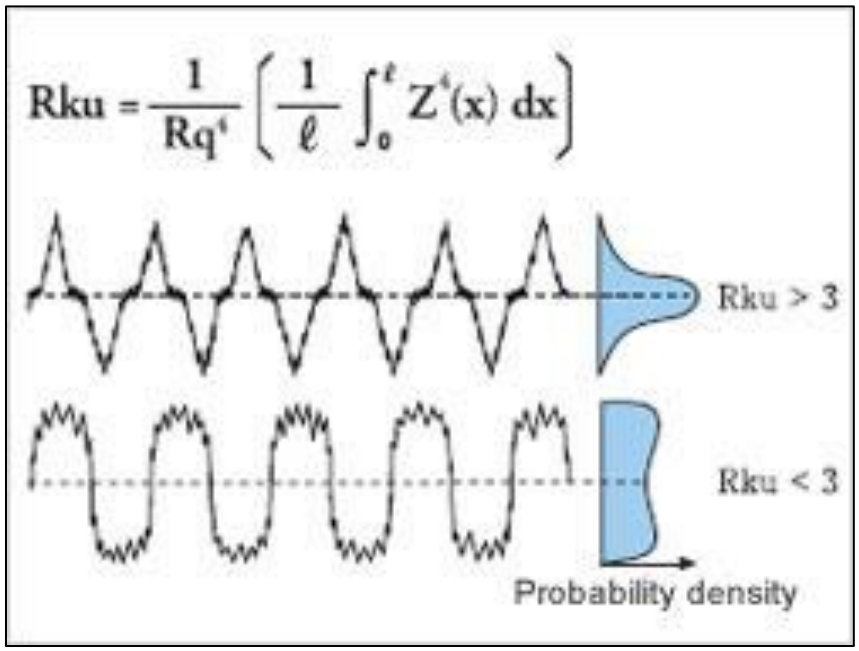

Figure 1-9: Schematic of Kurtosis of roughness profile [32].

Note that the symmetric Gaussian distribution has a kurtosis of 3. Distributions with K > 3 are called leptokurtic, and those with K < 3 are called platykurtic. In general, many engineering surfaces have symmetrical Gaussian height distribution [33].

Figure 1-8 and Figure 1-9 show the probability density functions for random distributions with different skewness, and symmetrical distributions (zero skewness) with different kurtosis [35].

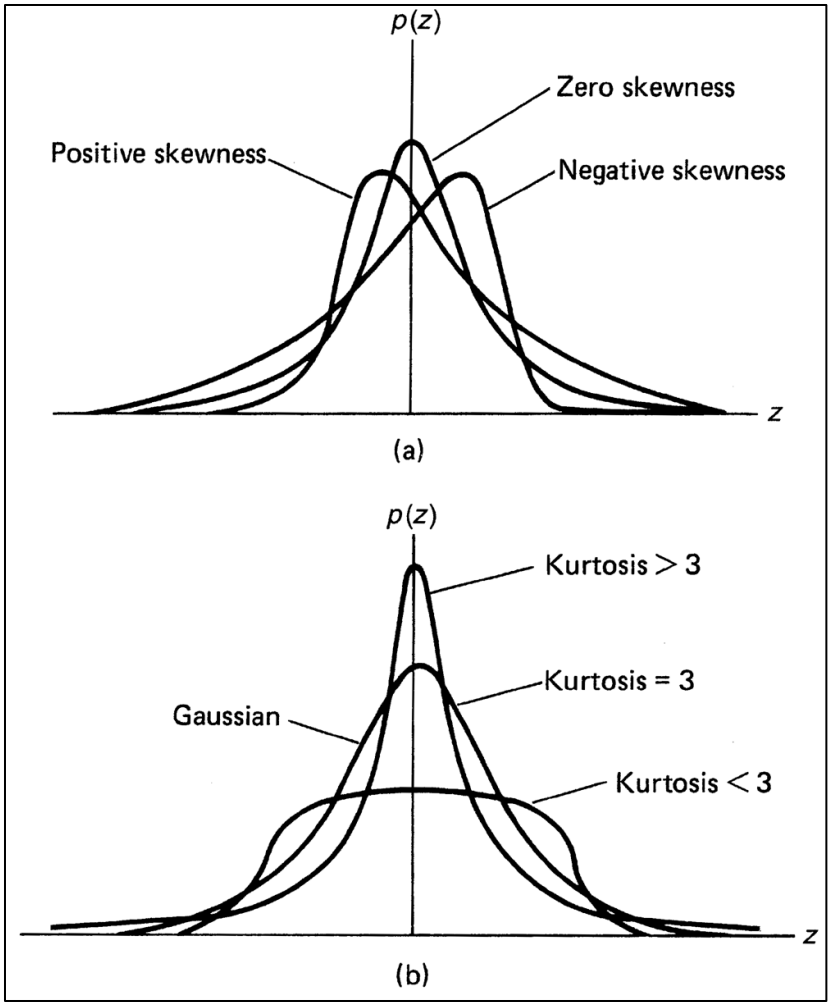

Figure 1-10: (a) Probability density functions for random distributions with different skewness, and for (b) symmetrical distributions (zero skewness) with different kurtosis [33].

1.7.5. Bearing Area Curves

The real contact area is smaller than a nominal contact area. The real area of contact, also known as the bearing area may be approximately found from a surface profile. The bearing area curve (BAC) first proposed by Abbott and Firestone [34] is also known as the Abbott–Firestone curve or the Abbott curve. It provides three numbers of $R^{\wedge}_{pk}$, $R^{\wedge}_{k}$ and $R^{\wedge}_{vk}$.

- Core roughness depth ($R_k^{\wedge}$) is the depth of the roughness core profile.
- Reduced peak height ($R_{pk}^{\wedge}$) is the mean height of the peaks expanded from the core area. It represents an estimate of the trivial peaks that will be worn off during the run-in period.
- Reduced valley depth ($R_{vk}^{\wedge}$) is the mean depth of the valleys prolonging from the core area. It denotes an evaluation of the depth of valleys that will retain lubricant in an operating surface.
- Minimum material ratio (M_{r1}) is the portion of the surface that consists of minor peaks above the core roughness.
- Maximum material ratio (M_{r2}) is the portion of the surface that will carry load during running of bearing. Figure 1-11 shows the parameters in BAC.

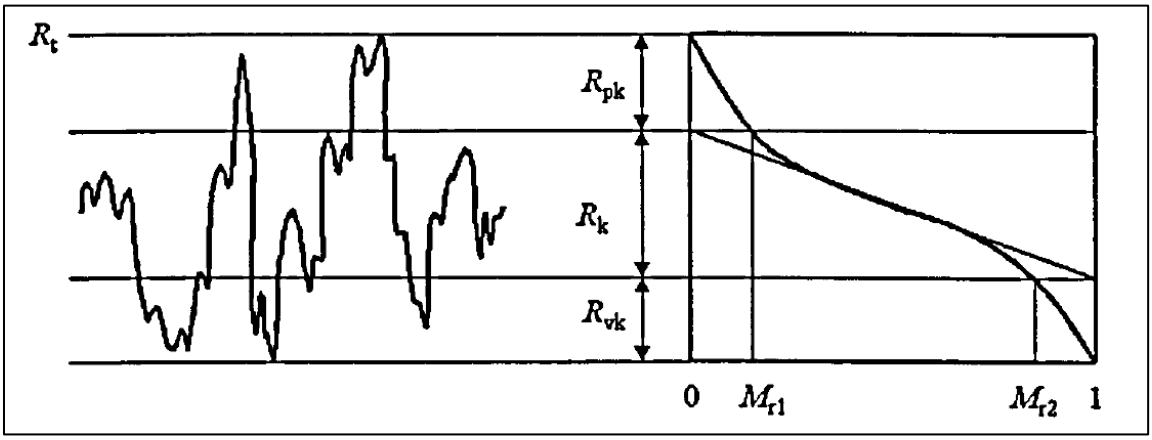

Figure 1-11: Parameters in Bearing Area Curve [34].

To produce a BAC from a surface profile, a parallel line (bearing line) is drawn with a small distance from a reference line (Figure 1-11). The length of each material intercept along the line is measured and these lengths are accumulated. Statistical

distribution of each point relative to reference line produces BAC. For a Gaussian surface, the most popular surface distribution profile, the BAC has an S-shaped look as shown in Figure 1-12. In the case of a surface map, bearing planes are drawn, and the area of each material intercept is measured. For a random surface, the bearing length and bearing area fractions are numerically identical.

The BAC is related to the cumulative distribution function (CDF). The fraction of heights lying above a given height z (i.e., the bearing ratio at height h) is given by [33]:

$$P(z > h) = \Delta z \sum_{z=h}^{\infty} p(z) \tag{1-19}$$

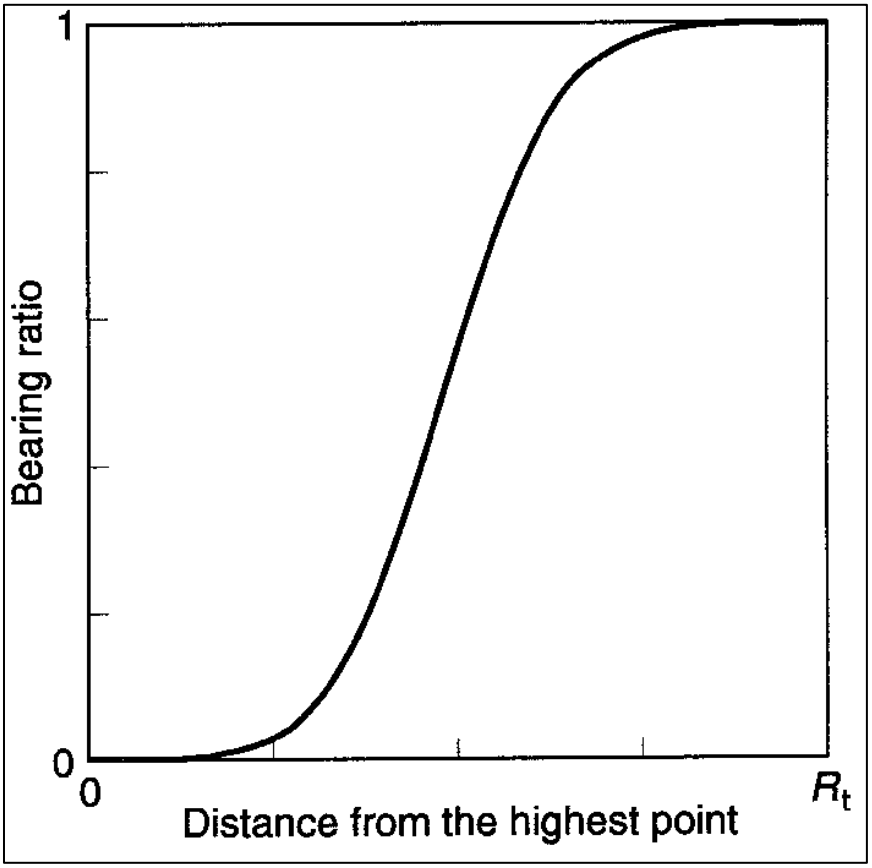

Figure 1-12: Schematic of bearing area curve [33].

1.8. Contact between rough surfaces

The contact between two rough surfaces starts with the contact between asperities and applying load causes asperities to undergo plastic or elastic deformation depending upon the magnitude of load. As a result, the real contact area is always smaller than a nominal one. Several types of modeling for real contacts have been proposed. A review of contact of the rough surfaces can be found in [35, 36].

Some of the experimental techniques that have been used to measure the real contact area are total internal reflection, Nomarski interferometry, neutrography, thermal and electrical resistance and computer simulation. The general results of experimental studies can be expressed as below:

- The real area of contact increases as the load increases due to an increase in the number of micro-contacts.
- The separation of the contacting surfaces is approximately inversely proportional to the logarithm of the load; the distribution of contact spot sizes is approximately log normal [36].
- Apparently, the density and average size of micro-contacts can vary over several orders of magnitude for different surfaces at the same load. It also appears that, contrary to an established belief, the real area of contact does not vary as the load but increases as its 0.8 power [36].
- The most promising finding by Woo is that bearing area is not in fact proportional to the load as universally believed previously [36].

1.9. Lubrication regimes

An investigation by the UK Government concluded that by applying the tribological principles, a savings of seven hundred million dollars per year is obtainable by reducing friction and wear [37]. Since then, tribology has been considered as a new trend which deals with wear, friction and lubrication. The purpose of lubrication is separating working surfaces, reducing friction without causing any damage to the surface and conveying heat from the contact. Depending on the lubricant film thickness and the degree of geometric comformity, lubrication regimes can be defined. Lubrication regimes also can most commonly define by the Stribeck curve. A Stribeck curve represents the general characteristic of a lubricated moving surface as a function of viscosity, velocity, and load [38].

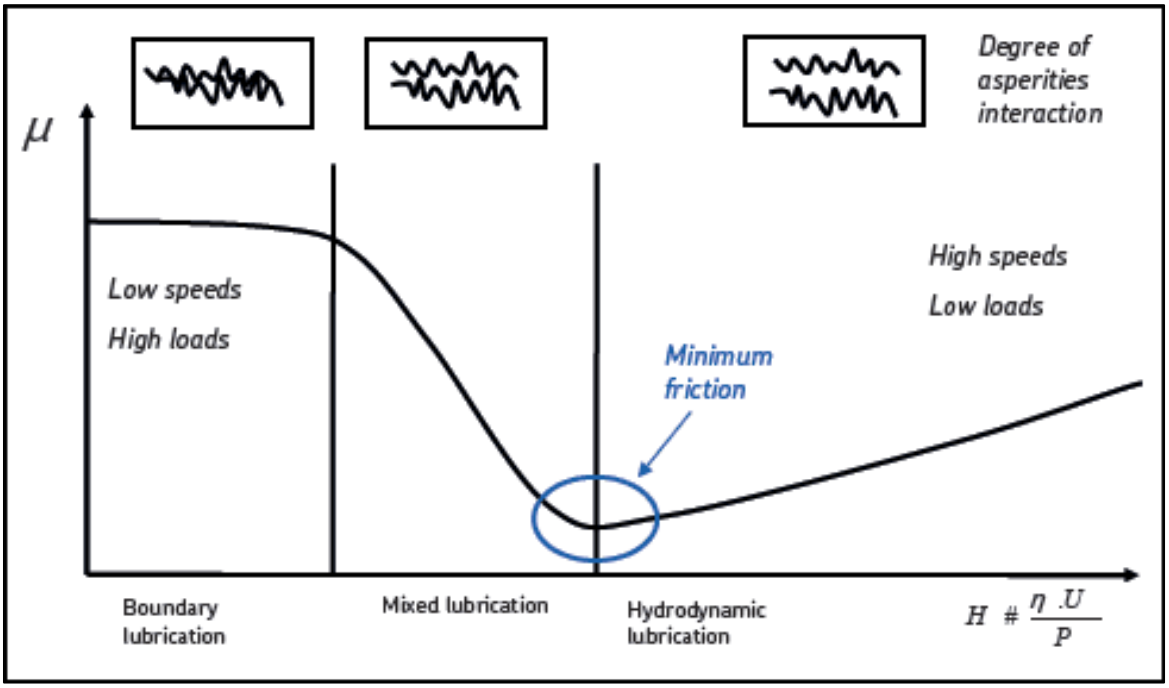

Figure 1-13: Stribeck curve and lubrication regimes. H is representing viscosity. U entrainment velocity and P load.

It is possible to identify four different forms of lubrication regimes in self-pressure generating lubricated contacts: hydrodynamic, elastohydrodynamic, partial or mixed and boundary (Figure 1-13).

Hydrodynamic or full film lubrication is the condition when the load carrying surfaces are separated by a relatively thick film of lubricant. In this regime (where there is no metal to metal contact), the moving surfaces are able to draw the lubricant into a wedge formed by the bounding surfaces since the entrainment velocity is significant to generate enough pressure to completely separate the surfaces and support the applied load. In this regime, the friction force is generated from the internal friction in the lubricant or shear resistant in the lubricant.

Elastohydrodynamic lubrication (EHL) is the condition that occurs when a lubricant is introduced between surfaces that are in rolling contact and under high contact pressure, such as ball and rolling element bearings. Therefore, the load is sufficiently high enough for the surfaces to elastically deform during the hydrodynamic action (Figure 1-14). This condition happens when geometrical comformity is poor and Hertzian contact pressure elastically deforms the contact. Also, high pressure increases the lubricant viscosity and thickness of the film. Contact pressures of above 1GPa (common in rolling element bearings) can cause the lubrication regime to remain in EHL as long as the velocity and viscosity stay within appropriate values. In non-conformal contacts such as rolling elements bearings, contact pressure varies between 100 to 4000 MPa. An equation governing the relationship between pressure and viscosity of oil has been derived by Barus [39]:

$$\eta = \eta_0 \exp(\alpha p) \qquad (1\text{-}20)$$

where α is the pressure-viscosity coefficient that normally is in the range 15–30 GPa^{-1}, η_0 is the dynamic viscosity under atmospheric conditions [40]. At 300 MPa the viscosity will have increased by a factor 90–8,000 [40]. Therefore, in the EHL regime, the residence time is short, and the pressure is high enough to make it impossible for the lubricant to escape the contact. Since the lubricant is liquid and almost incompressible, it separates the contact. Note that the theoretical minimum film thickness is dependent upon the sliding speed, the viscosity at room temperature and the pressure-viscosity coefficient of the lubricant. When the speed or viscosity decreases, the amount escaped lubricant increases and lubricant regime merges into mixed condition.

Partial or mixed lubrication regime occurs when the speed is low, the load is high or the temperature is enough high to reduce lubricant viscosity significantly – when any of these conditions occur, the tallest asperities of the bounding surfaces will protrude through the film and occasionally come in contact. This regime is called mixed because it is a mixture of boundary and EHL regimes. In this regime, the total load is shared by the lubricant and the asperities.

Boundary lubrication is the condition when the fluid films are negligible. Therefore, there is extensive asperity contact. In this regime, the physical and chemical properties of a lubricant become significantly important whereas the properties of the bulk fluid lubricant are insignificant. Components are working in a boundary lubrication regime when the load is substantially high or the entrainment velocity is considerably low. In these kinds of conditions, the only way to increase the film thickness is to increase viscosity. However, increasing viscosity comes at the cost of efficiency. Chemical additives in lubricants can play important roles as they can reduce the adhesion

between asperities; and reduce the friction by generating a tribo-film on the surface. High-pressure additives consisting of sulphur, chlorine and phosphorus atoms react with a steel surface and create a protective and slippery surface.

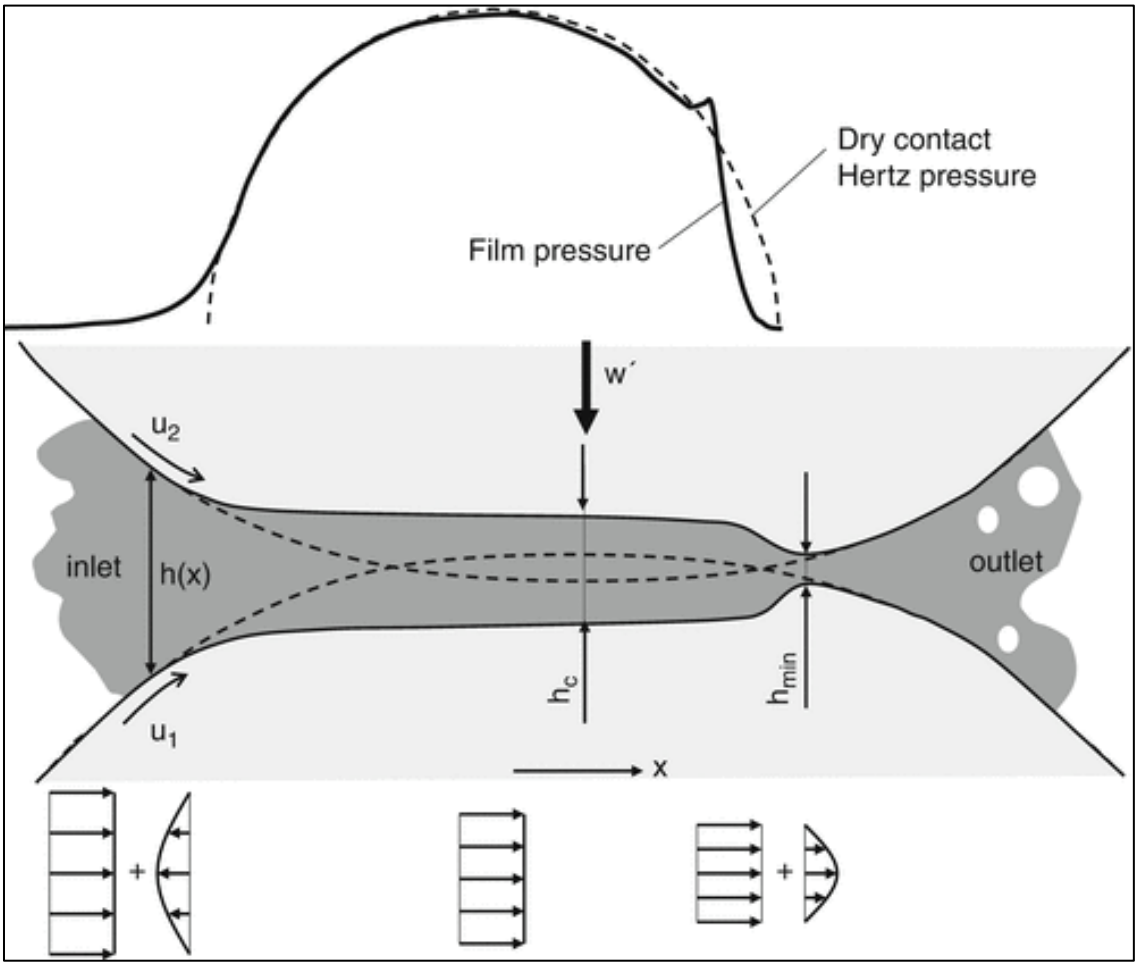

Figure 1-14: Typical film thickness profile for an EHL line contact. U is velocity and hc is central film thickness [40].

1.10. Lubricant film thickness for point and elliptical contact

Martin may have been the first tribologist who tried to calculate the lubricant film thickness [41]. Grubin made a huge contribution by introducing elastic contact theory of Hertz to the lubrication analysis that included the effect of pressure on viscosity [42].

However, nowadays, EHL film thickness is usually calculated according to Dowson. Hamrock and Downson developed a series of equations for several lubrication conditions from fully flooded to starvation [43, 44, 45, 46]. The central and minimum film thickness calculated by Hamrock and Dowson are given by the following expressions:

$$h_{cen} = 2.69\, U^{0.67}\, G^{0.53}\, W^{-0.067}\, (1 - 0.61\, e^{-0.73k}) R_e \quad (1\text{-}21)$$

$$h_{min} = 3.63\, U^{0.68}\, G^{0.49}\, W^{-0.073}\, (1 - 0.61\, e^{-0.68k}) R_e \quad (1\text{-}22)$$

where U, G and, W are dimensionless components and given by the following expressions:

$$U = 0.5(u_1 + u_2) \quad (1\text{-}23)$$

$$G = \alpha E^* \quad (1\text{-}24)$$

$$W = \frac{p}{E^* R_e^2} \quad (1\text{-}25)$$

k = (b/a) is the ellipticity ratio, a and b are the major and the minor semi-axis, respectively.

1.11. Lubricant film thickness for line contact

In 1959 Dowson and Higginson outlined the numerical solution of the complete isothermal elastohydrodynamic lubrication problem for line contacts in 1959. The equation is given by the following expressions [47]:

$$h_{min} = 2.65\, U^{0.7}\, G^{0.54}\, W^{-0.13}\, R \quad (1\text{-}26)$$

Where W is the load per unit length and would be expressed by:

$$W = \frac{p}{E^* R_e L} \tag{1-27}$$

1.12. Film parameter

Film parameter, also known as specific film thickness or lambda (λ) ratio is a dimensionless number representing the ratio of the minimum lubricant film thickness to the composite roughness of contact surfaces. This equation shows that surfaces have to be smooth in order to obtain full film lubrication. Full film lubrication occurs if λ is greater than 3 and boundary lubrication occurs if λ is less than 1 [48]. Consequently mixed lubrication is in between. The severity of each lubrication problem can therefore be predicted efficiently and rapidly. Dowson used equation 1-28 to estimate pitting life based on surface roughness. However, many elastohydrodynamically lubricated machine components are operating with no problems at $1 < \lambda < 3$ [49]. This could be due to the fact that flattening happens for asperities inside the contact area. However, Jacobson believes that dynamic change in the surface roughness due to cyclic contact may put a question mark in front of the use of the λ ratio as guide to the safe/un-safe operating limits for a lubricated contact [50].

$$\lambda = \frac{h_{min}}{\sqrt{R_{q1}^2 + R_{q2}^2}} \tag{1-28}$$

Recently (2010 and also 2014 edition), ISO 15144 was established to calculate the micropitting load capacity of cylindrical spur and helical gears using equation 29 for calculation of λ. In this equation composite roughness is calculated based on the arithmetic roughness of surfaces.

$$\lambda = \frac{h_{min}}{0.5\,(R_{a1} + R_{a2})} \tag{1-29}$$

ISO 15144 added another parameter (S) for calculation of minimum EHL film thickness (equation 30).

$$h_y = 1600\,\rho_{n,y}\,U^{0.7}\,G^{0.6}\,W^{-0.13}\,S_{GF,Y}^{0.22} \tag{1-30}$$

$S_{GF,Y}$ is the local sliding parameter.

$$S_{GF,Y} = \frac{\alpha_{\theta B,Y}\,\eta_{\theta B,Y}}{\alpha_{\theta M}\,\eta_{M}} \tag{1-31}$$

and:

- $\alpha_{\theta B,Y}$ is the pressure-viscosity coefficient at local contact temperature.
- $\eta_{\theta B,Y}$ is the dynamic viscosity at local contact temperature.
- $\alpha_{\theta M}$ is the pressure-viscosity coefficient at bulk temperature.
- $\eta_{\theta M}$ is the dynamic viscosity at bulk temperature.

The local contact temperature is the sum of the local flash and the bulk temperature.

Note that ISO 14155 is written for gear contacts with a high slide to roll ratio. However, for rolling element bearings, the local temperature is below the flash point of the oil.

The precision and accuracy of the Hamrock-Dowson and Dowson and Higginson equations have been confirmed by Lubrecht et al. in 2009 [51]. Considering both line contact and elliptical contact works, he showed that both the numerical pressure and film thickness results and the curve-fitted film thickness predictions are very accurate, even by today's standards [51]. However, for elliptical contact the ratio h_{min}/h_{cen} is not completely

settled. Therefore, equations 1-21 and 1-22 for elliptical contact as well as 1-26 for line contact are generally accepted by industry as reference equations for calculating minimum and central film thickness.

1.13. Tribological advantages of DLC coatings

Nowadays, the positive effect of tribological coatings on machine components, such as gears and bearings is clear and many independent studies have shown substantial decrease in surface failures due to tribological coatings [52, 53, 54].

Moreover, developing a coating to enhance the resistance of the surface to contact fatigue, micropitting, wear, scuffing and other surface related failures has been a goal of concern to tribologists for many years [55]. Among coatings developed over the last four decades, diamondlike carbon coatings (DLC) have shown a considerable potential in reducing and diminishing many surface failures [53]. The footprint of DLC coatings can be found in many industries such as bearings [56, 57], gears [58, 59], automotive valve-train applications [60, 61], piston pins [62] and pistonrings [63], cam followers [64] , spark-ignited, direct-injection fuel systems [65], cutting and forming tools [66, 67], etc. In the biomedical field, studies have been performed chiefly for the use of DLC in orthopedic applications [68, 69], and in the computer industry; this is generally related to the head-disk interface [70, 71, 72, 73].

DLC is an alloy of sp^2 and sp^3 bonded carbon along with hydrogen which then may or may not be doped with metal and ceramic agents based on application and functionality [53]. The mechanical properties of the DLC coatings are highly sensitive to the composition and processing parameters as well as doping agents [74, 75, 76]. Tungsten

(W), titanium (Ti), chromium (Cr) and silicon (Si) and their carbides (WC, TiC) are of the most common agents used for doping in DLC coating.

Among all metal doped diamondlike carbon coatings (Me-DLC), tungsten carbide doped diamond-like amorphous carbon coatings (WC/a-C:H) have received considerable attention regarding wear and delamination under high Hertzian contact pressure [77].

Many studies have shown tribological advantages of having the coating on one or more counter parts [78, 79, 80, 81], although, some studies showed there is no apparent benefit in using DLC coatings [82, 83, 84].

In [54], Doll briefly discussed how tribological coatings have been used for improving lives of bearings in boundary and mixed lubrication regimes. Doll mentioned MC/a-C:H coatings and specifically TiC/a-C:H and WC/a-C:H coatings can increase the fatigue life under poor lubrication conditions, increase debris damage life in bearings as well as adhesion resistance which leads to improve false brinelling and fretting life.

In 2012, Moorthy compared the effect of tungstan doped DLC (W-DLC) with the commercial name of BALINIT-C and a Nb-S coating on the micropitting and surface fatigue resistance of gears. In this study, the back-to-back gear tests were carried out on uncoated gears and also on gears coated with BALINIT-C and Nb–S coatings in order to compare their contact fatigue performance [85]. W-DLC is a hard but elastic coating, therefore it has a high wear resistance and at the same time high durability. The Nb-S coating is much softer, but this coating penetrates well inside the micro-valleys on the as-ground surface masking the peaks and valleys [85].

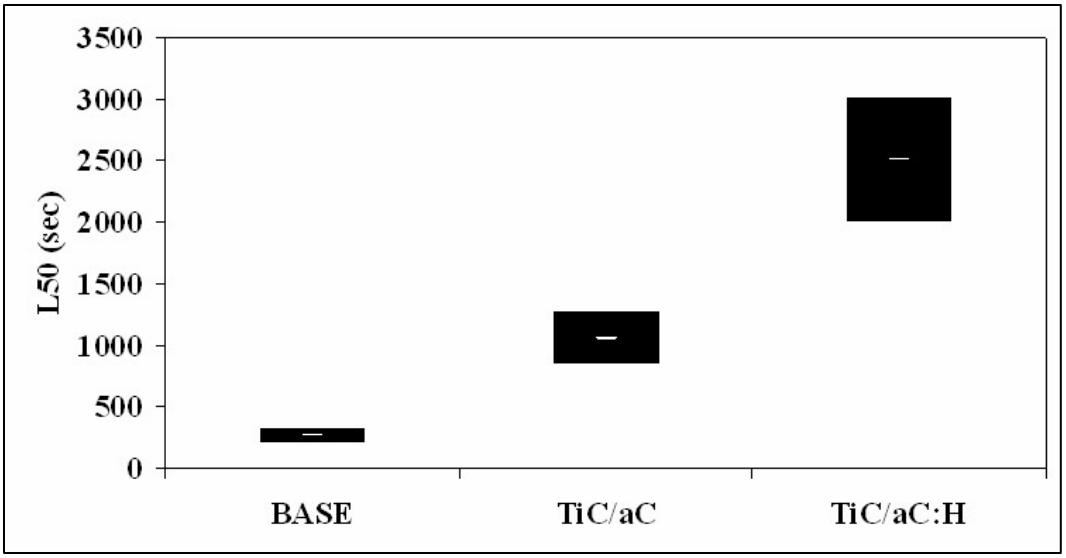

a)

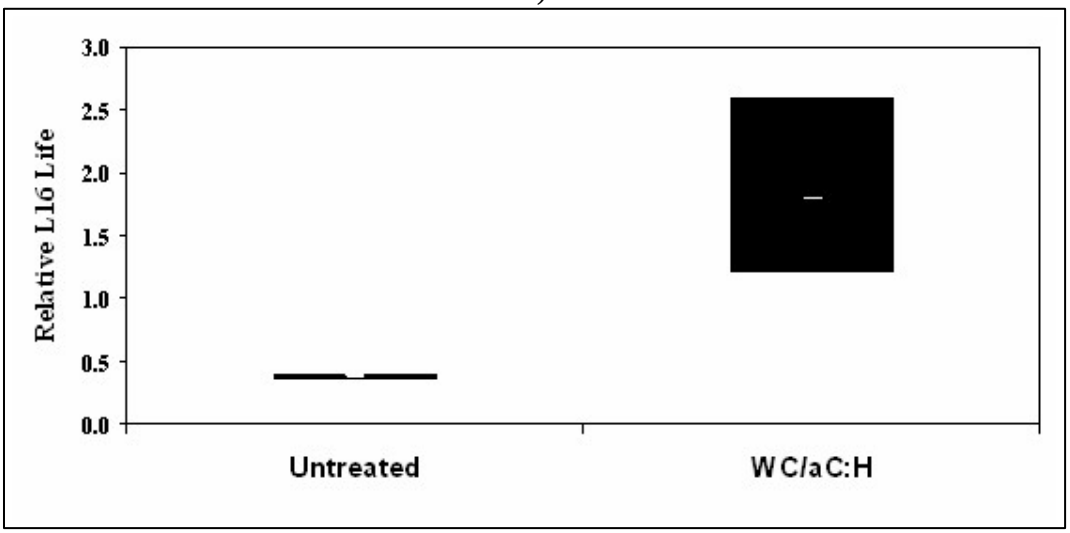

b)

Figure 1-15: a) L_{50} time to rib-roller end failure of tapered roller bearings with and without coated roller ends. Tests were performed with an applied thrust load of 4448 N at a speed of 2700 rpm in a condition that mimics a loss of lubrication. b) Results of laboratory testing showing the resistance to bearing life reduction caused by metallic debris provided by WC/aC:H coatings on rollers of tapered roller bearings [54].

The results of this study indicated the uncoated gears show a gradual progression of micropitting damage and the associated loss of gear tooth profile in the dedendum region between the start of active profile (SAP) and the pitch-line. SAP is the intersection of the limit diameter and the involute profile. In case of W-DLC coated gears, the

micropitting is largely reduced by the effect of polishing and removing of surface irregularities. A minimum level of micropitting damage was observed on the Nb-S coated gears. This may be attributed to good retention of Nb–S coating during contact fatigue and good penetration of Nb–S coating masking microscopic surface irregularities and thereby removing local stress concentration [86]. In that study, gears with the same coating were running against each other.

CHAPTER II

EQUIPMENT AND MACHINES

2.1. Overview

In this chapter, a brief explanation about machines and equipment used in this project is provided.

2.2. CFUMS

Closed-field Unbalanced Magnetron Sputtering (CFUMS) is a type of physical vapor deposition (PVD) process. Sputter deposition was first described by Grove (1852) and Plücker (1858) more than 160 years ago. They reported the formation of metal films due to vaporization by sputtering. Closed field systems were introduced by Hitachi in 1986 and unbalanced magnetron sputtering was presented by Windows and Savvides in the same year. However, modern magnetron sputtering has developed rapidly from 1990 to the point where it has become established as the process of choice for the deposition of a wide range of industrially important coatings [87].

2.2.1. History

Magnetron sputtering can be divided into two categories: conventional or balanced which was introduced in the early 1970s and unbalanced introduced in the late 1980s. Balanced and unbalanced refers to the magnetic field intensity of the permanent magnets located behind the targets. An incorporation of unbalanced magnetron

technology into multi-source, closed-field systems in the early 1990s transformed the capabilities of this technique, and has subsequently been responsible for its rise in application. Closed-field unbalanced magnetron sputtering (CFUBMS) is an exceptionally versatile technique, suitable for the deposition of high-quality, well-adhered films of a wide range of materials at commercially useful rates [88].

2.2.2. Principle of CFUMS

In a traditional sputtering process, a target (or cathode) plate is bombarded by energetic ions generated in a glow discharge plasma, situated in front of the target.

2.2.2.1. Magnetron sputtering

The bombardment process causes the removal of target atoms, particles, and secondary electrons. Condensation of target particles on the substrate produces a thin film [87]. Secondary electrons emitted from the target surface play an important role in maintaining the plasma. However, conventional magnetron sputtering has several limitations such as low deposition rates, low ionization efficiencies in the plasma, and high substrate heating effects. Development of unbalanced magnetron sputtering has mitigated these limitations substantially.

Magnetrons make use of the fact that a magnetic field configured parallel to the target surface can constrain secondary electron motion to the vicinity of the target [88]. Collision of secondary electrons to the target substantially increases the probability of an ionizing electron and atoms and consequently results in a dense plasma in the target region which means intensification of sputtering rates and, therefore, higher deposition rates at the substrate. In addition, the increased ionization efficiency achieved in the magnetron mode allows the discharge to be maintained at lower operating pressures

(typically, 10^{-3} mbar, compared to 10^{-2} mbar) and lower operating voltages (typically -500V, compared to -2 to -3 kV) than is possible in the basic sputtering mode [88].

2.2.2.2. Balanced and unbalanced magnetron sputtering

Balanced and unbalanced magnetron configurations are shown schematically in Figure 2-1. Balanced describes a condition where the fields of outer and central magnetic poles are the same and therefore plasma is confined at the vicinity of target. Type 1 unbalanced magnetron is when the central pole is strengthened relative to the outer pole. Therefore, the plasma density is lower near the substrate, which leads to deposited films with porosities on the order of 1000 times greater than a fully dense material [89]. Films of this type have a number of diverse potential applications, such as catalysts, pyrophoric devices, or non-reflective coatings [88]. Type 2, unbalanced magnetron is when the outer poles are strengthened relative to the central pole. Therefore, the magnetic field is not closed and some lines are directed towards the substrate. Secondary electrons that follow these lines can travel to the substrate, and as a result, the plasma can reach the substrate easier. This has several advantages:

- Substantial decrease in the negative bias voltage of substrate as the plasma is already close to the substrate
- Uniform coatings with less internal stress are producible
- The ion current drawn at the substrate and deposition rate are directly proportional to the target current

Ion current densities higher than 1 mA/ cm^2 are needed to produce a uniform and dense film on the substrate. However as shown in Figure 2-1, the ion current density is insufficient for the first two methods. Ion current density can be increased by applying a

negative bias voltage to the substrate. However, higher negative bias voltages can increase the number of defects and the internal stress of the films. Thicker films would be more prone to delamination from a substrate. Unbalanced magnetron sputtering can overcome this problem as it requires a lower bias voltage than other traditional PVD methods.

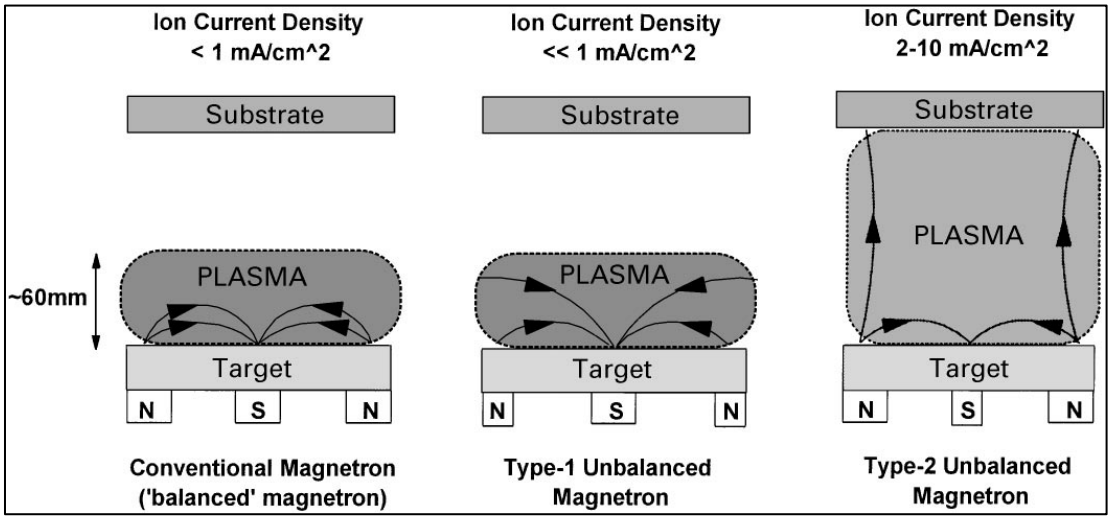

Figure 2-1: Schematic representation of the plasma confinement observed in conventional and unbalanced magnetrons [88].

2.2.2.3. Closed-field and mirror-field configuration

To apply a uniform film or coating on substrates with complex geometries, multiple magnetron sources should be used and the substrate should be translated or rotated in front of each target in the chamber.

Figure 2-2 shows three configurations for a dual magnetron sputtering set up. The closed-field configuration occurs when the magnetic arrays in adjacent magnetrons are configured with opposite magnetic polarities. Conversely, a mirror-field condition is

achieved when the magnetic arrays in adjacent magnetrons are configured with identical magnetic polarities. Opposite to the closed field, in the mirrored case, some of the field lines are pointing to chamber walls and therefore some secondary electrons get lost resulting in a low plasma density in the substrate region. The influence of configuration on ion-to-atom ratio on the substrate is shown in Figure 2-3. Clearly, a closed field configuration has 2-3 times greater ion-to-atom ratio on the substrate than either mirror or a single magnetron configuration [90].

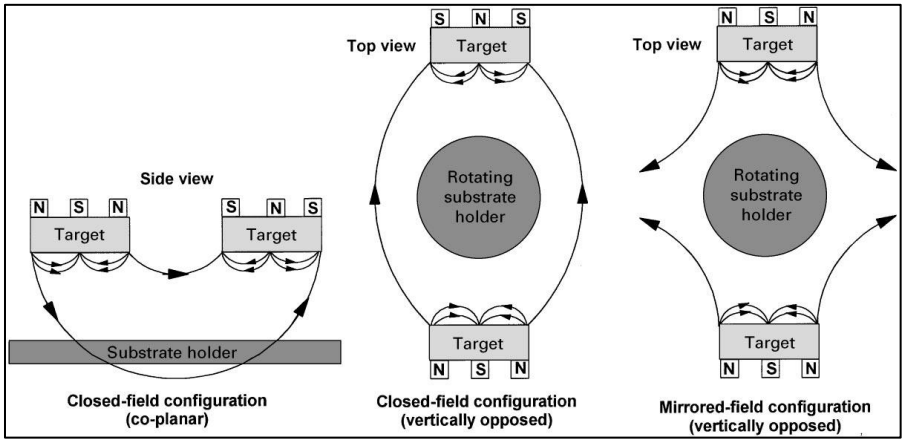

Figure 2-2: Dual unbalanced magnetron configurations [88].

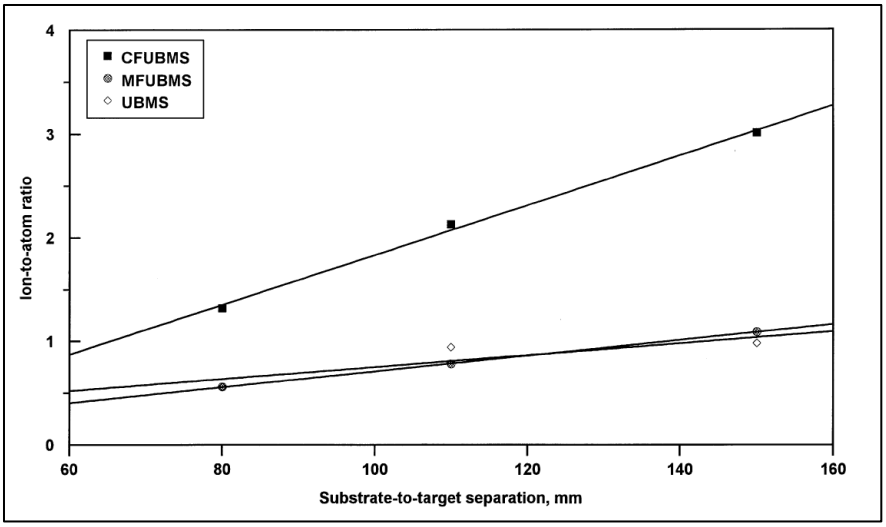

Figure 2-3: The variation with substrate-to-target separation in the ion-to-atom ratio incident at the substrate for closed field (CFUBMS), mirrored field (MFUBMS) and single magnetron (UBMS) configurations [90].

2.2.3. Advanced coatings by CFUMS

CFUMS has several advantages. CFUMS is capable of generating complex composite coatings such as (TiAl)N, (TiZr)N and (CrZr)N [91]. Multiple targets in closed field configuration can overcome limitations of conventional sputtering systems and make it possible to achieve almost any type of composite coatings. Also, by sputtering the targets at different rates, almost any desired alloy composition can be attained. Nano-layered composite coatings such as metal doped molybdenum disulfide (MoS_2/metal) and DLC coatings are examples of coatings that were commercially developed by CFUMS for tribological applications [92]. MoS_2/metal is relatively soft and can be applied for solid lubrication purposes but DLC is a hard coating that can mitigate surface failures in bearings and gears [93].

The tribological behavior of a tungsten carbide diamond-like carbon coating (WC/a-C:H) deposited by CFUMS on 52100 bearing steel in the Timken Surface Engineered Laboratories (TESL) is the topic of this dissertation. The physical properties and deposition process of this coating will be explained in detail in future chapters.

2.2.4. CFUMS in TESL

The actual image and schematic diagram of the CFUMS system at TESL is shown in Figure 2-4 a and b. This system was designed through a collaboration between the Timken company and the Fraunhofer Institute in Braunschweig, Germany. Two chromium targets used in that deposition system are shown in Figure 2-4c. The volume of chamber is about 0.44 m^3 (30× 30× 30 in^3) and the minimum vacuum pressure achievable is about 10^{-6} Torr. However, the typical working pressure is about 10^{-2} to 10^{-3} Torr. It is equipped with water-cooled targets, so little radiated heat is generated. A PLC controller controls target shutters, water circulation, power supplies, carousel rotation and valves. Several pressure and temperature sensors have been installed to measure the gas flow rate, and circulating water temperature. It has four magnetrons positioned on the four faces of a square with length of 76.2 cm (30 in). The size of the targets is 38.1× 12.7×2.3 cm (15× 5× 0.9 in). Substrates can be held with or without magnets (depends upon the geometry of samples and deposition parameters) and rotated in the chamber in one, two, and three axis. The applied current, bias voltage, gas flow etc. are controlled by software to achieve almost any alloy composition or composite coating with several layers as far as not more than four targets is necessary.

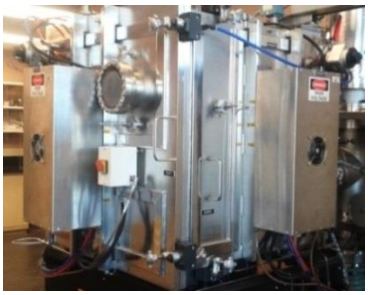

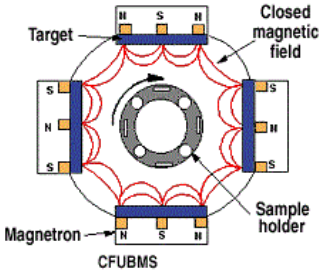

a) CFUMS in TSEL b) Schematic of CFUMS c) Used targets

Figure 2-4: a) Actual and b) schematic of quad targets CFUMS available in TSEL. Position of two sequential magnetron targets is shown with red arrows. c) Two used Chromium targets.

For the specified WC/a-C:H coating used in the current study, two tungsten and two chromium targets were used. Argon is used for generating the plasma and for plasma cleaning of the substrates surfaces. During plasma cleaning, a bias voltage of -500 VDC was applied to samples. Argon plus acetylene were used to supply the carbon content of the coating. The coating is a layered material consisting of a 100 nm-thick Cr layer that forms strong chemical bonds to the native iron oxide surface layer on steel [94]. In the next layer, the composition is gradually changed from Cr to WC/a-C:H. The thickness of this gradient layer is also about 100 nm thick. Finally, the top layer of WC/a-C:H is approximately 900 nm thick. This yields a total coating thickness of approximately 1.1 μm. More information about the coating microstructure and process parameters are available in references [95] and [96] respectively.

2.4. PCS Micropitting Rig

The description of the micropiting rig (MPR) is provided by the manufacturer of the rig [97]. The MPR is a computer controlled three-contact disc machine in which there are three ‘counterface’ rings of equal diameter positioned apart with a smaller diameter roller located in the middle and in contact with all the rings.

2.4.1. MPR specification

The description of the micropiting rig (MPR) is provided by the manufacturer of the rig [97]. The MPR is a computer controlled three-contact disc machine in which there are three ‘counterface’ rings of equal diameter positioned apart with a smaller diameter roller located in the middle and in contact with all the rings. This arrangement allows the test roller to be subjected to a large number of rolling contact cycles in a short period of time and hence significantly reduces testing time. At a typical entrainment speed of 3.5m/s, the central test roller will experience approximately one million contact cycles per hour. Figure 2-5a and 5b show the Micropitting rig and the chamber [97]. The rig has an on-board processor, which allows the speed(up to 4 m/s), slide-roll ratio(up to 200%), temperature(up to 135˚C), and load(up to 1250 N) to be automatically controlled. Two servo-controlled motors are used to control the speeds of the rings and the roller separately, therefore allowing any combination of slide-roll ratio and entrainment speed to be set. Since the rig is computer controlled, it is possible to perform both simple and complicated test steps under precisely controlled conditions, allowing the effect of lubricant compositions on micropitting, macropitting or failure load testing to be studied [97].

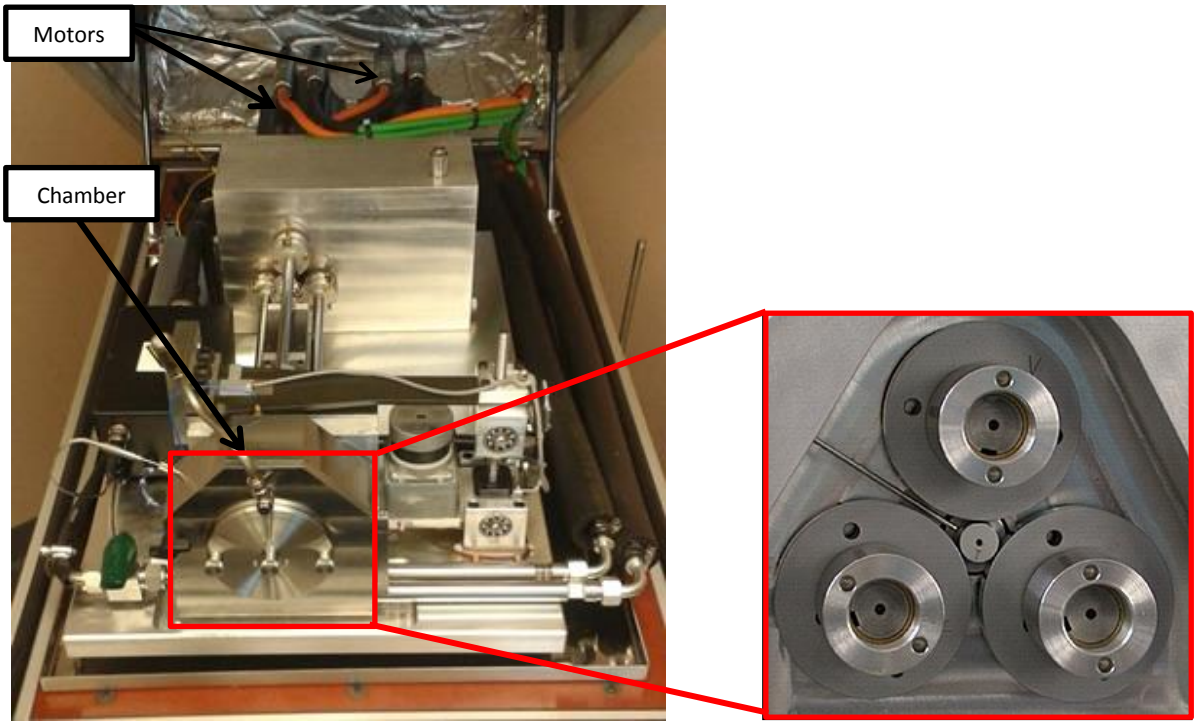

a) MPR under the hood

b) MPR chamber

c) PCS roller

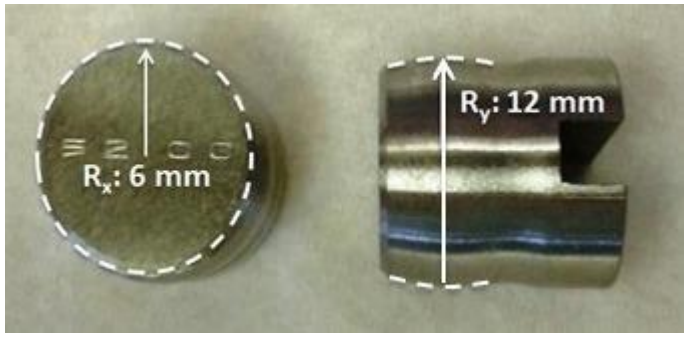

d) TKR roller

Figure 2-5: a) PCS MPR. b) Details of MPR chamber. Temperature measurement sensor can be seen close to the contact. c) PCS roller that makes a line contact. d) TKR roller that makes elliptical contact.

A dip lubrication system is used to supply lubricant into the contacts. The test requires a relatively small volume (150 ml) of oil into which the two lower rings are dipped. An electric cartridge heater is used to adjust the temperature of the test chamber,

which in turn heats up the test lubricant. A temperature probe is inserted into the test chamber with the tip of the probe close to the contact region [97].

The load is applied by means of a motorized ball-screw, acting through a loading arm. Strain gauges are attached on the loading arm to measure the applied load. The rig is equipped with a piezoelectric accelerometer that is used to measure the vibration in the contact. Once a macropit propagates on the test roller, the increased measured vibration level is detected by the control system and the test is stopped automatically. The number of cycles to failure ("Life") is recorded [97].

The test head design allows a test to be stopped at any time, the load removed and the rotation stopped. The central roller can then be withdrawn for inspection, without disturbing either the lubricant or the three rings. The roller specimen can then be placed back in position and the test can continue. This is particularly useful in the study of both micropitting and macropitting, where physical examination of the specimen is essential.

The rig has comprehensive safety features. A test will be automatically stopped when any preset limit for temperature, vibration level, or friction is exceeded. The temperature limit uses the lubricant bulk temperature to trigger the shutdown of a test. In addition, there is also a safety alarm temperature sensor inside the test head. Vibration and friction coefficient limits are detected using an accelerometer mounted on the test head and a torque sensor respectively [97].

2.4.2. Discs and rollers

Two types of discs have been used for these experiments: PCS discs and TKR discs. PCS discs were supplied by the MPR manufacturer, and TKR discs provided by the Timken Company. The hardness and geometry of the discs are similar. Both types have a

cylindrical shape (R_x: 27 mm) with the hardness of 62 HRC. However, their composition and surface roughness values are slightly different. PCS discs are made of 5210 case carburized steel and TKR discs are made of 52100 through hardened. Details of surface roughness will be discussed in roughness section.

Similarly, two types of rollers, one with a line contact and the other one with an elliptical contact were examined against the cylindrical discs. Both types of rollers have similar geometries except in the contact area. Roller type 2 (TKR) has a barrel shape (R_x: 6 mm, R_y: 12 mm) which leads to an elliptical Hertzian contact area and less edge stress. Roller type 1 (PCS) has no crown at the contact area and therefore produces a line contact in contact with cylindrical discs. The geometry of rollers; type 1 (PCS) and 2 (TKR) are presented in Figure 2-5c and 5d respectively. In addition, the composition of the two types of roller is slightly different; PCS rollers are made of 5210 steel heat treated to a case hardness of 57 HRC and TKR rollers are made of 52100 with a hardness of 62 HRC. In the experimental section, more details are given for surface roughness and heat treatment of rollers.

2.5. 3D surface Profilometer

The Zygo NewView™ 7300 white light interferometer (profilometer) is a powerful tool available in TESL for characterizing and quantifying surface roughness, step heights, critical dimensions, and other topographical features with excellent precision and accuracy. It is shown in Figure 2-6. All measurements are nondestructive, fast, and require no sample preparation. Profile heights ranging from < 1 nm up to 20000 µm at high speeds, independent of surface texture, magnification, or feature height are measureable.

The measurement technology of Zygo NewView™ 7300 is Scanning White-light Interferometry (SWLI). SWLI is a versatile technology that provides a noncontact, 3-D method of measuring surface roughness. The interference microscopy technology combines an interferometer and microscope into one instrument.

Illumination from a white light beam passes through a filter and then a microscope objective lens to the sample surface. The objective lens is coupled with a beam splitter so some of the light is reflected from a reference mirror. The light reflecting back from the surface recombines with the reference beam. The recombined beams create bright and dark bands called “fringes,” which make up the interferogram. Fringes represent the object’s topography [98].

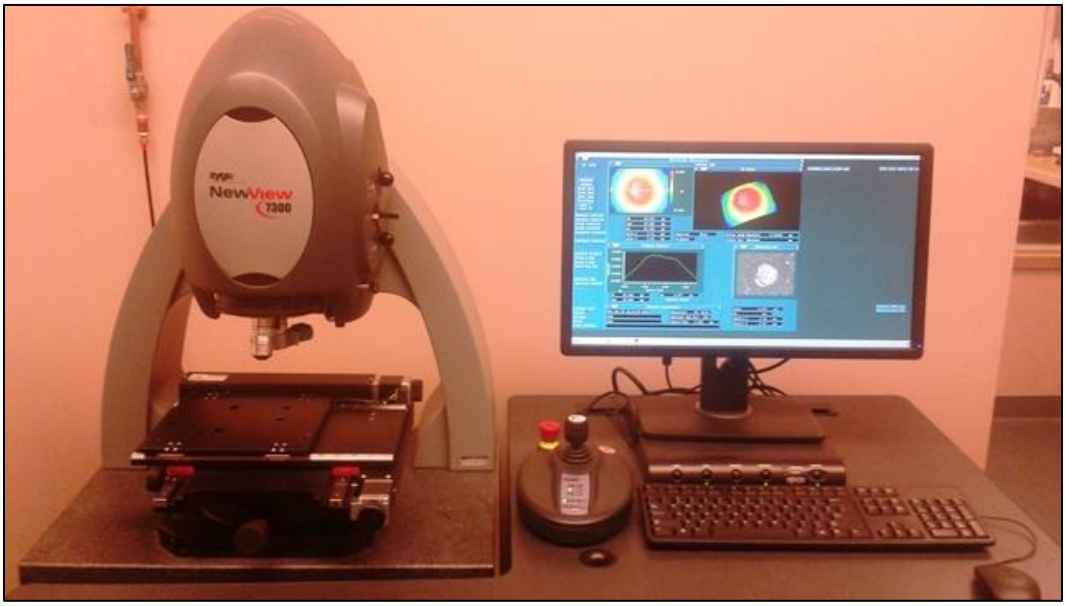

Figure 2-6: Zygo NewView™ 7300 available in TSEL

The pattern of these fringes is captured on a CCD camera array for software analysis. By obtaining several frames of intensity information for each point, the system

can recreate the sample surface. The frames are passed through an algorithm to convert those intensity signals into height information [98].

Microscope-based white light optical profilers are capable of measuring a variety of surface types, including ground and polished surfaces, steps and films. They do this by mapping surface heights that range from sub-nanometers to microns across areas that range from microns to millimeters in a single measurement. This rapidly provides surface roughness, shape and waviness data.

When the required measurement areas are larger than the field of view, a stitching procedure can be employed that involves a number of partially overlapping measurements being combined into one surface profile. Stitching, however, requires that regions overlap, with the overlapping data aligning adjacent measurements. Because overlap regions are measured more than once, overall measurement time increases [98].

2.6. Additional equipment

Other experimental equipment used in this study is listed below:

- Thermolyne FB 1300 laboratory furnace with working temperature range of 100 to 1100 ˚C and chamber size of (10 x 9.5 x 11) cm. Heat treatment of MPR rollers and disc has been done in conventional laboratory size furnace.
- Mikronite polishing machine. The Mikronite process is a high-energy centrifugal system. Eight vessels filled with abrasive media and parts are rotated with high speed that causes high energetic impact of media with parts that eventually polishes the surface of parts. The media within the vessel can vary depending on the goal, but it is commonly a combination of ground walnut shells and an

abrasive such as silicon carbide or aluminum oxide the same materials found in sandpaper [99].

- Fowler 54-770-650-1 Digital Rockwell Hardness Tester. This model meets requirement of EN-ISO 6508 and ASTM-E18 Standards, has a resolution of 0.5 of Rockwell unit and 10 kgf preload/ 60, 100, 150 kgf load. This machine has automatic loading and unloading, automatic holding of test force with large LCD backlit display.
- Metallography equipment: Struers cutting and polishing machines along with metallographic sample preparation equipment. The ACCUTOM-5 (STRUERS) is a microprocessor controlled cut-off machine with a diamond wheel. This machine has a high-precision stepper motor that makes it able to position in steps of 5 mm with variable speed. Cold mounting resin, polishing papers, clothes and diamond slurries provided by Allied company.
- Optical microscope, capable of taking pictures with magnification up to 1000 times.
- Scanning Electron Microscope (SEM JEOL JSM 5310) for taking high magnification and resolution pictures of micropits, cracks and failures of the coatings.
- ISL HOUILLON Viscometer used to measure the viscosity of oil samples.
- The Fischerscope X-Ray XDAL spectrometer (an XRF machine) allows us to check the thickness of coating before and after running.

- Thermo Scientific Nicolet 6700 spectrometer FT-IR (Fourier transform infrared spectroscopy) is used to check if there is any oxidation or significant change in oil composition after micropitting tests.
- FIB (Focused ion beam) and TEM (Transmission electron microscopy) are used to study the delamination of coating. FIB has similar principles as SEM, except that the rastering beam over the sample is an ion beam instead of the electron beam, mostly gallium. The sputtering action of Ga ions on the substrate provides a precise machining capability, applicable for thin films and coatings with almost no phase changing, delamination or plastic deformation.

CHAPTER III

EXPERIMENTAL PROCEDURE

3.1. Overview

The general aim of this research project is to study the effect of two tribological coatings: Black oxide and WC/a-C:H, on the micropitting and surface fatigue behavior of 52100 bearing steel. Therefore, several variables are considered: surface roughness, hardness, load, entrainment velocity, slide to roll ratio etc.

As-received rollers and discs have a hardness of 62 HRC. To change the hardness of rollers and discs to desired values, conventional heat treatment in a furnace has been used in air. A thin layer of oxide produced due to the heat treatment, was removed in the Mikronite. The as-received surface roughness (R_a) of discs and roller was 0.4 μm. After heat treatment and finishing the surface roughness decreased to 0.2 μm. Coatings were then applied to the specimens. Tests were stopped after attaining a certain number of cycles and the surfaces of roller and/or discs were characterized by 3D optical Profilometer, optical microscopy and SEM. Additional characterizations techniques such as FIB, TEM, FTIR have also been done on a limited number of specimens. All tests were performed in either boundary or mixed lubrication regimes.

3.2. Materials and substrates

PCS discs and rollers are made of case carburized 5210 steel with a hardened depth of 1 mm and an initial surface roughness of 0.4 or 0.2 μm for discs and 0.2 μm for rollers. The contact between a PCS roller and a disc leads to a line contact. Figure 2-5c shows the feature of a PCS roller and discs are recognizable in Figure 2-5b. The hardness of the discs is typically 62 HRC and that of the roller is 57 HRC. The hardness values were chosen in order to generate pitting on the roller with less surface damage created on the discs. Rougher discs (0.4 μm) generate macropitting and smoother discs (0.2 μm) generate micropitting on the surface of the roller.

Timken fabricated discs and rollers are made of through hardened 52100 steel with typical hardness of 62 HRC and an initial surface roughness of 0.4 μm (discs) and 0.2 μm (rollers). Geometries of the Timken-fabricated rollers and discs are shown in Figure 2-5d. The contact between Timken-fabricated roller and discs generates an elliptical contact.

As it shown in Table 3-1, the difference between composition of 5210 and 52100 is negligible. However, the difference between heat treatments (case carburized and through hardened) may affect micropitting behavior.

Table 3-1: Chemical composition of AISI 5210 and SAE52100

Steel	C	Si	Mn	Cr	Ni	Others
5210	0.97	0.25	0.35	1.5	max 0.30	Cu max 0.30
52100	0.98-1.1	0.15-0.35	0.25-0.45	1.3-1.6		P max 0.025, S max 0.025

3.3. Lubricant

The test oil used in these experiments is an ISO viscosity grade 10 polyalphaolefin (PAO ISO 10) containing no extreme pressure (EP) or anti-wear (AW) additives in order to avoid their effects on the test results. Oil viscosity was measured by a ISL Houillon Viscometer. The viscosity of ISO 10 was measured experimentally at 40 and 100 ˚C and then extrapolated to 75 and 90 ˚C, assuming a linear relation between temperature and viscosity. Viscosity values of ISO 10 utilized in the calculation of λ at 40, 75 and 90 ˚C is 0.01, 0.0059 and 0.0041 Pas, respectively with a resolution of ± 0.0005. Temperatures of 40, 75 and 90 ˚C were testing temperatures.

3.4. Tribological coatings

In this section the deposition procedure, characteristics, and mechanical and physical properties of the two tribological coatings used in this research project are summerized. Prior to the deposition of the coatings an automated process used on the specimens. The ultrasonic alkaline detergent removes organic and inorganic contaminations from the surface. After cleaning, specimens are coated with WC/a-C:H by CFUMS or black oxide by a hot bath.

3.4.1. WC/a-C:H coating

The WC/a-C:H coating is a layered material consisting of a 100 nm-thick Cr layer that forms strong chemical bonds to the FeO surface layer on steel [94]. In the next layer, the composition is gradually changed from Cr to WC/a-C:H. The thickness of this gradient layer is also about 100 nm thick. Finally, the top layer of WC/a-C:H is approximately 900 nm thick. This yields a total coating thickness of approximately 1.1 μm. Before applying the coating, the surface of the specimens is subjected to a plasma

bombardment in the chamber to remove any remained contamination from previous cleaning process. In this study our focus mostly is on the mechanical properties of the coating such as hardness and young modulus. More information about the coating microstructure and process parameters is available in references [95] and [96] respectively. However, it should be noted the hardness of this coating is about 11-13 GPa and the young's modulus is about 120 GPa.

3.4.2. Black Oxide

A hot bath process was used to achieve a black oxide coating on the surfaces of rollers and discs. This procedure consists of three steps: a pre-treatment to achieve the steel surface, a black oxide conversion treatment, and a post-treatment to stabilize the black oxide.

In the pre-treatment step, the surface of steel is degreased by first washing with hexane, then isopropanol and is finally deoxidized using a one molar sulfuric acid solution. In the conversion step, parts are placed in the hot bath solution for 20 minutes in order to achieve a uniform black oxide layer with thickness of about one micrometer. The hot bath solution consists of dissolved 70% KOH, 20% KNO_3 and 10% KNO_2 in deionized water at 135˚C. In the post-treatment step, the black oxide is stabilized by rinsing the parts in deionized water and rapidly drying them with warm air. The post-treatment step prevents further oxidation of black oxide by removing the corrosive elements used to convert the steel surface.

There is not much a difference between the appearance of black oxide and WC/a-C:H coated parts. Both of them have a black shiny color. However, unlike WC/a-C:H,

black oxide is relatively soft. The hardness of black oxide is between 5.5 to 6.5 GPa [100].

CHAPTER IV

WC/a-C:H COATING ON MPR DISCS AND ROLLER

4.1. Overview

In this section, the micropitting behavior of coated and uncoated parts is presented first when the WC/a-C:H coating is applied to discs and secondly to rollers. Finally, the micropitting result of the WC/a-C:H coating on the roller or disc are compared with the results of the case when the black oxide coating is on both roller and discs.

4.2. WC/a-C:H coating on discs

To study the effect of the WC/a-C:H coating on the micropitting behavior of uncoated steel, initially coating was applied to the discs.

4.2.1. WC/a-C:H coating on discs, PCS samples (Line contact)

Coated discs ran against the uncoated roller and the results are compared with steel/steel contact. (i.e. no coating on discs or the roller). It is noted that the contact between PCS samples is line contact. Table 4-1 shows the test matrix for first series of experiments.

In the first series, rollers run under three escalating contact stresses of 1.2, 1.5 and 1.7 GPa for 0.8, 0.8 and 1.6 million cycles respectively which result in 3.2 million total number of cycles for each run. Other variables such as maximum calculated contact

stress, temperature, and calculated initial λ are presented in Table 4-1. The results of the first series of tests are presented in Table 4-2.

Figure 4-1 shows the surface of rollers after running against coated and uncoated discs. In general, the presence of the coating on the discs causes early stage micropitting or a high rate of abrasive wear on the roller as the roughness of the coated discs increases. On the other hand, in steel/steel contact, rollers can run for more than 35 million cycles (10 runs) with no significant sign of surface damage when the surface of discs are 0.1 μm (Ra). An increase in the surface roughness of discs causes the roller to undergo micropitting after 4 runs or 14 million cycles. A further increase in roughness of discs (0.4 μm) causes early macropitting in first run on the roller as it can be seen in Figure 4-1g. Figure 4-2 shows the surface of uncoated rollers running against WC/a-C:H coated discs for tests number 1.1 and 1.2 from Table 4-1 in three sequential runs. Each run has 3.2 million cycles at 1.2, 1.5 and 1.7 GPa maximum contact stress as it mentioned in Table 4-1. Micropitting on the surface of roller is recognizable even after first run. Range of depth of pits is reported in micrometer.

Table 4-1: Micropitting test matrix. P represents the calculated contact stress, u is the entrainment velocity, SRR is the slide to roll ratio, and λ is the ratio of the calculated minimum lubricant film thickness to the composite surface roughness (Ra). D represents Disc and R represents Roller.

Test	Coating		H (HRC)		R_a (μm)		P_{max} (GPa)	u (m/s)	SRR %	T (˚C)	λ
	D	R	D	R	D	R					
1.1	Y	N	62	57	0.1	0.25	1.2-1.5-1.7	3	20	90	0.72
1.2	Y	N	62	57	0.2	0.25	1.2-1.5-1.7	3	20	90	0.54
1.3	Y	N	62	57	0.3	0.25	1.2-1.5-1.7	3	20	90	0.36
1.4	Y	N	62	57	0.4	0.25	1.2-1.5-1.7	3	20	90	0.18
2.1	N	N	62	57	0.1	0.25	1.2-1.5-1.7	3	20	90	0.72
2.2	N	N	62	57	0.2	0.25	1.2-1.5-1.7	3	20	90	0.54
2.4	N	N	62	57	0.4	0.25	1.2-1.5-1.7	3	20	90	0.18

Table 4-2: Results of the MPR Tests of first series

Test	Coating		H (HRC)		R_a (μm)		Results
	D	R	D	R	D	R	
1.1	Y	N	62	57	0.1	0.25	Micropitting on roller
1.2	Y	N	62	57	0.2	0.25	Micropitting on roller
1.3	Y	N	62	57	0.3	0.25	Micropitting and wear on roller
1.4	Y	N	62	57	0.4	0.25	Abrasive on roller
2.1	N	N	62	57	0.1	0.25	No considerable damage on roller or discs
2.2	N	N	62	57	0.2	0.25	Micropitting on roller
2.4	N	N	62	57	0.4	0.25	Macropitting

Figure 4-2 shows the surface of an uncoated roller running against uncoated discs in three random runs; tests number 2.1 and 2.2 from Table 4-1. The criterion for micropitting in this series of tests is when the depth of pits reaches almost 5 micrometer.

Therefore, test number 2.1 is not considered as a micropitted sample. Additional tests and an increase in the number of cycles does not change the surface or generate wear.

This result is consistent with previous reports on the effect of surface roughness on fatigue life of steel/steel contact. It has been reported that an increase in the surface roughness (i.e. a decrease in λ ratio) increases the rate of micropitting and surface fatigue [24].

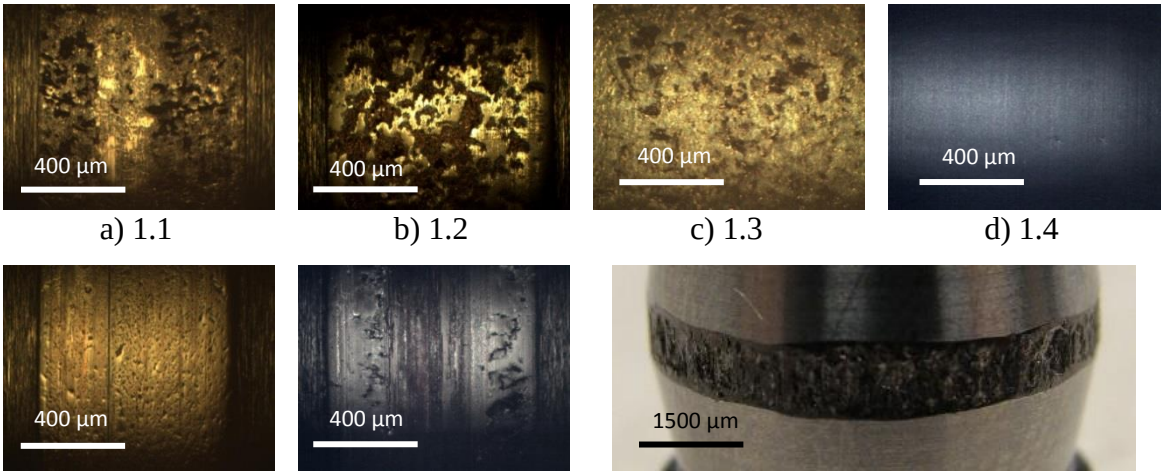

a) 1.1 b) 1.2 c) 1.3 d) 1.4

e) 2.1 f) 2.2 g) 2.4

Figure 4-1: Surface of rollers in the category of line contact. The upper row is the surface of rollers after running against WC/a-C:H coated discs and roughness of discs gradually increases. (1.1) the surface of roller after 3.5 million cycles running against WC/a-C:H coated discs with Ra: 0.1 µm. (1.2) the surface of roller after 3.5 million cycles running against WC/a-C:H coated discs with Ra: 0.2 µm. (1.3) The surface of roller after 3.5 million cycles running against WC/a-C:H coated discs with Ra: 0.3 µm. (1.4) the surface of roller after 7 million cycles running against WC/a-C:H coated discs with Ra: 0.4 µm. High abrasive rate does not let the roller to undergo micropitting. The bottom row is steel/steel contact and the roughness of discs gradually increases: (2.1) the surface of roller after 35 million cycles running against uncoated discs with Ra: 0.1 µm. Some dents can be seen on the surface, but no sign of fatigue and micropitting. (2.2) the surface of roller after 14 million cycles running against uncoated discs with Ra: 0.2 µm. (2.4) the surface of rollers after 3.5 million cycles running against uncoated discs with Ra: 0.4 µm.

Test 1.1: WC/a-C:H/Steel Contact
Disk Ra: 0.1 μm

a) 1st run | b) 2nd run | c) 3rd run

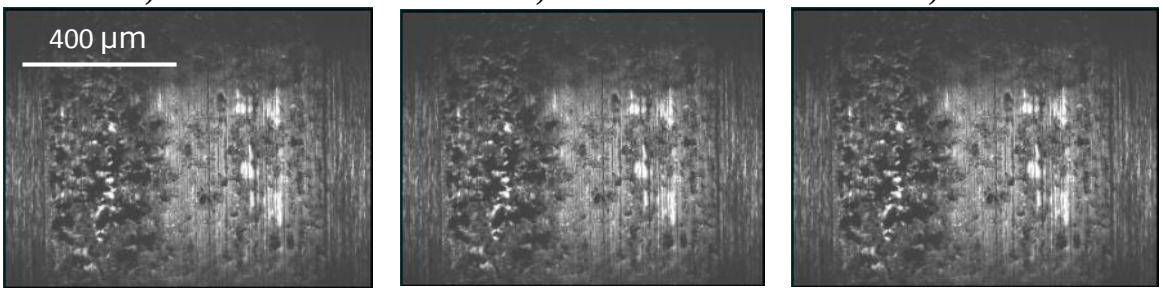

Pits depth: 4-4.5 μm | Pits depth: 4-4.5 μm | Pits depth: 4-4.5 μm

Test 1.2: WC/a-C:H/Steel Contact
Disc's Ra: 0.2 μm

d) 1st run | e) 2nd run | f) 3rd run

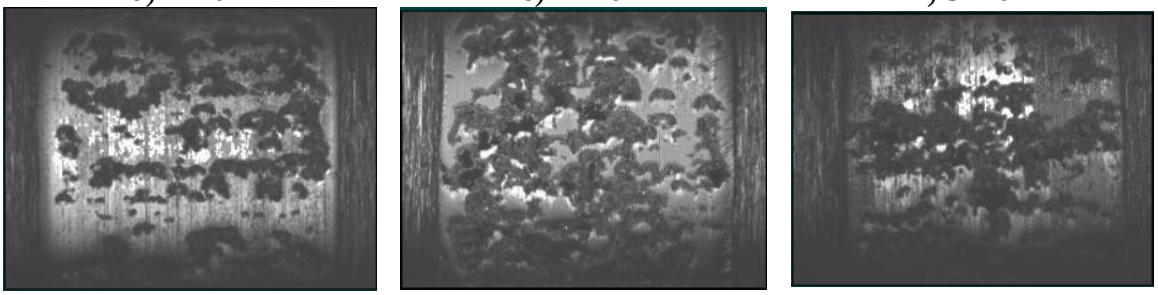

Pits depth: 4.7-5.6 μm | Pits depth: 4.5-5.5 μm | Pits depth: 3.4-4.0 μm

Figure 4-2: Progress of micropitting on tests 1.1 and 1.2 from Table 4-1. Photos are taken after each run (3.2 million cycles in 1.2-1.5 and 1.7 GPa Hertzian contact pressure). Magnification is 50x.

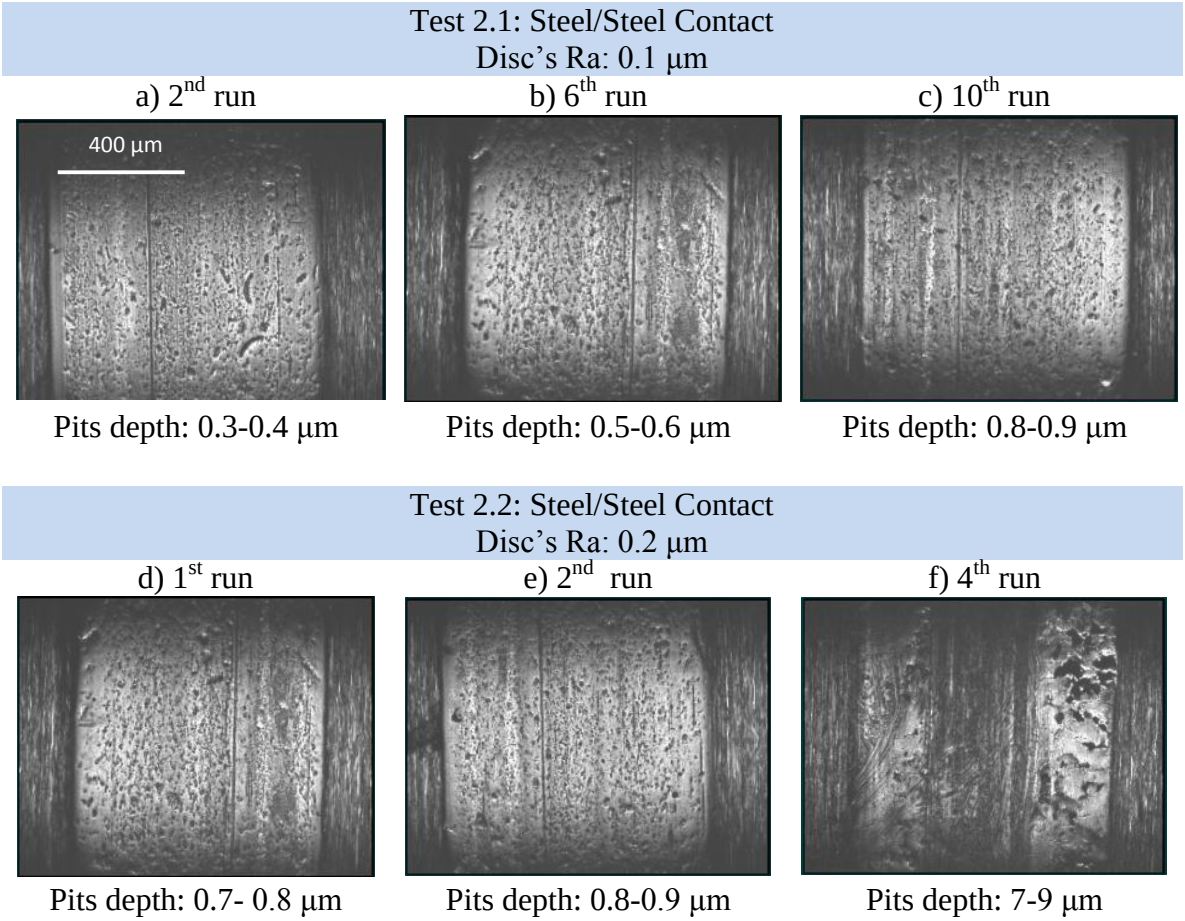

Figure 4-3: Progress of micropitting on tests 2.1 and 2.2 from Table 4-1. Photos are taken after each run (3.2 million cycles in 1.2-1.5 and 1.7 GPa Hertzian contact pressure). Magnification is 50x. No micropitting observed on the surface or roller of test 1.1 after 35 million cycles (11 runs).

λ ratio and micropitting failure are directly related in the steel/steel contact; as λ increases (or surface roughness decreases) micropitting decreases significantly. As is shown in Figure 4-4, when the roughness of discs is 0.1 µm (λ: 0.72) no micropitting is observed on the surface of roller after 10 runs (35 million cycles). However, discs with surface roughness of 0.4 µm (λ: 0.18) can cause severe macropitting on the roller after approximately 2.5 million cycles.

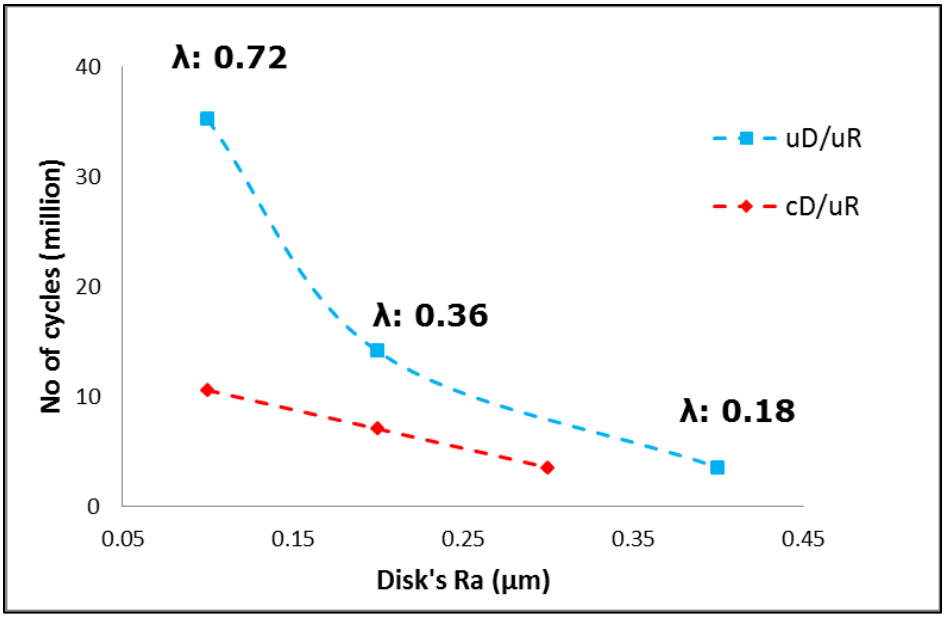

Figure 4-4: Number of contact cycles to micropiting failure on the surface of rollers running against WC/a-C:H coated and uncoated discs. Failure criterion is when that depth of pits reaches 5 µm. uD/uR points to uncoated discs/uncoated roller contact and cD/uR points to WC/a-C:H coated discs/uncoated roller contact.

Applying the coating to a disc considerably accelerates micropitting and wear on the rollers that is, the micropitting life of an uncoated roller running against the WC/a-C:H coated discs/uncoated roller contact is always less than the steel/steel contact (Figure 4-4), as long as the roughness of the discs is less than 0.3 µm. Coated discs rougher than 0.3 µm causes a high rate of abrasive wear on the roller, but there is no sign of micropitting since there is not enough time for the substrate to undergo fatigue process.

Measurement provided by PCS MPR is the vertical displacement of the loaded disc. Vertical displacement is representative of elastic deformation of the roller and discs as well as wear on both discs and roller. However, it mostly shows the wear on the roller. The roller is relatively softer than the discs and the number of stress cycles on a roller is almost 14.5 times greater than that of a disc. Wear rates are compared for test 1.4 and 2.4

of Table 4-1 in Figure 4-5. Results show that the uncoated roller does not show any sign of micropitting when it runs against rough coated discs (0.4 μm) as it shown in Figure 4-2d. Nevertheless, the steady state wear rate is higher on the uncoated roller when it runs against coated discs. Therefore, it can be concluded that the coating on the rough discs acts as a polishing source. The rate of abrasive wear on the roller is large enough that the roller surface does not undergo a fatigue process. Also, the surface finish of the roller is considerably smooth and isotropic.

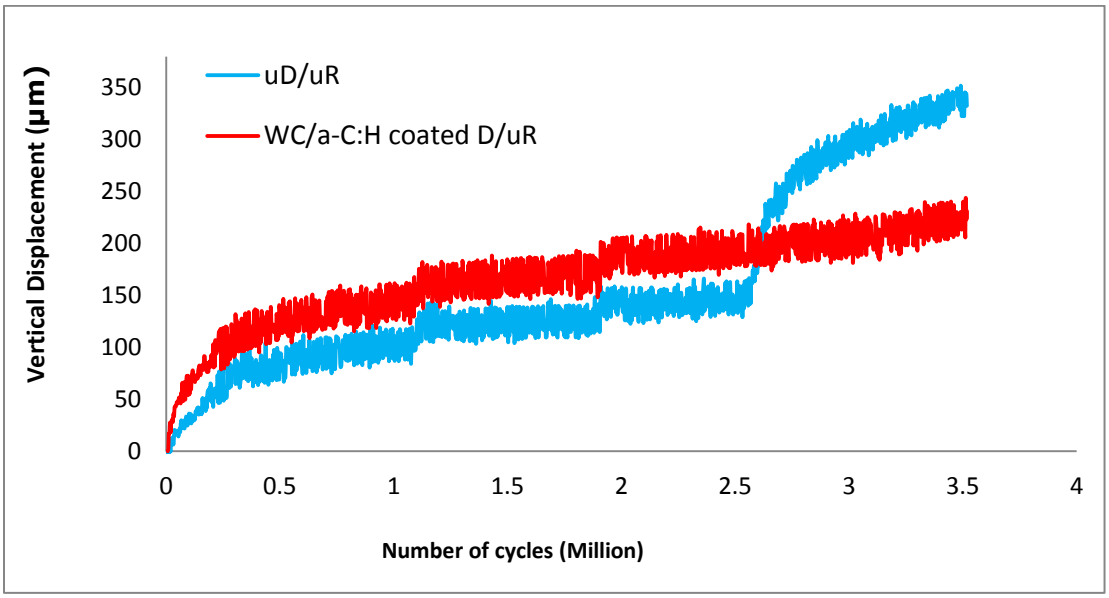

Figure 4-5: Vertical displacement vs. number of cycles in test 1.4 and 2.4 of Table 4-1. Higher rate of abrasive wear on the roller against WC/a-C:H coated discs. The pick on the steel/steel contact graph shows the transition point from micropitting to macropitting on the surface of roller.

Table 4-3: Average Coefficient of friction in three contact stresses and number of cycles when micropits depths reached 5 micrometer.

Test	Coating		Roughness	Friction coefficient			Micropitting at (million cycles)
	Discs	Roller	Disc	At 1.2 GPa	At 1.5 GPa	At 1.7 GPa	
1.1	Y	N	0.1	0.0493	0.0521	0.0536	10.5
1.2	Y	N	0.2	0.0614	0.0612	0.0613	7
1.3	Y	N	0.3	0.0632	0.0625	0.0703	3.5
1.4	Y	N	0.4	0.0658	0.0660	0.0707	---
2.1	N	N	0.1	0.0400	0.0446	0.0497	35
2.2	N	N	0.2	0.0480	0.0497	0.0532	14
2.4	N	N	0.4	0.0674	0.0714	0.0728	3.5

Another measurement provided by the PCS MPR is the coefficient of friction. The average coefficient of friction for tests in Table 4-1 is presented in Table 4-3. It observed that an increase in the contact stress slightly increases the coefficient of friction. Moreover, the coefficient of friction of the WC/a-C:H/ steel contact is almost as same as the steel/steel contact.

Table 4-4: Material properties and test parameters in micropitting experiments for elliptical contact category.

Test	Coating		H (HRC)		R_a (μm)		P_{max} (GPa)	u (m/s)	SRR %	T (˚C)	λ
	D	R	D	R	D	R					
3.1	Y	N	62	57	0.4	0.25	1.5	1	2	40	0.09
3.2	Y	N	62	57	0.2	0.25	1.5	1	2	40	0.18
3.3	Y	N	62	62	0.2	0.25	1.5	1	0	40	0.18
3.4	Y	N	62	62	0.2	0.07	1.5	1	0	40	0.47
4.1	N	N	62	57	0.4	0.25	1.5	1	2	40	0.09
4.2	N	N	62	57	0.2	0.25	1.5	1	2	40	0.18
4.3	N	N	62	57	0.2	0.25	1.5	1	0	40	0.18

4.2.2. WC/a-C:H coating on discs, Timken samples (Elliptical contact)

Timken-fabricated discs and rollers are made of through-hardened 52100 steel with hardness of 62 HRC. With their elliptical contact, rollers are run under a constant contact stress of 1.5 GPa instead of using three escalating contact stresses. Surfaces of rollers are studied after 0.1 or 0.3 or 0.5 million stress cycles based on the micropitting progressive rate or until surface fatigue cracks or pitting occurs. Parameters of maximum calculated contact stress, temperature, and calculated initial λ are presented in

Table 4-4.

In this experimental set, two mean roughness values are used as base lines for coated and uncoated discs; (R_a: 0.2 μm) representative of smooth surface which causes low wear rate on the roller and (R_a: 0.4 μm or Rq: 0.56 μm) representative of rough surface which causes a high abrasive wear rate on the roller. Beside roughness, the influence of slide to roll ratio (SRR) on micropitting is also studied.

The results of micropitting and friction coefficient for the category of elliptical contact is presented in Table 4-5 and the surfaces of rollers, running against coated and uncoated discs with different roughness values are presented in Figure 4-6.

.

Table 4-5: The surface failure (micropitting and/or wear) of roller and coefficient of friction (COF) of the category of elliptical contact

Test	Contact		R_a (μm)	SRR	Friction coefficient	Micropitting at (million cycles)	Statement
	D	R	D				
3.1	Y	N	0.4	2	0.0574	----	Abrasive wear
3.2	Y	N	0.2	2	0.0481	1	micropitting
3.3	Y	N	0.2	0	0.0114	2	micropitting
3.4	Y	N	0.2	0	0.0220	1.8	micropitting
4.1	N	N	0.4	2	0.0663	----	No micropitting
4.2	N	N	0.2	2	0.0608	----	No micropitting
4.3	N	N	0.2	0	0.0350	----	No micropitting

In this category, no sign of micropitting was observed on the roller in the steel/steel contact probably due to a lower contact stress (1.5 GPa) in comparison with the line contact (PCS rollers, 1.7 GPa). General results of the elliptical contact and the line contact are similar: A high rate of abrasive wear and no sign of micropitting are observed on the roller after running against rough coated discs (R_a: 0.4 μm) and early micropitting on the roller after running against smooth coated discs (R_a: 0.2 μm).

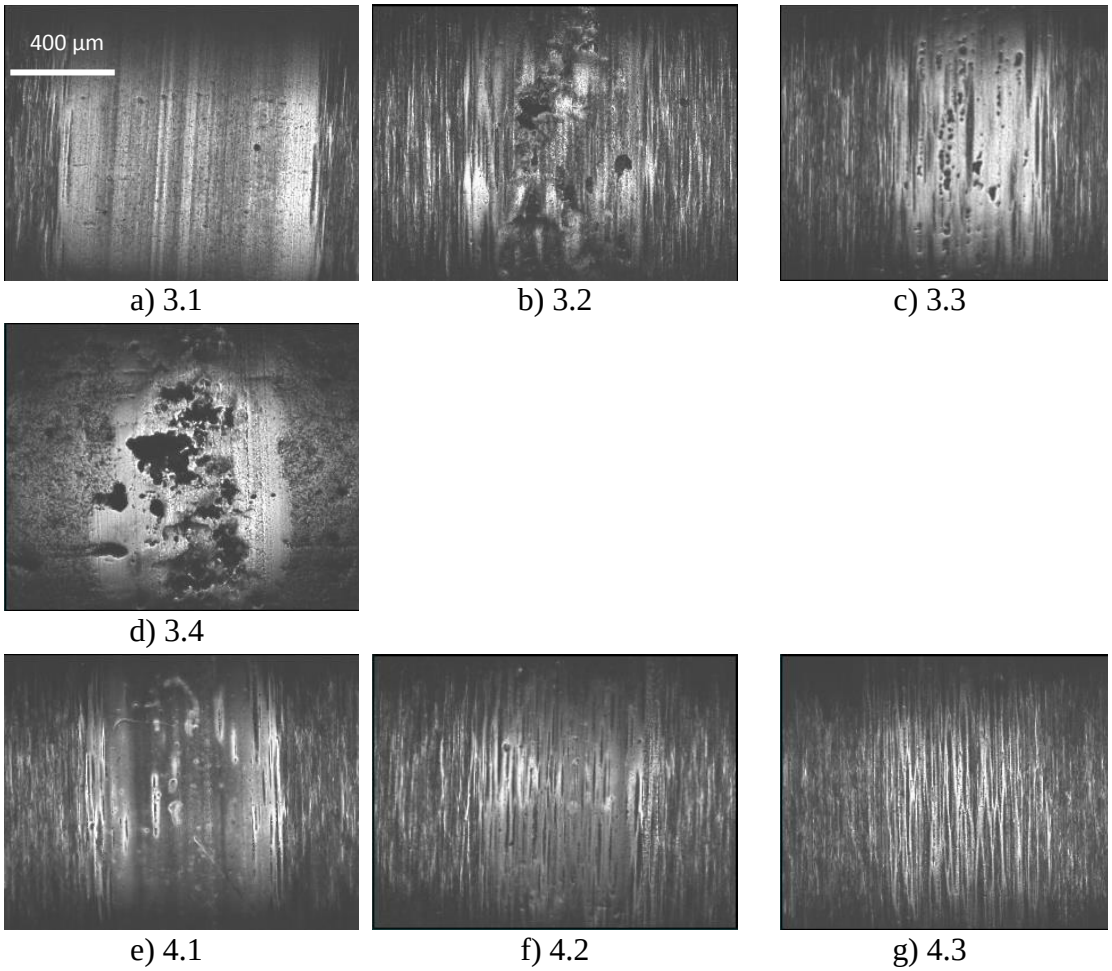

Figure 4-6: Surface of rollers in the category of elliptical contact. The upper row is the surface of rollers after running against WC/a-C:H coated discs (cD/uR contact) and roughness of discs gradually decreases. (3.1) The surface of roller after 2 million cycles running against WC/a-C:H coated discs with Ra: 0.4 µm and 2% SRR. (3.2) The surface of roller after 2 million cycles running against WC/a-C:H coated discs with Ra: 0.2 µm and 2% SRR. (3.3) The surface of roller with initial R_a of 0.25 µm after 4 million cycles running against WC/a-C:H coated discs with Ra: 0.2 µm and 0% SRR. (3.4) the surface of roller with initial R_a of 0.07 µm after 3.8 million cycles running against WC/a-C:H coated discs with Ra: 0.2 µm and 0% SRR. The bottom row is steel/steel contact and the roughness of discs gradually decreases: (4.1) the surface of roller after 2 million cycles running against uncoated discs with Ra: 0.4 µm and 2% SRR. (4.2) the surface of roller after 2 million cycles running against uncoated discs with Ra: 0.2 µm and 2% SRR. (4.3) the surface of roller after 4 million cycles running against uncoated discs with Ra: 0.2 µm and 0% SRR.

4.2.2.1. Effect of sliding

Figure 4-7 shows the surface of uncoated rollers after running against uncoated and coated discs. Figure 4-7a shows the surface of roller from the test 4.2 of

Table 4-4. No sign of micropitting can be seen on the surface of roller in steel/steel contact after 2 million cycles. The parallel test of WC/a-C:H coated discs/uncoated roller contact is test 3.2 of

Table 4-4. The surface of roller is shown in Figure 4-6c and 4-6d after 1 and 2 million cycles respectively. The surface of the roller undergoes fatigue and heavy micropitting after running against WC/a-C:H coated discs. Beside surface fatigue, the effect of shear is noticeable as well. For highlighting the effect of shear, Figure 4-7b is presented which shows the surface of roller of test 3.3 of Table 4-4. Figure 4-7b shows the roller after WC/a-C:H coated discs at 0.0% SRR. Comparing the morphology of the pits on the surface of rollers after running against WC/a-C:H coated discs with 0.0% SRR (Figure 4-7b) and 2.0% SRR (Figure 4-7c) indicates that shear stress considerably accelerates micropitting and surface fatigue. However, the roller suffers from micropitting even at 0.0% SRR. This indicates that although shear stress makes a huge contribution in acceleration of micropitting of steel/steel contacts, the nature of micropitting is fatigue (Oila el. al [5]) and correlated to cyclic stress on the elastically deformed volume under the contact area.

Figure 4-8a and b display the surfaces of uncoated rollers after 1.5 million cycles tested against WC/a-C:H-coated (Ra: 0.4 μm) discs (Test 3.1) and WC/a-C:H-coated (Ra: 0.2 μm) discs (Test 3.2), respectively. The WC/a-C:H coating on the rough discs

has not only removed the grind lines in the wear track on the roller, but has also removed a considerable amount of the profile of the roller, which can be observed more clearly in the profile trace shown in Figure 4-8c.

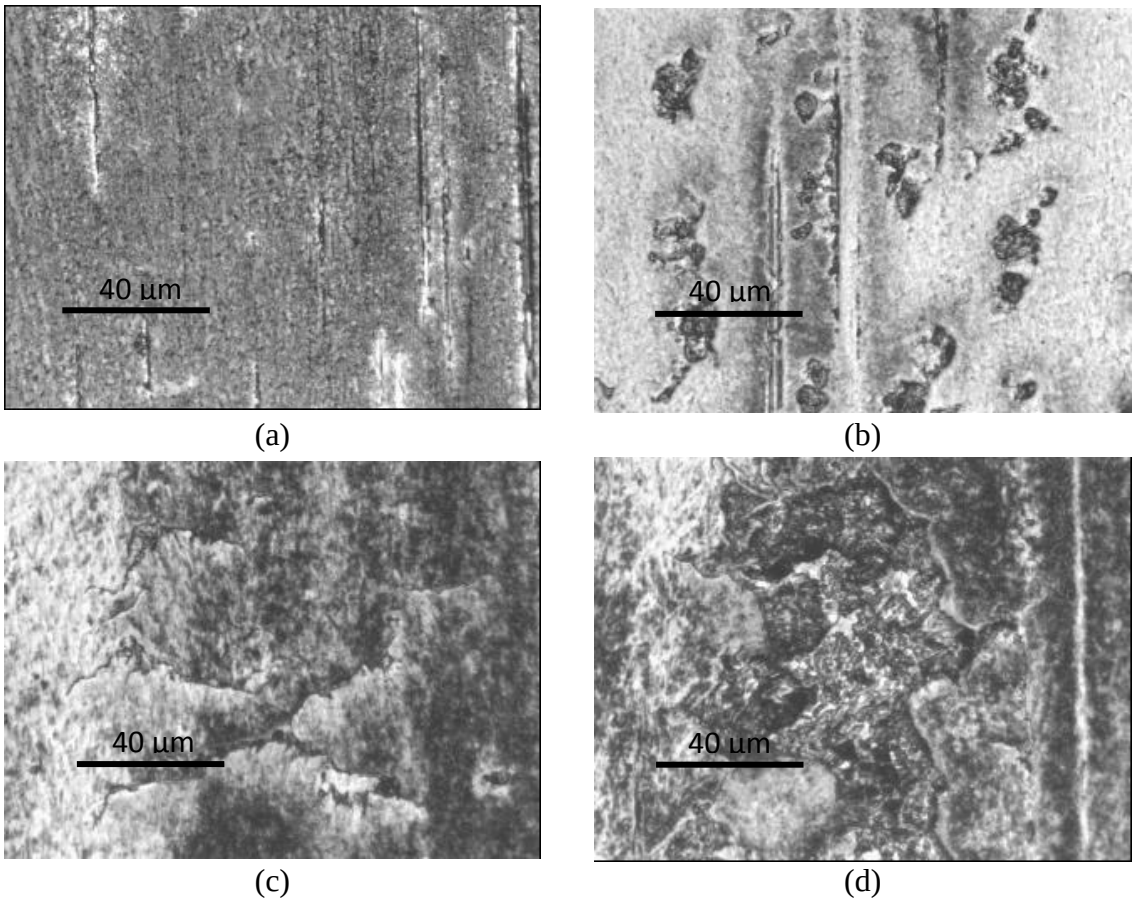

(a) (b)

(c) (d)

Figure 4-7: (a) The surface of roller after 2 million cycles running against uncoated discs (Steel/steel contact) with 2.0% SRR. No sign of surface fatigue or spallation. (b) The surface of roller after 2 million cycles running against WC/a-C:H coated discs (WC/a-C:H coated discs/uncoated roller contact) with 0.0% SRR. Pits have equiaxial morphology, (c) The surface of roller after 1 million cycles running against WC/a-C:H coated discs (WC/a-C:H coated discs/uncoated roller contact) with 2.0% SRR. (d) The surface of roller after 2 million cycles running against WC/a-C:H coated discs (WC/a-C:H coated discs/uncoated roller contact) with 2.0% SRR. The effect of shear on the morphology of pits is noticeable.

In comparison, the uncoated roller that was tested against the Ra = 0.2 µm discs in Test 3.2 exhibited micropitting after just 1.5 million stress cycles. In addition to the micropitting, mild polishing in the wear scar is observed without any measurable loss of roller profile, as shown in Figure 4-8d. The machined roller profile (Ry = 12 mm) is no longer present, and the disc-roller contact is much larger and less elliptical. As a result, the Hertzian contact stress of the test has been greatly reduced from its initial value of 1.5 GPa.

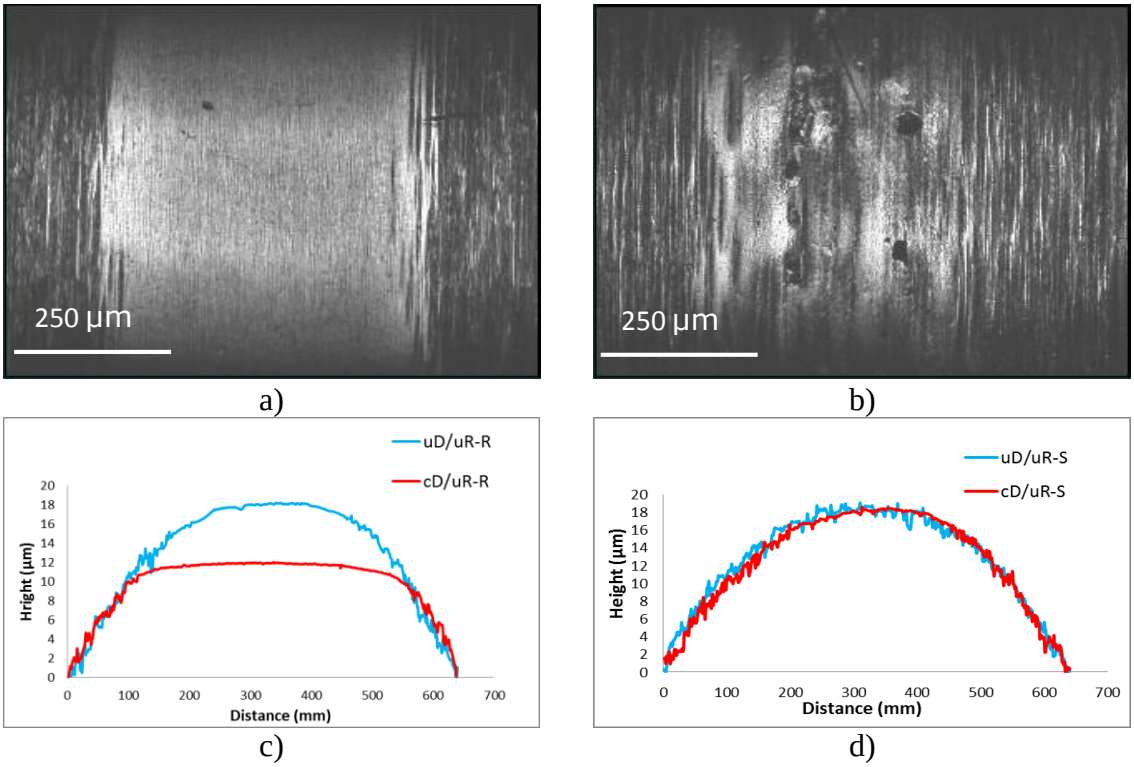

Figure 4-8: (a) Wear track of uncoated rollers after 1.5 million cycles tested against WC/a-C:H-coated rough discs (Ra = 0.4 µm) in Test 2.1. (b) Wear track of uncoated roller tested against WC/a-C:H-coated smooth discs (Ra = 0.2 µm) in Test 2.2. (c) Comparison of roller profiles (Ry) from Test 1.1 (Ra = 0.4 µm uncoated disc against Ra = 0.25 µm uncoated roller) and Test 2.1 (Ra = 0.4 µm coated disc against Ra = 0.25 µm uncoated roller). (d) Comparison of roller profiles (Ry) from Test 1.2 (Ra = 0.2 µm uncoated disc against Ra = 0.25 µm uncoated roller) and Test 2.2 (Ra = 0.2 µm coated disc against Ra = 0.25 µm uncoated roller).

When two surfaces come into contact under high Hertzian contact pressure, asperities of mating surfaces elasto-plastically deform so that the applied load can be supported. The plastic deformation of the WC/a-C:H asperities should be considerably less than those of the uncoated part, since the coating is harder than the through-hardened AISI 52100 steel. Therefore, if the roughness of the coated component is relatively large, the coating asperities will continue to remove material from the uncoated part until either the contact pressure minimizes due to a change in the profile of the uncoated part, or the lubricant film thickness completely separates the asperities of the mating surfaces. This effect is displayed graphically in Figure 4-9, where the contact stress has been calculated from Ry measurements of the roller surfaces periodically during testing involving Ra = 0.4 μm discs without and with the WC/a-C:H coating (Test 3.1 and 4.1 from Table 4-4). The contact stress between the coated discs and roller in Test 3.1 was decreased from 1.5 to nearly 1 GPa, the reduction through wear in the contact stress from the uncoated contacts in Test 4.1 was much less due to a much smaller change in the roller profile. Most of the wear on the rollers occurs during the early stages in Tests 4.1 and 3.1.

4.3. Coating on the roller, Timken roller (Elliptical contact)

Previously mentioned, the geometries of the Timken discs and roller create elliptical contact. Discs were heat-treated to a hardness of 62 HRC, while the roller hardness values were 53, 57, and 62 HRC. To achieve the hardness of 53 and 57 HRC, samples were kept in furnace at 310 and 330 ˚C for 3 hours in air atmosphere. To remove a thin oxide layer formed during heat treatment, the samples were super-finished using the Mikronite process. It is acknowledged that the 53 and 57 HRC roller hardnesses are lower than those typically specified for rolling element bearing steels. However, using

this wide range of roller hardness in the MPR tests allows for a clearer observation on the influence of hardness on this damage mode and confirmation of the efficacy of bearing steel hardness specifications.

Table 4-6 shows the test matrix of parallel tests for comparison between uncoated discs/WC/a-C:H coated roller contact and steel/steel contact.

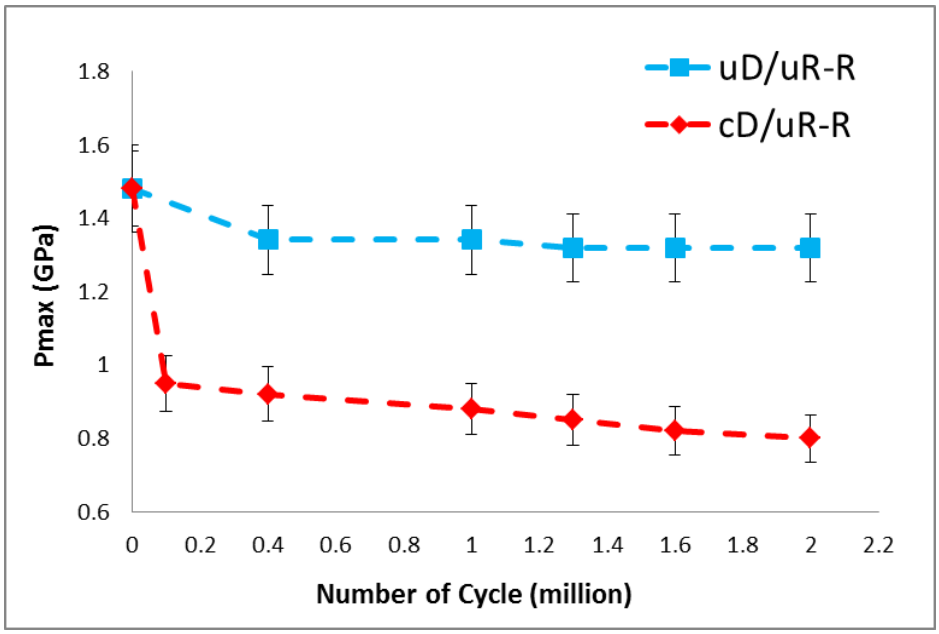

Figure 4-9: Calculated maximum Hertzian contact stress plotted versus cycles for Tests 1.1 (uncoated Ra = 0.4 μm discs versus uncoated Ra = 0.25 μm roller) and 2.1 (coated Ra = 0.4 μm discs versus uncoated Ra = 0.25 μm roller). Pmax is calculated from Ry measurements of the roller surfaces taken at different cycles during the tests. uD/uR-R points to uncoated disc/uncoated roller with rough disc and cD/uR-R points to coated disc/uncoated roller with rough disc.

Table 4-6: Micropitting test matrix. P represents the calculated contact stress, u is the entrainment velocity, SRR is the slide to roll ratio, and λ is the ratio of the calculated minimum lubricant film thickness to the composite surface roughness (Ra).

Test	Coating		HRC		Ra (μm)		P	u	SRR	T	λ
	D	R	D	R	D	R	(GPa)	(m/s)	(%)	(˚C)	
5.1	N	Y	62	62	0.4	0.2	2.25/ 2.55/	2	0	40	0.13/ 0.13/
5.2	N	Y	62	57	0.4	0.2	2 / 2.25/	2	0	40	0.13/ 0.13/
5.3	N	Y	62	57	0.4	0.2	2	2	10	40	0.14
5.4	N	Y	62	62	0.2	0.4	1.5	1	0	40	0.09
5.5	N	Y	62	57	0.4	0.2	1.7	2	2	75	0.07
5.6	N	Y	62	53	0.4	0.2	1.5	2	2	75	0.12
6.1	N	N	62	62	0.4	0.2	2.25	2	0	40	0.13
6.2	N	N	62	57	0.4	0.2	2	2	0	40	0.14
6.3	N	N	62	57	0.4	0.2	2	2	10	40	0.14
6.4	N	N	62	62	0.4	0.2	1.7	1	2	40	0.09
6.5	N	N	62	57	0.2	0.2	1.7	2	2	75	0.07
6.6	N	N	62	53	0.2	0.2	1.5	2	2	75	0.12
6.7	N	N	62	57	0.4	0.2	1.5	1	2	40	0.09

The MPR test results are gathered in Table 4-7. The number of stress cycles tested (N) and friction coefficients (μ), measured for each test are also shown. A better understanding of the difference between micropitting, surface fatigue and wear in Table 4-7, can be obtained from Figure 4-10. Figure 4-10a shows micropitting, Figure 4-10f shows surface fatigue and cracking, and Figure 4-10c shows wear.

Table 4-7: Results of the MPR Tests for steel/steel contact vs uncoated disc/ WC/a-C:H coated roller contact

Test	Coating		N	μ	Comments
	D	R	Millions		
5.1	N	Y	1/ 6/ 3.5	0.05	No wear or micropitting, delamination of coating at 2.5 GPa
5.2	N	Y	15/ 7/ 6	0.035	No wear or micropitting,
5.3	N	Y	0.5	0.085	No wear or micropitting, partially delamination of coating
5.4	N	Y	7	0.08	High rate of wear on discs
5.5	N	Y	30	0.05	No wear or micropitting
5.6	N	Y	10	0.05	No wear or micropitting
6.1	N	N	1	0.057	Micropitting
6.2	N	N	2	0.045	Micropitting
6.3	N	N	0.5	0.09	Wear + slightly cracking
6.4	N	N	10	0.07	Mild wear
6.5	N	N	8	0.06	Polishing
6.6	N	N	2	0.06	Surface fatigue+ Micropitting
6.7	N	N	30	0.05	Polishing

Several observations can be made from the Table 4-7. First, no micropitting but significant abrasive wear occurs whenever at least one of contacts was coated with a rough surface (Ra = 0.4 μm). Second, harder and rougher discs can cause micropitting damage on softer and smoother rollers. In Test 6.6, for example, the roller is 9 points softer than the discs on the HRC scale, while in Test 5.2, the WC/a-C:H coating (12–13 GPa hardness) makes the surfaces of the discs much harder than the 57 HRC roller. Third, higher sliding causes wear to be the dominant material removal mechanism and

not micropitting at this level of specific film thickness ($0.1 < \lambda < 0.2$). Finally, neither wear nor micropitting occurs when (a) low-roughness, uncoated, comparably hard disc and roller surface are in contact and the contact stress is relatively lower ($P_h \approx 1.5$ GPa), or (b) low-roughness coated rollers are tested in all tested contact stresses range.

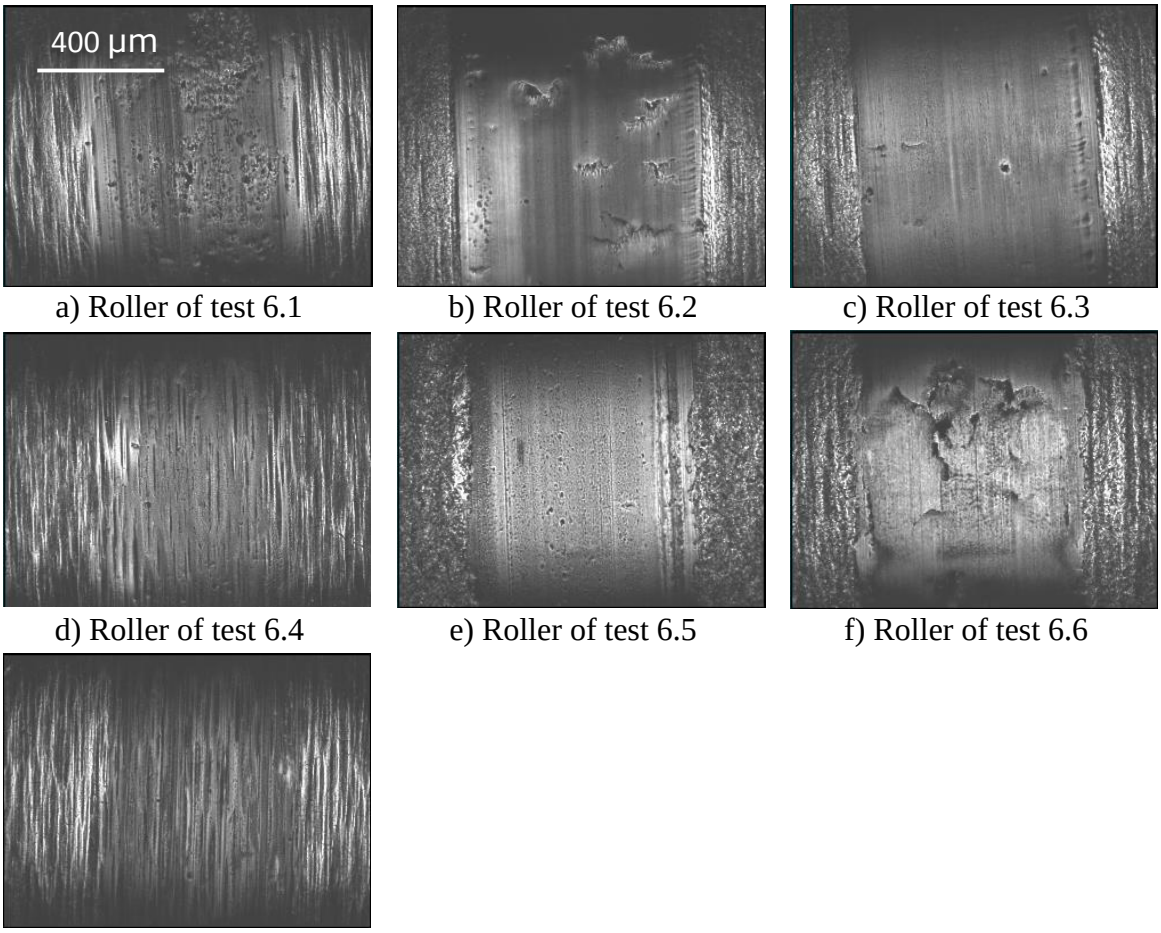

a) Roller of test 6.1 b) Roller of test 6.2 c) Roller of test 6.3

d) Roller of test 6.4 e) Roller of test 6.5 f) Roller of test 6.6

g) Roller of test 6.7

Figure 4-10: A comparison of the wear tracks on uncoated rollers after tests 6.1 to 6.7.

Friction coefficients of the contacts are dependent upon applied load, oil viscosity, additives, coating, contact area, surface roughness, texture, and other factors. Values for the friction coefficient are high when the coated part has a rough surface or when the slide to roll ratio is high. The uncoated smooth discs exhibit a slightly higher

friction coefficient when mated against uncoated rollers, as compared to discs that are in contact with WC/a-C:H coated rollers.

Figure 4-10 shows the surface of uncoated rollers that have run against uncoated discs. Comparing the result of tests; 6.2, 6.5 and 6.7 in Table 4-6 illustrates that there might be a threshold force for the initiation of micropitting. Results from tests 6.2 and 6.3 show that a higher slide to roll ratio generates a high rate of wear on the roller which may prevent micropitting damage from occurring. However, in these experiments, if micropitting is more pronounced in low slide to roll ratios, the reason could be that the initial film thickness parameter is low. More sliding means more asperity interaction and a higher rate of wear (Compare Figure 4-10b and 4-10c).

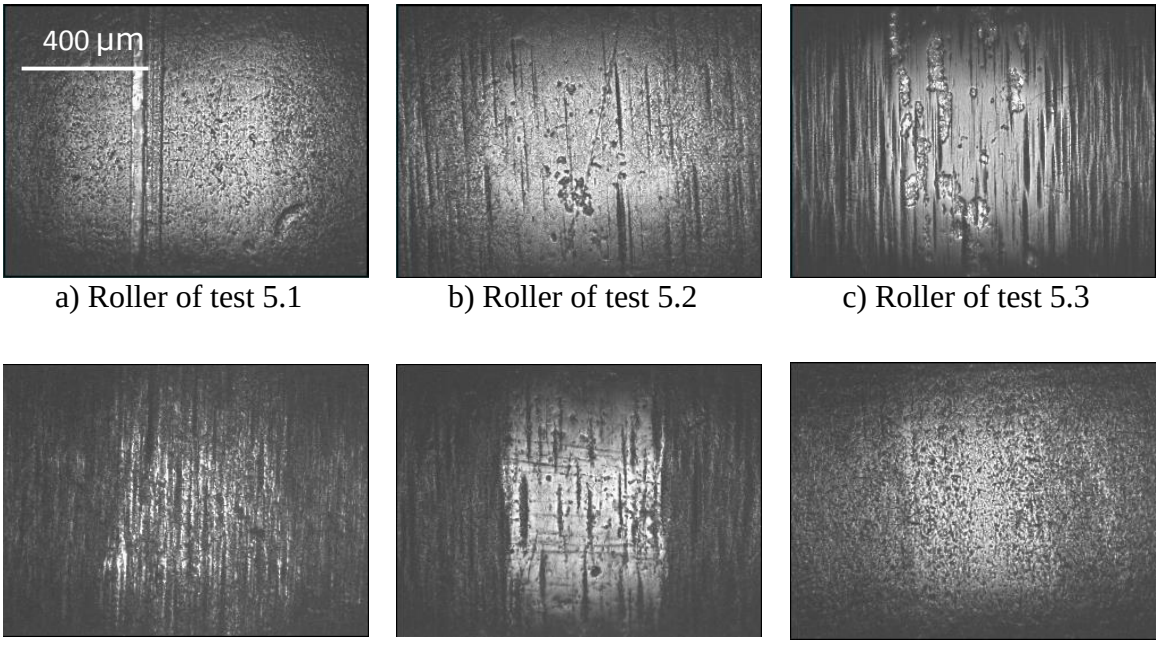

a) Roller of test 5.1 b) Roller of test 5.2 c) Roller of test 5.3

d) Roller of test 5.4 e) Roller of test 5.5 f) Roller of test 5.6

Figure 4-11: A comparison of the wear tracks on uncoated rollers after tests 3.1 to 3.6.

Figure 4-11 shows the surface of coated rollers that have run against uncoated discs. There is no micropitting or measurable wear on the surface of the coated rollers. Figure 4-11a shows the surface of a coated roller in test 5.1 after 10 million cycles running against 3 sets of discs in which the contact stress periodically increased. Delamination or fatigue failure of coating can be observed at a nominal contact stress level of 2.5 GPa.

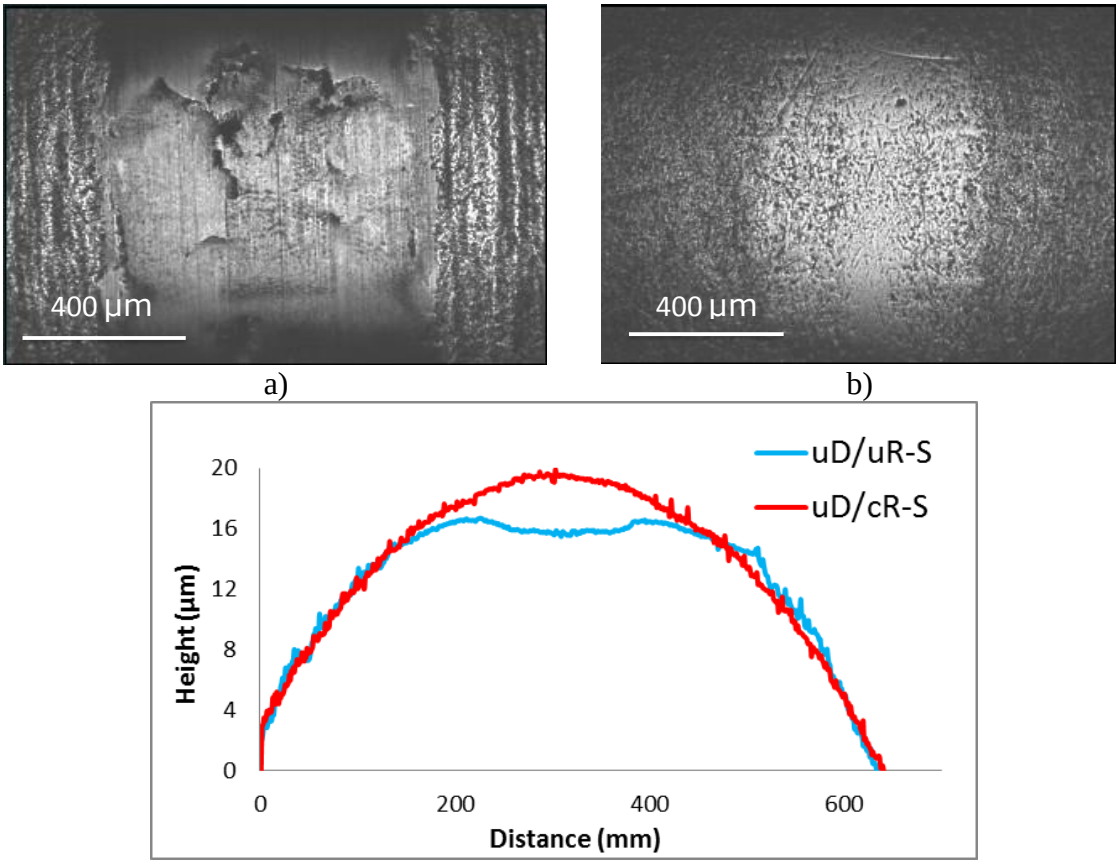

Figure 4-12: (a) Wear scar on roller from Test 1.3 (smooth, uncoated discs versus smooth, uncoated 53 HRc roller). (b) Wear scar on roller from Test 3.3 (smooth, uncoated discs versus smooth, WC/a-C:H-coated 53 HRc roller). (c) Comparison of roller profiles (Ry) from Test 1.3 (smooth, uncoated discs versus smooth, uncoated 53 HRc roller) and Test 3.3 (smooth, uncoated discs versus smooth, WC/a-C:H-coated 53 HRc roller).

Wear scars and Ry profiles on rollers from Tests 6.6 (smooth, uncoated discs vs. smooth, uncoated 53 HRC roller) and 5.6 (smooth, uncoated discs vs. smooth, WC/a-C:H-coated 53 HRC roller) are compared in Figure 4-12a–c. The wear scar of the uncoated roller in Figure 4-12a displays a large amount of surface fatigue and cracking after 2 million cycles, which is consistent with its lower hardness (53 HRC) and that of the contacting discs (62 HRC). The surface fatigue in the wear scar can be seen more clearly in Figure 4-12c, where the Ry profile has become negative. The wear scar of the coating on the roller is shown in Figure 4-12b. Only a slight burnishing has occurred, and the profile and surface roughness in the wear scar do not appear to be significantly altered from their initial states. Finally, in Figure 4-13a and b, wear scars are shown that were produced on the discs from a coated roller (Test 5.4 after 7 million stress cycles for roller) with larger roughness values (Ra = 0.4 μm), respectively.

The WC/a-C:H coating on the rough roller was aggressive to the discs, and removed a considerable amount of material although the number of stress cycles on a disc is almost 13.5 times smaller than the roller. By comparing Figure 4-13a and Figure 4-8c, it can concluded the coating on the rough surface causes a high rate of abrasive wear on the uncoated counterpart.

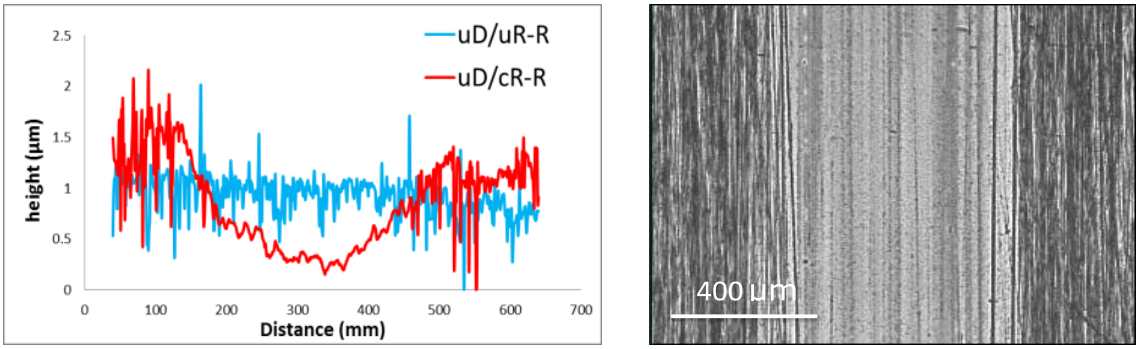

a) b)

Figure 4-13: (a) Comparison of the Ry profiles of an uncoated disc before and after the tests against rough coated roller (Test 3.3). (b) Wear scar on disc from Test 3.3 (uncoated Ra = 0.2 µm discs versus coated Ra = 0.4 µm rollers) after 7 million cycles of roller contact (each 14.5 contacts of roller is equal to one contact of a disc).

4.4. Discussion

Bearings with WC/a-C:H-coated rollers display excellent tribological and rolling contact fatigue performance [93, 101]. However, in these MPR tests, uncoated rollers suffered from either large amounts of abrasive wear or micropitting when tested against coated discs, while tests involving coated, low-roughness rollers and uncoated discs (Tests 5.x) showed no signs of micropitting.

In the MPR testing, asperities on the surface of the roller plastically deform under load, which can create work hardening and eventually lead to micropitting. The proclivity of steel to work harden depends upon the hardness [102]; that is, softer steel will work harden more rapidly than harder ones. Regarding surface fatigue and micropitting initiation, there might be a correlation between the yield strength and contact stress. By comparing the results of Tests 6.1, 6.2 and 6.4 to 6.6 from Table 4-7, it can be seen the contact stress that preserved surface fatigue and micropitting was relatively close to the yield strength of the roller. Specifically, the results of tests 1.5 and 1.6 show that the 57 HRC (6.2 GPa) roller does not experience micropitting for up

to 30 million cycles; whereas the 53 HRC (5.5 GPa) roller suffers from surface fatigue before 2 million cycles. If the yield strength (σ_y) is approximately one-third of hardness (H) [103], then the yield strengths of the H = 6.2 GPa and H = 5.5 GPa rollers are σ_y = 2.1 GPa and σ_y = 1.8 GPa, respectively. It is believed that although the calculated maximum contact stress of 1.5 GPa at a slide-roll ratio of 2% is sufficient to work harden the asperities of the σ_y = 1.8 GPa roller and develop micropitting in Test 1.3, that stress level with SRR = 2% is insufficient to do the same on the surface of the σ_y = 2.1 GPa roller in Test 1.2. Moreover, coating the discs with even considerably harder coating could potentially increase rate of pitting on the softer roller as it shown in test 2.2 from Table 4-7.

The objective of this study was to investigate the influence that a WC/a-C:H coating has on the micropitting damage of bearing steel, and compare those results with uncoated contacts. Comprehensive and detailed studies on micropitting damage of uncoated contacts can be found in Oila et al. [4, 5, 3] and Morales-Espejel et al. [24].

In steel/steel contact, wear is correlated with the roughness of discs; discs with smooth surface roughness (R_a< 0.2 μm) causes mild wear on the roller and as the roughness increases other type of wear such as micropitting (0.2 < R_a < 0.3) and macropitting (R_a > 0.3 μm) are manifesting due to work hardening of asperities. However, a decrease in applied load ceases the occurrence of micropitting on the roller. This implies that although the λ ratio and sliding are important components for accelerating micropitting, the ratio of applying load to the substrate hardness needs to pass a critical value to cause fatigue on the surface. In other words, micropitting failure is a combination of fatigue due to cyclic loading and shear due to sliding. However, it

seems micropitting is more load dependent than λ ratio as addressed by Chiu et al. as well [104].

In WC/a-C:H coated discs/uncoated roller contact, wear regimes are different than steel/steel contact; Early micropitting on the roller after running against coated discs with smooth surface roughness (R_a< 0.2 μm) and high rate of abrasive wear on the roller after running against rough coated discs (R_a > 0.3 μm).

High abrasive wear can be explained by the high hardness of WC/a-C:H which is almost twice that of 52100 Steel. However, interestingly smooth coated discs can cause early micropitting even in 0.0% SRR. Although there is an intrinsic sliding in any contact problems, the amount of intrinsic sliding is considerably small when the applied SRR is 0.0% especially in elliptical contact.

The amount of abrasive wear observed in these experiments greatly depended upon the surface roughness of the contact and which surface had the WC/a-C:H coating. For example, the uncoated roller in Test 6.1 and the uncoated discs in Test 5.4 exhibited a large amount of abrasive wear when they were run against the coating on rough (Ra = 0.4 μm) discs and roller surfaces, respectively. On the other hand, if the roughness of the coated part was lower (i.e., Ra = 0.2 μm), the abrasive wear of the counter face was greatly reduced, and polished or burnished counter faces were created. Regardless of whether the coating was on the disc or roller, the wear volume of the WC/a-C:H-coated part was negligible, and the WC/a-C:H-coated component maintained its initial roughness throughout the test.

When two surfaces come into contact under high Hertzian contact pressure,

asperities of mating surfaces elasto-plastically deform so that the applied load can be supported. The plastic deformation of the WC/a-C:H asperities should be considerably less than those of the uncoated part, since the coating is harder than the through-hardened AISI 52100 steel. Therefore, if the roughness of the coated component is relatively large, the coating asperities will continue to remove material from the uncoated part until either the contact pressure minimizes due to a change in the profile of the uncoated part, or the lubricant film thickness completely separates the asperities of the mating surfaces. This effect is displayed graphically in Figure 4-9, where the contact stress has been calculated from Ry measurements of the roller surfaces periodically during testing involving Ra = 0.4 μm discs without and with the WC/a-C:H coating. The contact stress between the coated discs and roller in Test 5.1 was decreased from 1.5 to nearly 1 GPa, the reduction through wear in the contact stress from the uncoated contacts in Test 6.7 was much less due to a much smaller change in the roller profile. Most of the wear on the rollers occurs during the early stages in Tests 6.7 and 5.1.

The wear volume of the uncoated counterpart was significantly reduced when the coating was applied to the smoother surfaces. Since the wear rate of the coated part is very low, the total wear volume arises primarily from the uncoated steel counter faces. The change in the separation between the centers of the discs and the rollers (i.e., the displacement) measured during Tests 6.6 (uncoated Ra = 0.2 μm discs vs. uncoated Ra = 0.2 μm 53 HRC rollers) and 5.6 (uncoated Ra = 0.2 μm discs vs. coated Ra = 0.2 μm 53 HRC rollers) is plotted versus stress cycles in Figure 4-14a after in first 2 million cycles of tests (Figure 4-14b shows the same results for the tests 6.5 and

5.5 from Table 4-6). The displacement curves, approximate measurements of wear depth, indicate that about 33% less material is removed from the uncoated steel specimens when they are in contact with the coating rather than the uncoated steel. Moreover, Test 5.6 (uncoated Ra = 0.2 μm discs vs. coated Ra = 0.25 μm 53 HRC rollers) achieved more than five times more cycles without micropitting or wear than Test 6.6 (uncoated Ra = 0.2 μm discs vs. uncoated Ra = 0.25 μm 53 HRC rollers), which exhibited micropitting before 2 million cycles. Also, the profile of the same rollers has been shown in Figure 4-12 after 2 million cycles for uncoated and 10 million for coated roller. Interestingly, the 53 HRC roller suffers from surface fatigue and cracking, however, 57 HRC roller suffers from wear and both of these material removal manifestation can be mitigated by coating.

Figure 4-15a–d illustrate the surface morphologies of discs after running against an uncoated roller (Test 6.2) and a WC/a-C:H-coated roller (Test 5.2) after about 2 million cycles. The grind lines are still evident on the surfaces of the disc from Test 6.2 (Figure 4-15a–b) and the disc from Test 5.2 (Figure 4-15c–d), although the coating on the roller in Test 5.2 appears to have visually altered the appearance of the grind lines on the disc. Ra, Rq, and Rsk values obtained from the 3D surface measurements in Figure 4-15 are gathered in Table 4-8. It appears that while Ra and Rq are almost the same for each disc, there is a significant change observed in Rsk. Rsk values became negative on both disc surfaces, and the disc that ran against the coated roller has an Rsk value approaching -1. Negative Rsk values have been reported to have a positive influence on the fatigue life of rolling element bearings [105] in low λ conditions. It has been postulated that the oil residing in the valleys can be squeezed out during elastic

deflections of the surface and bring lubricant to an otherwise starved contact region [106].

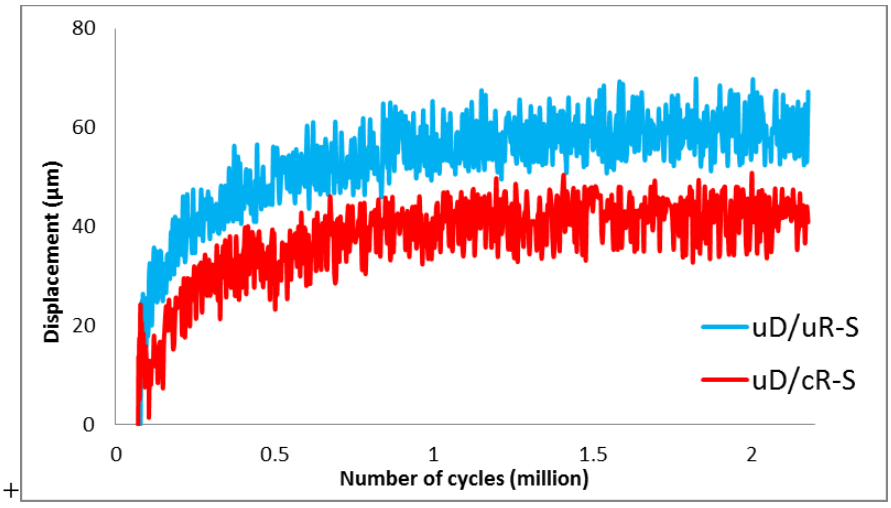

a)

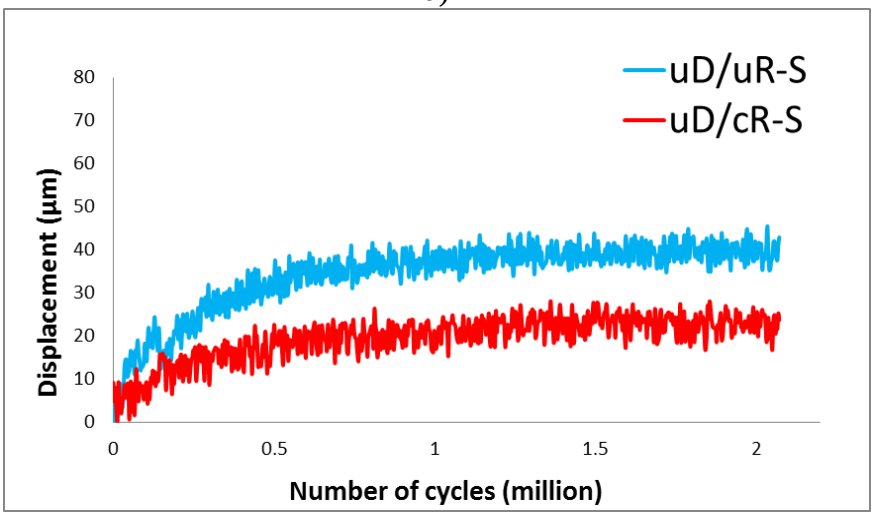

b)

Figure 4-14: The change in the separation between the centers of the discs and the rollers (i.e., displacement) measured during a) Tests 6.6 (uncoated Ra = 0.2 µm discs vs. uncoated Ra = 0.2 µm 53 HRC rollers) and 5.6 (uncoated Ra = 0.2 µm discs vs. coated Ra = 0.2 µm 53 HRC rollers) plotted versus stress cycles. b) The same results for the rollers with hardness of 57 HRC.

Table 4-8: Surface Roughness Parameters after 2 Million Cycles of Discs from Tests 6.2 and 5.2

Value	Initial Values	Test 6.2 Disc (steel-steel)	Test 5.2 Disc (steel-WC/a-C:H)
Rq (μm)	0.19 ± 0.01	0.13 ± 0.01	0.15 ± 0.01
Ra (μm)	0.13 ± 0.01	0.09 ± 0.01	0.09 ± 0.01
Rsk	0.03 ± 0.01	-0.30 ± 0.01	-0.88 ± 0.01

Coatings such as WC/a-C:H are not known to exhibit adhesive wear against steel at low temperatures [107]. On the other hand, steel-steel contacts can experience both abrasive and adhesive wear in low λ or dry conditions. Many studies have reported that the friction coefficient of diamond-like carbon-steel contacts is less than that of steel-steel contacts [53]. Results in this study indicate that the measured friction coefficients of the steel-WC/a-C:H contacts depend upon the roughness of the coated component.

Interestingly, comparison of the friction coefficients involving rough surfaces in Tests 5.1 and 6.1 indicates that the presence of the coating slightly increases the frictional losses. However, this could be attributed to the significant amount of abrasive wear occurring in these tests.

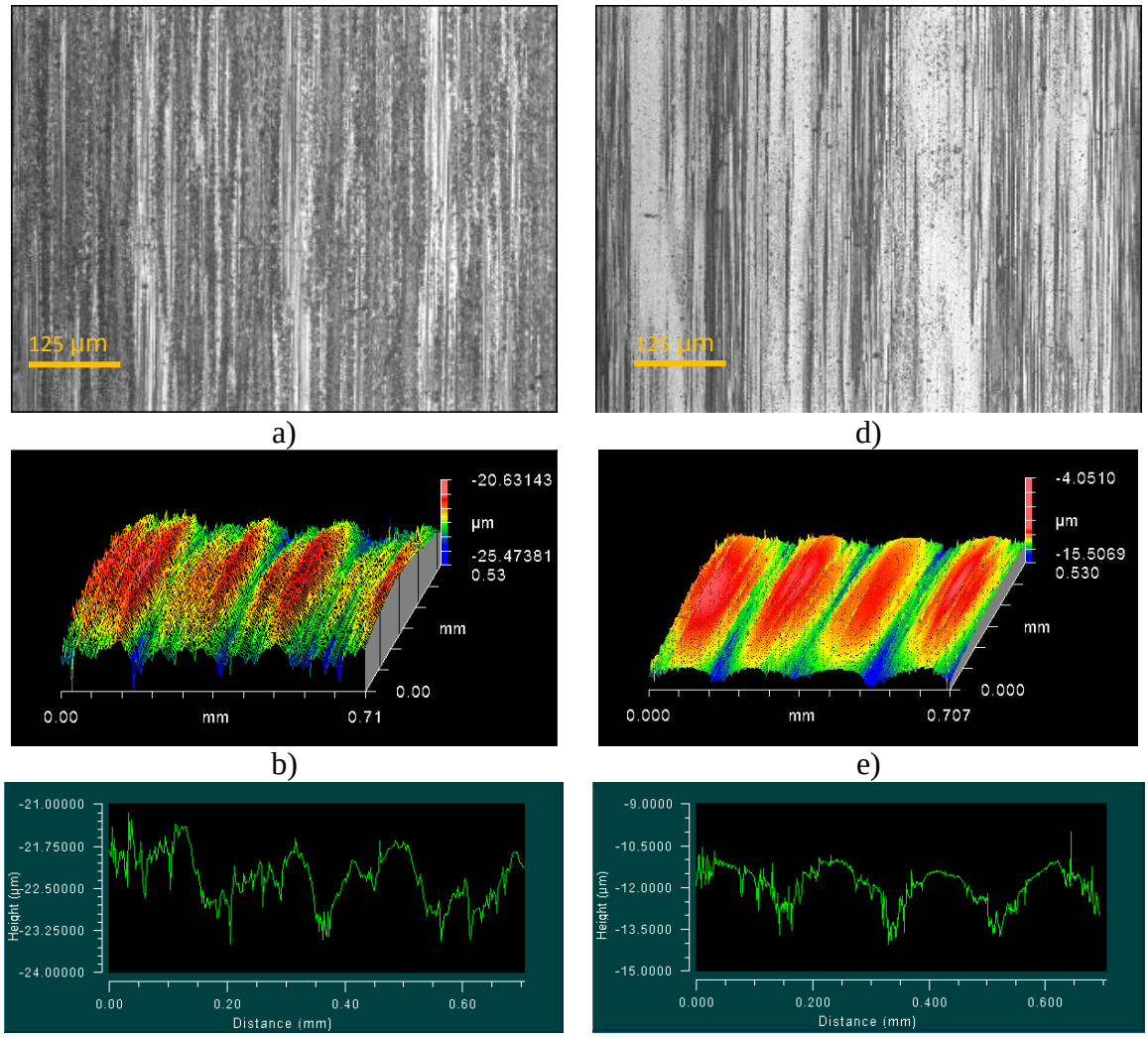

Figure 4-15: The surface of a disc after Test 6.2 and 5.2 from Table 4-6 after 2 million cycles. The surface of the uncoated disc after uncoated roller; a) Intensity map, b) Oblique plot and c) Surface profile. The surface of the same disc after WC/a-C:H coated smooth roller; d) Intensity map, e) Oblique plot and f) Surface profile.

Results of testing of the WC/a-C:H coating on smooth surfaces indicate that whereas the presence of the coating on the discs promotes the early onset of micropitting on the roller (before about 1 million cycles), when the coating is applied to the roller, no micropitting or high rate wear occurs on either the roller or the discs after 10 million and more cycles. The fact that the micropitting behavior of an uncoated part against a coated part, disc or roller, is not consistent gives rise to a couple of hypotheses. First, it could be due to the difference in stress cycles; each disc experiences 1 stress cycles compared to 13.5 stress cycles of the roller. Therefore, asperities on the roller may go under plastic deformation and/or fatigue before causing fatigue on the discs surfaces.

Second, the origin may also reside in the relative geometries of the roller and a disc. The roller radius is about five times smaller than a disc. A contact between a disc and a roller causes the same contact stress amplitude in both pieces. However, the size and depth of the maximum Von-Mises stress is larger and closer to the surface in the roller than in the disc. More experiments and study is required to clarify that if the relative geometry of the contact plays a significant role in micropitting and surface contact fatigue phenomena.

CHAPTER V

BLACK OXIDE VERSUS WC/a-C:H COATING

5.1. Overview

As previously mentioned, two tribological coatings have received considerable attention regarding micropitting resistance: Black oxide by and DLC. Studies show that the best performance is achieved when black oxide is applied to both mating surfaces and when DLC is applied to only one surface [53]. In this chapter, the micropitting behavior of through-hardened SAE 52100 rollers with and without a WC/a-C:H coating that are in contact with uncoated steel discs is examined. These results are compared to experiments conducted on rollers and discs with a black oxide surface treatment.

5.2. Design of experiment

As shown in Table 5-1, three specific tribological contacts are examined: 1) conventional steel on steel contact, 2) black oxide on black oxide contact (BO/BO), and 3) steel on WC/a-C:H coated rollers. Experiments are performed using three slides to roll ratios: -10%, 0% and +10%. Slide to roll ratio is calculated based on the relative rolling speeds of disc and roller.

$$\boldsymbol{u_e = \frac{u_d + u_r}{2}} \tag{5-1}$$

$$\boldsymbol{SRR} = \frac{\boldsymbol{u_d} - \boldsymbol{u_r}}{\boldsymbol{u_e}} \quad (5\text{-}2)$$

Positive sliding indicates that the disc is running faster than the roller and negative sliding implies that the roller is running faster the disc.

Sliding decreases the lubricant film thickness and may cause change in the wear regime. Moreover, lubricant film thickness and friction coefficient may behave differently in negative and positive sliding regimes [108].

5.3. Results and discussion

Images of roller surfaces taken after 0.5 million cycles are shown in Figure 5-1. Inspection of these images indicates that micropitting is the dominant wear mechanism for steel/steel and BO/BO contacts with SRR= 0.0%. No micropitting or surface fatigue is evident on the WC/a-C:H coated roller tested at SRR = 0%. At SRR = ±10%, abrasive wear appears to be the dominant wear mode for the steel/steel and Bo/Bo contacts and a few pits and cracks are observed on the roller surfaces involved in the steel/steel and BO/BO tests. Whereas the WC/a-C:H coating on the rollers tested at SRR = -10% exhibits small areas of distress, the coating appears to be intact on rollers tested at SRR = 0% and +10%.

Table 5-1: Material properties and test parameters in micropitting experiments

Test	Contact	SRR %
1.1	Steel on Steel	-10.0
1.2	Steel on Steel	0.0
1.3	Steel on Steel	+10.0
2.1	Black oxide on Black oxide	-10.0
2.2	Black oxide on Black oxide	0.0
2.3	Black oxide on Black oxide	+10.0
3.1	Steel on WC/a-C:H	-10.0
3.2	Steel on WC/a-C:H	0.0
3.3	Steel on WC/a-C:H	+10.0

The calculated initial λ ratio and other micropitting testing parameters such as oil temperature, entrainment velocity, and contact stress are gathered in Table 5-2.

Table 5-2 General conditions of micropitting test

Discs		Rollers		u	Load	P_{max}	T	λ
H (HRC)	Ra(μm)	H (HRC)	Ra (μm)	m/s	N	GPa	˚C	
62	0.4	57	0.2	2	170	2	40	0.35

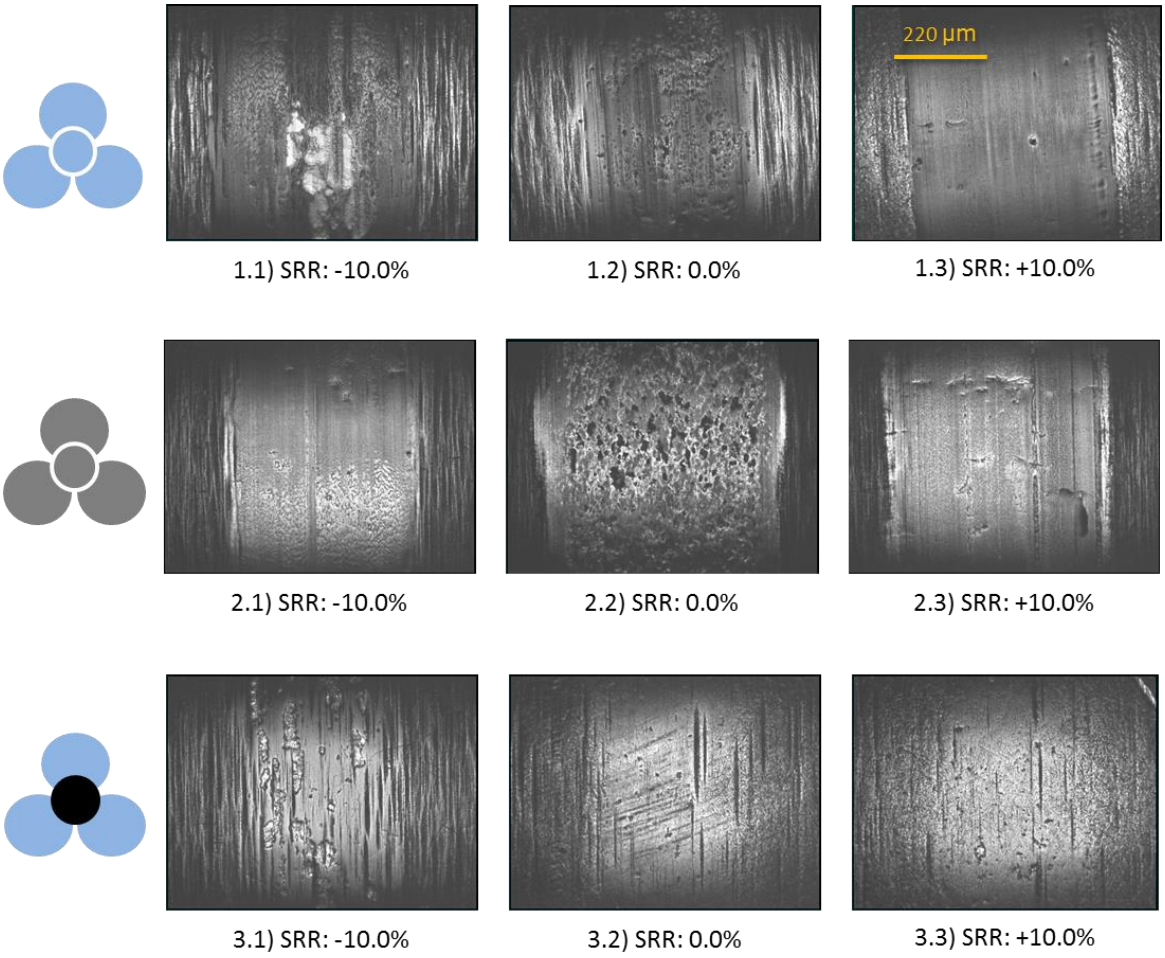

Figure 5-1: Surface of rollers after 0.5 million cycles running at P_{max} = 2 GPa in three groups of steel/steel contact (1.1 to 1.3), Black oxide/black oxide contact (2.1 to 2.3) and Steel/WC/a-C:H coated roller contact (3.1 to 3.3) three slide to rolling ratios. This figure is labelled based on test numbers in Table 5-1.

Roller profiles measured before and after testing are shown in Figure 5-2. While no change in profile of the WC/a-C:H coated rollers is observed for all three values of SRR, the profiles of rollers tested in the BO/BO and steel/steel contact are noticeably altered. Wear is responsible for the altered profiles, and the largest amount of wear occurring in any test is on the roller tested in the BO/BO contact at SRR = 0%. The wear occurring on this roller is similar to that observed on the downwind row of spherical

roller bearings used to support the main shafts of wind turbines, where micropitting removes enough material to seriously alter the profile of the raceway and generate extreme levels of contact stress that generate low cycle raceway spalls [1].

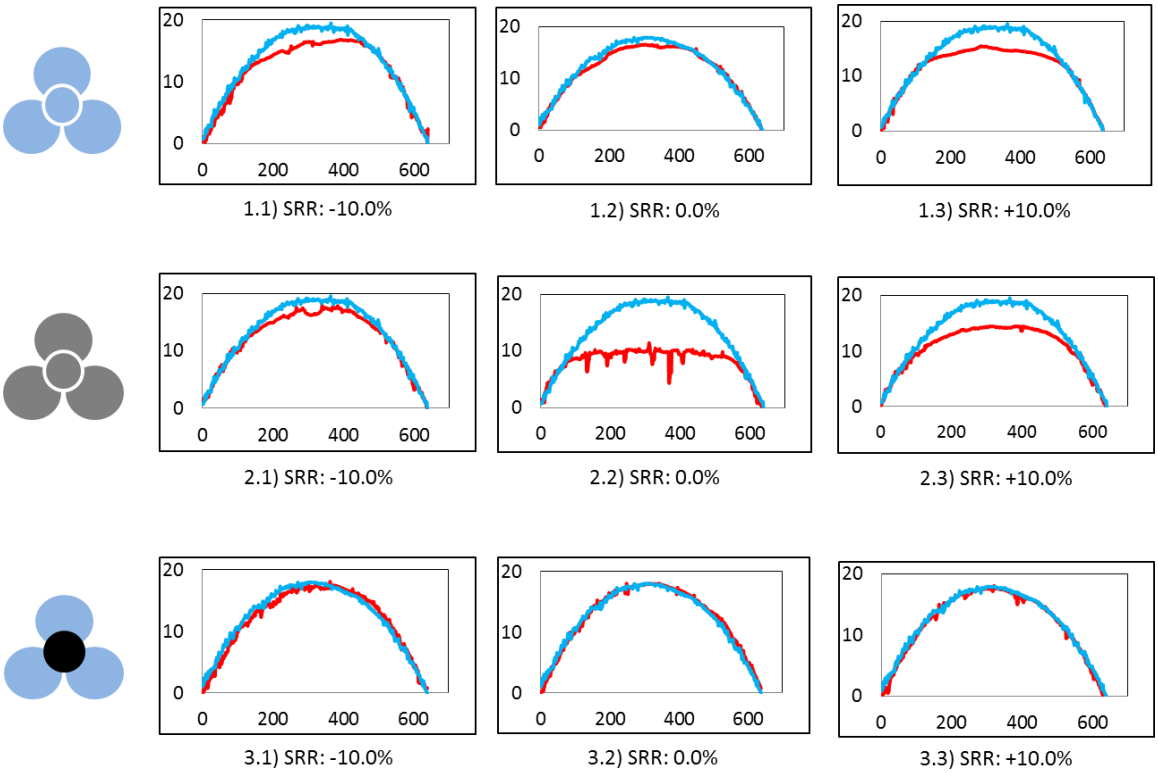

Figure 5-2: 2D profile of rollers before and after micropiting test generated from 3D Profilometer data Surface for three groups of steel/steel contact (1.1 to 1.3), Black oxide/black oxide contact (2.1 to 2.3) and Steel/WC/a-C:H coated roller contact (3.1 to 3.3) in three slide to rolling ratios. Unit of vertical axis is micron and horizontal axis is millimeter. No wear observed on the WC/a-C:H coated rollers. This figure is labelled based on test numbers in Table 5-1.

Wear and rate of wear is measured in situ in the micropitting rig through a measurement of the vertical displacement between the axis of the upper disc and the roller. Whereas the vertical displacement associated with changes in the applied load is due to the elastic deformation of the roller and discs, abrasive wear of discs and roller is

responsible for the vertical displacement occurring with stress cycles at a constant load. Since the applied load is constant in these experiments, the displacements shown in Figure 5-3 represent the combined wear of the discs and roller. The rate of wear (slope of the displacement) is much larger for the BO/BO contact at SRR=0% (5-3.2.2) than with any other test. Displacement slopes measured in Figure 5-3 are plotted for each materials pair in Figure 5-4. It is observed that the steel/steel and steel/WC/a-C:H contacts display a similar trend regarding the effect of sliding on increasing the wear rate in a boundary or mixed lubrication regime; a higher rate of wear for finite SRR and a lower rate of wear for SRR = 0%. The BO/BO contact exhibits exactly the opposite behavior. Additional information is gleaned from a comparison of the wear rates shown in Figure 5-4 with the measured profiles in Figure 5-2. Specifically, whereas wear of the steel/steel contact is shared between the roller and discs for all three SRR settings, all of the wear of the steel/WC/a-C:H contact occurs on the discs, if there is any. A lower rate of wear for black oxide in |SRR| >0.0% probably can be attributed to the fact that black oxide has a better lubricity. Therefore, black oxide can reduce shear stress between asperities and show lower rate of wear. On the other hand, black oxide has a porous microstructure and its hardness is lower than steel and much lower than WC/a-C:H. Therefore, at |SRR|= 0.0% sliding when the dominant wear mechanism is surface fatigue, black oxide is inferior to WC/a-C:H. Additionally, in the BO/BO tests performed at SRR = ±10%, wear is also shared between the rollers and the discs. It is important to note that these results may only extend to the testing conditions of current study. The black oxide performance might be better at higher values of λ and/or lower levels of contact stress where the

primary drivers for micropitting are sliding and entrainment velocity rather than contact stress.

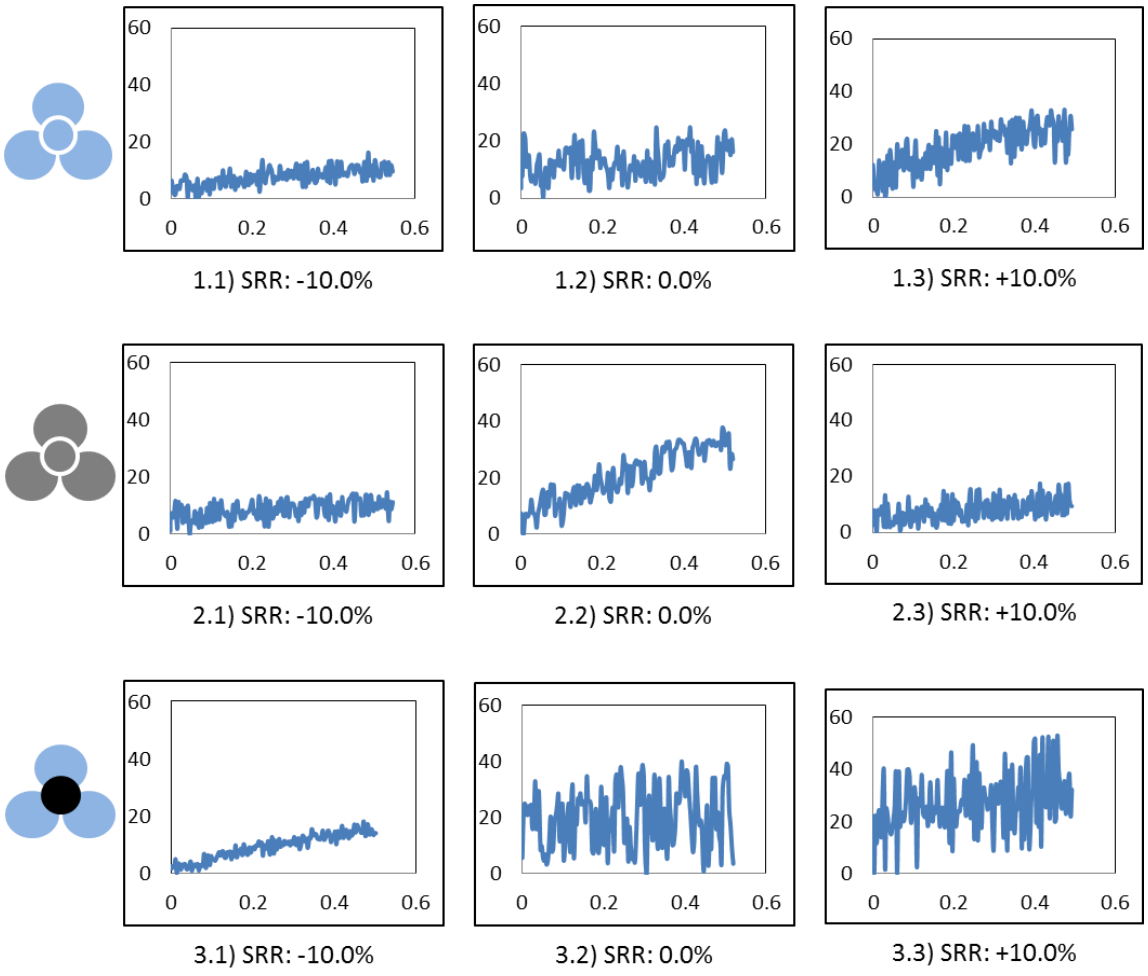

Figure 5-3: Vertical displacement (representing the total wear of roller and discs) for three groups of steel/steel contact (1.1 to 1.3), Black oxide/black oxide contact (2.1 to 2.3) and Steel/WC/a-C:H coated roller contact (3.1 to 3.3) in three slide to rolling ratios. Vertical axis is displacement (μm) micron and horizontal axis is number of cycles (million). No wear is observed on the WC/a-C:H coated rollers. This figure is labelled based on test numbers in Table 5-1.

Friction coefficients measured during the testing are displayed in Figure 5-5. The friction coefficients appear to depend more strongly on SRR than on the surface composition. All of the friction coefficients appear to be constant throughout the testing

except for the BO/BO test performed at SRR = 0%. The gradual decrease in friction seen in Figure 5-5.2.2 may be associated with the high rate of disc and roller wear and change in roller profile occurring in this test.

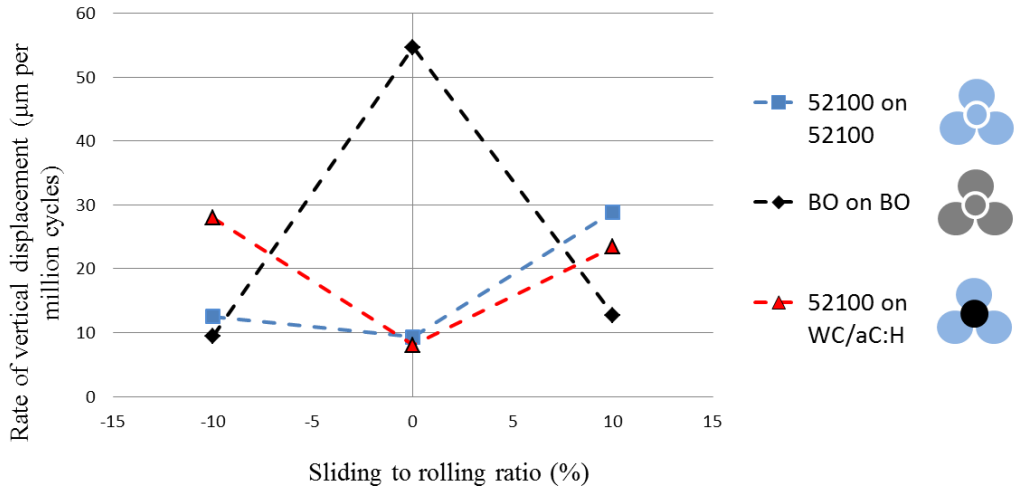

Figure 5-4: Rate of vertical displacement for three groups of steel/steel contact (1.1 to 1.3), Black oxide/black oxide contact (2.1 to 2.3) and Steel/WC/a-C:H coated roller contact (3.1 to 3.3) in three slide to rolling ratios. Wear rate is considerably high for BO/BO contact in 0.0% sliding and it has lowest rate of wear in ±10.0% sliding due to better lubricity of black coating.

Based upon the results of the previous section, black oxide does not appear to be an attractive candidate technology for rolling element bearings that must operate in application conditions where the contact stress is large and the λ value is small. On the other hand, the WC/a-C:H coated roller did not show any evidence of wear or micropitting for SRR = 0% and SRR = +10%, although some areas of the coating appeared to delaminate in the SRR = -10% test.

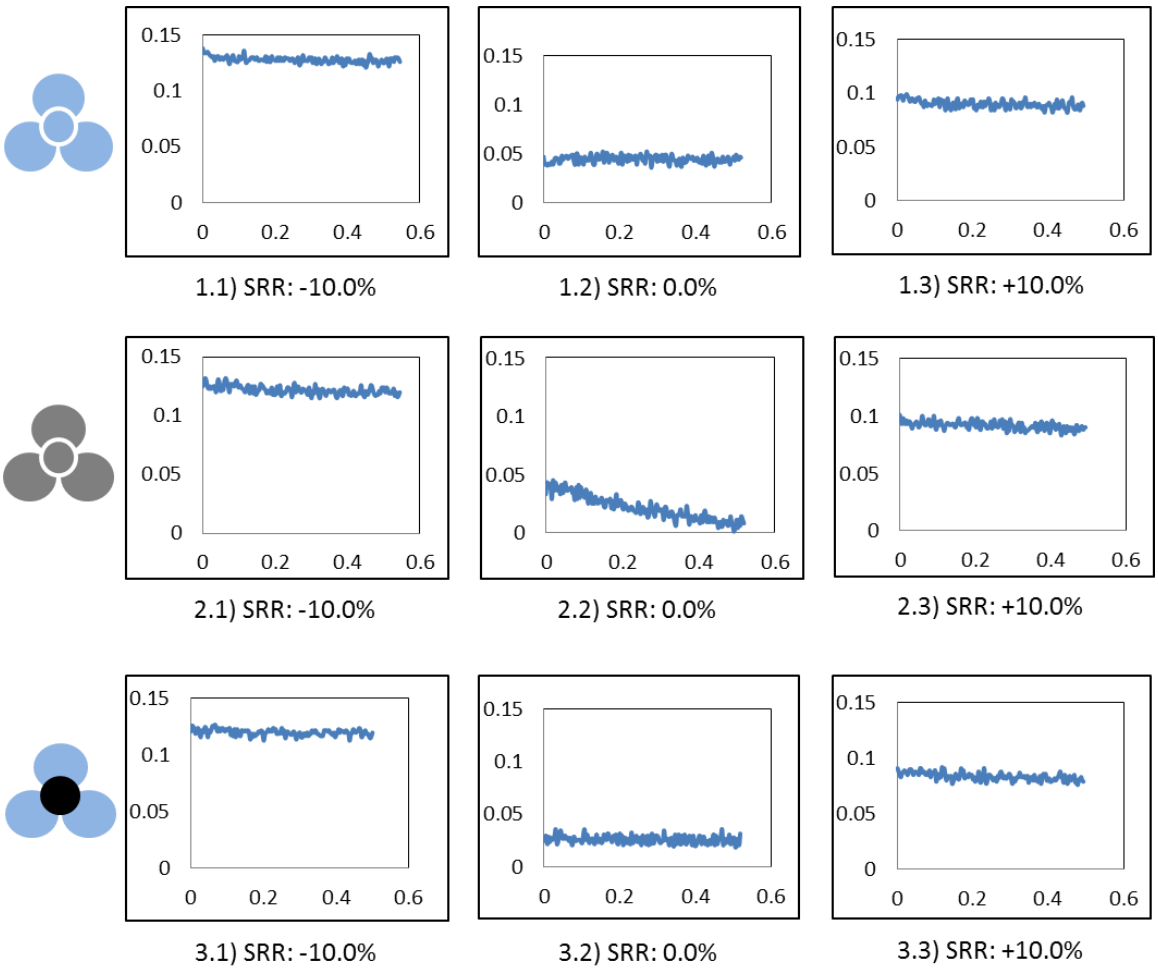

Figure 5-5: Coefficient of friction displacement for three groups of steel/steel contact (1.1 to 1.3), Black oxide/black oxide contact (2.1 to 2.3) and Steel/WC/a-C:H coated roller contact (3.1 to 3.3) in three slide to rolling ratios. Friction coefficient is gradually decreasing in BO/BO contact in 0.0% sliding because of change in shape and conformity of contact. This figure is labelled based on test numbers in Table 5-1. Vertical axis is friction coefficient and horizontal axis is number of cycles (million).

5.4. Conclusions

The goal of this chapter is to determine if a black oxide surface treatment and a WC/a-C:H coating can mitigate the type of micropitting wear observed on main shaft spherical roller bearings of modular wind turbines. Three materials pairs were examined in a micropitting test rig: untreated steel on steel, black oxide on black oxide and steel on

a WC/a-C:H coating in three SRR regimes of -10%, 0% and 10%. Tests were conducted at high contact stresses and low λ, similar to conditions experienced by the downwind row of a spherical roller bearings used to support the main shafts of 1.5 MW modular wind turbines. Based upon the results of this study, it is concluded that whereas the WC/a-C:H coating is very effective at mitigating micropitting, black oxide surface treatments are not. However, the black oxide surface treatment appears to provide an enhancement in wear resistance over a steel/steel contact when significant sliding is present since the black oxide treated surfaces rapidly polish and attain a low roughness interface.

CHAPTER VI

DELAMINATION OF WC/a-C:H COATING

6.1. Overview

In this chapter, the delamination of the WC/a-C:H coating is studied. In general, three types of coating delamination are observed for contact stresses less than 2 GPa: flaking (Figure 6-1), delamination due to edge stress (Figure 6-2) and random delamination due to high contact stress between asperities (Figure 6-4b or 6-4e). Six types of coating delamination have been identified by Yonekura et al. [109]. These six types of delamination are referred to random delamination in this study. Table 6-1 shows the results of coating delamination on coated discs or rollers.

6.2. Delamination of WC/a-C:H coating on discs

Flaking is the sub-micron delamination of a coating where sharp asperities fracture due to high contact pressure. Therefore, flaking occurs on samples with high surface roughness (Ra: 0.4 μm) on the roller or discs. Under these conditions, flaking of the coating provides carbon that goes into solution in the test oil as shown in Figure 6-1b. Flaking ceased as soon as the surface roughness (Ra) decreased to 0.2 μm. Fourier transform infrared spectroscopy (FTIR) examination did not show any oxidation of the oil. Size of flaked particles varies between 5 to 50 μm.

Delamination due to edge stress happens only when the coating is applied to discs (Figure 6-2). Delamination due to edge stress is rooted in relative geometry of the contacting specimens and usually occurs on the larger diameter component of contact unless contact curvatures have been designed with close consideration to avoid edge stress.

For MPR samples, the disc is cylindrical; and the roller is barrel shaped and significantly smaller in diameter than the disc. The Ry[1] is 0 for the disc and 12 for the roller which leads to more uniform distribution of compression stress in the Y direction of the roller under Hertzian contact stress. In addition, hydrostatic stress develops more rapidly in the roller versus the disc. Hydrostatic pressure causes slightly increase in the young modulus [110] yet it is negligible. The advantage of larger hydrostatic pressure in the roller causes slightly recession in the disc. Recession of the disc causes a sharp change in the stress profile on the surface of disc -perpendicular to direction of rolling- at the two edges/ends of the contact.

Although, the coating has a low Young's modulus, since it has a layered microstructure and consists of nano-size grains, it behaves relatively like a brittle material and can fracture and delaminate under tensile stress. This type of delamination is an early stage delamination that occurs at a medium range of contact stress (P_{max} > 1.5 GPa) and a low number of cycles (0.1 million cycles).

[1] Assume that X is rolling direction and Y is the perpendicular direction to the X in the rolling surface.

Table 6-1: General results of coating delamination on coated discs or rollers

Test	Coating		Ra		P	Cycles	Finishing of	Comments
	D	R	D	R	(GPa)	million	the coated part	
1.1	Y	N	0.4	0.2	1.7	3.5	Longitudinal	Flaking
1.2	Y	N	0.4	0.2	1.5	2	Longitudinal	Flaking
1.3	Y	N	0.2	0.2	1.7	3.5	Longitudinal	Edge stress delamination
1.4	Y	N	0.2	0.2	1.5	2	Longitudinal	Edge stress delamination
1.5	Y	N	0.2	0.2	1.5	2	Longitudinal	Edge stress delamination
1.6	Y	N	0.2	0.07	1.5	1.5	Longitudinal	Edge stress delamination
2.1	N	Y	0.2	0.4	1.5	7	Longitudinal	Flaking
2.2	N	Y	0.2	0.2	1.5	30	Longitudinal	No delamination
2.3	N	Y	0.2	0.2	1.5	15	Longitudinal	No delamination
2.4	N	Y	0.4	0.2	1.5	12	Isotropic	No delamination
2.5	N	Y	0.4	0.2	1.7	8.5	Isotropic	No delamination
2.6	N	Y	0.4	0.2	2	5	Longitudinal	No delamination
2.7	N	Y	0.4	0.2	2 / 2.25/ 2.55	15/5/4	Longitudinal	Partial delamination delamination/coating failure
2.8	N	Y	0.4	0.2	2 / 2.25/ 2.42	2/6/6	Longitudinal	Partial delamination delamination/coating failure
2.9	N	Y	0.4	0.2	2.25/ 2.55/ 3	1/6/4	Isotropic	Partial delamination delamination/coating failure
2.10	N	Y	0.2	0.2	2/ 2.25	18/ 16	Longitudinal	Local delamination

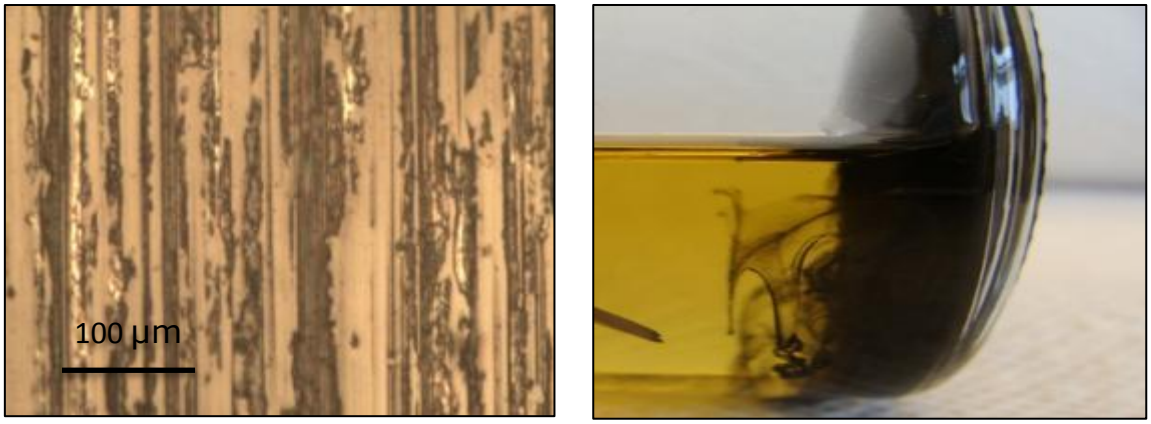

a) b)

Figure 6-1: a) Flaking of coating on a coated disc with surface roughness of 0.4 µm. b) Oil sample of test 1.1 from Table 6-1 after one day. Precipitation of black particles can be observed.

Coating delamination on the roller initiates at the center of contact in the location that maximum contact stress has been generated. Therefore, it is expected that edge delamination will occur when the coating is applied to the discs and center delamination can occur when the coating applied to the roller.

a) b) c)

Figure 6-2: a) Schematic of delamination of coating on the coated disc due to edge stress. b) Actual surface of a coated disc from test 1.3 with delamination on both sides of contact. c) 2D height profile of Figure 6-2b.

6.3. Delamination of WC/a-C:H coating on roller

In MPR testing, the combination of coated roller/uncoated discs performs better than the coated disc/uncoated roller combination in regard to coating delamination and tribological failures of the contacts.

As described earlier, the coating on the roller with the smooth surface roughness ($Ra < 0.2$ μm) does not suffer from flaking or edge stress. As a result, coated rollers can tolerate medium range of contact stresses up to 2 GPa for a high number of cycles (30 million cycles) with no delamination as shown in Figure 6-3.

At a higher contact stress (above 2 GPa), delamination of coating depends upon the quality of the surface of the substrate, hardness of substrates and SRR. Sliding increases the coefficient of friction from 0.05 at $|SRR|=0.0\%$ to around 0.1 at $|SRR|=2.0\%$ or $|SRR|=10.0\%$. Coatings that were applied on isotropically finished rollers showed better performance regarding delamination at higher contact stresses. In some cases, coating can tolerate contact stresses up to 2.5 GPa for 30 million cycles without a significant amount of delamination.

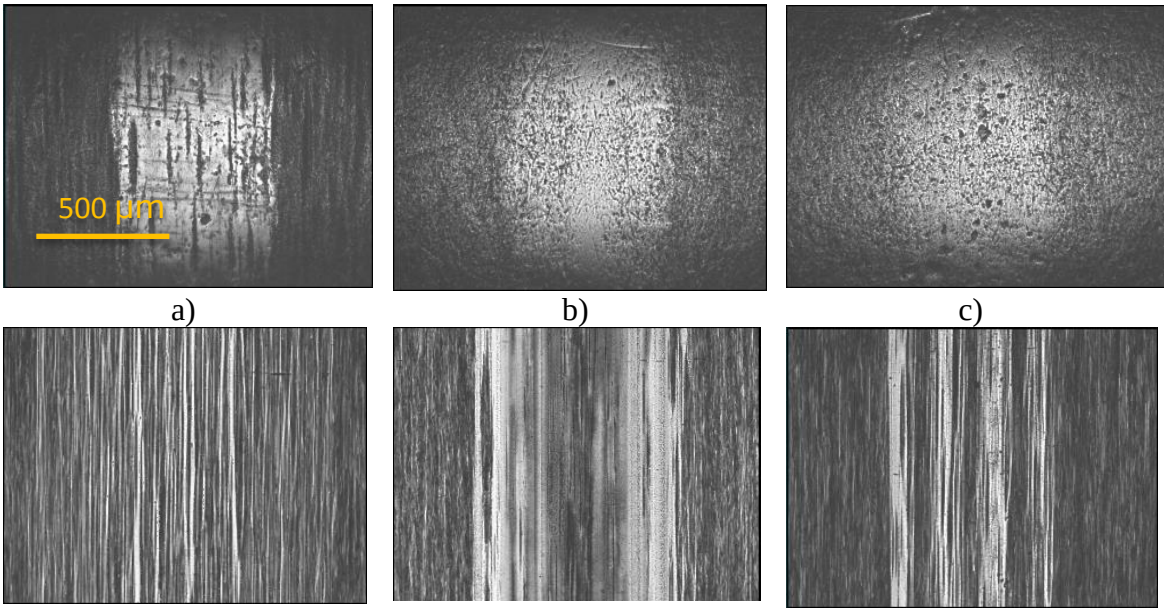

Figure 6-3: Surface of coated rollers with no delamination at medium range of contact stress (1.5 <P_{max}< 1.7 GPa). a) Roller of test 2.3 from Table 6-1, after 30 million cycles, P_{max}: 1.5 GPa and 2% sliding to rolling ratio. b) Roller of test 2.4 from Table 6-1, after 12 million cycles, P_{max}: 1.5 GPa and 2% sliding to rolling ratio and hardness of roller is 53 HRC. c) Roller of test 2.5 from Table 6-1, after 8.5 million cycles, P_{max}: 1.7 GPa and 2% sliding to rolling ratio. d) Surface of counterpart disc for test 2.3 from Table 6-1 which slightly has polished after 30 million cycles of roller equal to 2.07 million cycles for an element on a disc. e) Surface of counterpart disc for test 2.4 from Table 6-1 which slightly has polished after 12 million cycles of roller equal to 0.83 million cycles for an element on a disc. Isotropic finishing on roller causes higher rate of wear on longitudinal finished disc. f) Surface of counterpart disc for test 2.5 from Table 6-1 which slightly has polished after 8.5 million cycles of roller equal to 0.58 million cycles for an element on a disc.

6.4. Delamination, wear and the orientation of surface roughness

Increases in average surface roughness (Ra) of coated part intensify the delamination of coating. In addition, for a constant surface roughness, the direction of grinding lay has an effect on the delamination as well as the rate of abrasive wear on the uncoated counterpart. Regarding delamination of the coating, the best performance is achieved by applying the coating on isotropically finished surfaces in a pure rolling condition (|SRR|=0.0%). Effect of roughness on the uncoated counterpart is relatively negligible compared with the effect of roughness on the coated part. However, the

roughness of the counterpart is still important during the first few thousand cycles or running-in time on the delamination of coating. After running-in, asperities on the surface of the uncoated counterpart have worn away since there is considerable hardness difference between coating and AISI 52100 Steel. The rate of abrasive wear depends on the quality of the surface finish of the coated part; the rougher the surface of the coated part, the higher the rate of abrasive wear on the uncoated counterpart. For example, when the coated part has a surface roughness of 0.4 μm, the rate of abrasive wear is high enough to change the profile of the uncoated part and decrease the contact pressure by 35%. On the other hand, the coating on the smooth isotropically finished roller with a surface roughness (Ra) below 0.2 μm polishes the asperities on the surface of the uncoated discs even when the contact stress is higher than 2 GPa. However, at stresses greater than this, the coating has a higher risk of delamination.

Comparing Figure 6-3d and 6-3e suggests that the superfinishing process creates an isotropic surface on the roller with a low Ra and consequently a higher λ ratio. Rate of abrasive wear on the surface of the counterpart decreases dramatically after running-in; however, since there is no chemical affinity between the DLC and steel, there is no adhesive wear on the contact surfaces and consequently the roughness of the surfaces becomes as low as 0.07 μm.

6.5. High contact stress

Random delamination at high contact stresses (P_{max} >2 GPa) depends upon the quality of the roller finish, amount of sliding and contact stress. In order to study the systematic delamination of the coating, coating were applied to super finished rollers (Ra: 0.2 μm) and the coated rollers were subjected to contact stresses ranging from 2 to 3 GPa.

Figure 6-4 shows the surface of coated rollers with roller hardness values of 57 and 62 HRC that were subjected to periodically increased contact stress with and without sliding. Results show that the threshold contact stress for coating failure is about 2.5 GPa in pure rolling condition (|SRR|=0.0%). It should be noted that the actual contact stress is higher than 2.5 GPa since the discs were machined in a manner that produced surfaces with sinusoidal longitudinal micro-groves. Although, the threshold stress for partial or random delamination may change based on the quality of surface, sliding and hardness of substrate, random delamination in the presence of sliding (|SRR|=±10.0%) tends to happen at a contact stress around 2 GPa for rollers with longitudinal surface finishing (Figure 6-4d and Figure 6-5c).

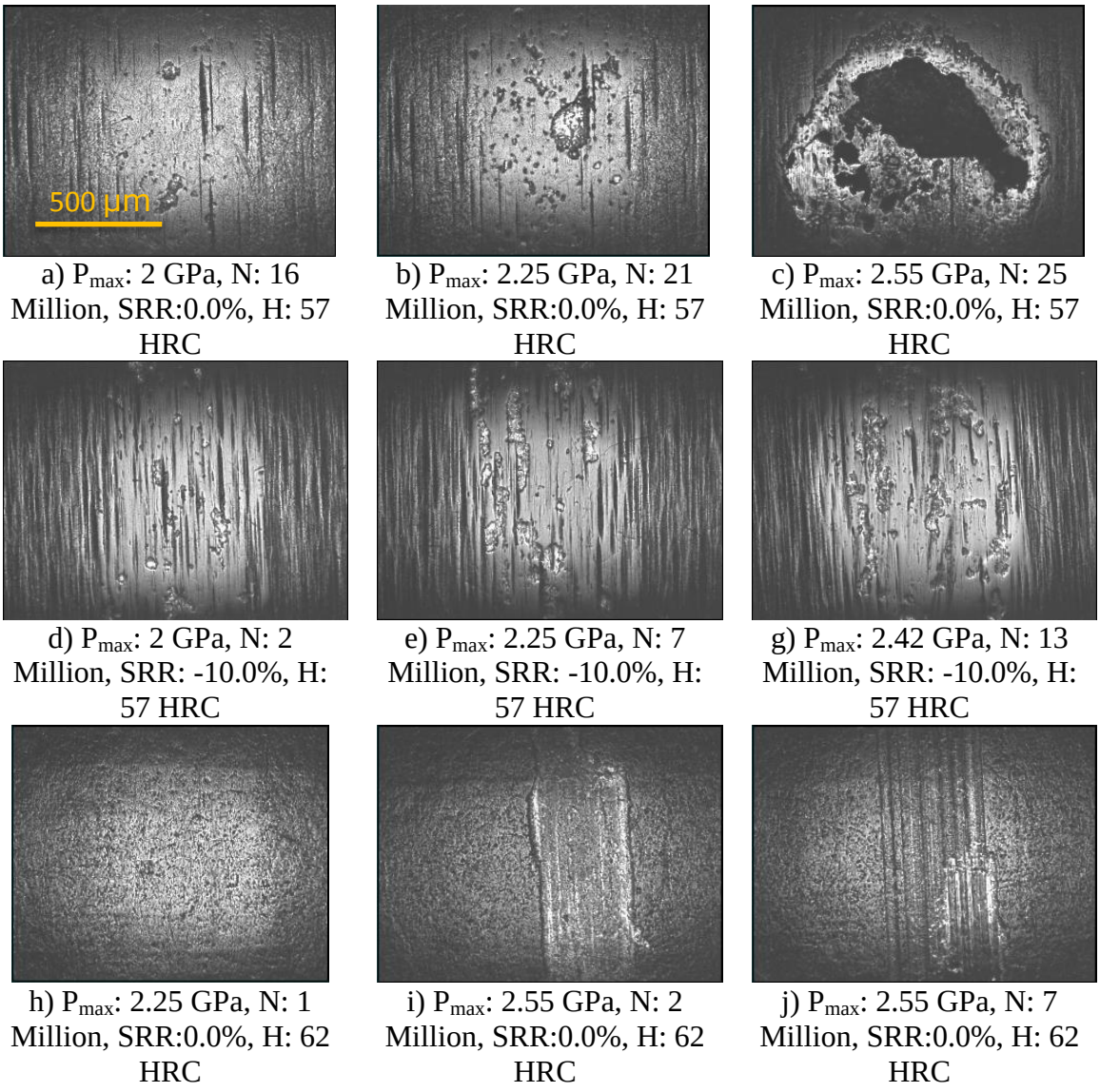

a) P_{max}: 2 GPa, N: 16 Million, SRR:0.0%, H: 57 HRC

b) P_{max}: 2.25 GPa, N: 21 Million, SRR:0.0%, H: 57 HRC

c) P_{max}: 2.55 GPa, N: 25 Million, SRR:0.0%, H: 57 HRC

d) P_{max}: 2 GPa, N: 2 Million, SRR: -10.0%, H: 57 HRC

e) P_{max}: 2.25 GPa, N: 7 Million, SRR: -10.0%, H: 57 HRC

g) P_{max}: 2.42 GPa, N: 13 Million, SRR: -10.0%, H: 57 HRC

h) P_{max}: 2.25 GPa, N: 1 Million, SRR:0.0%, H: 62 HRC

i) P_{max}: 2.55 GPa, N: 2 Million, SRR:0.0%, H: 62 HRC

j) P_{max}: 2.55 GPa, N: 7 Million, SRR:0.0%, H: 62 HRC

Figure 6-4: Gradually increase in coating delamination by increase in number of cycles and contact stress. 3 counterpart discs have hardness of 62 HRC and longitudinal surface roughness (Ra) of 0.2 µm. a) Test 2.7 from Table 6-1 at 16 million cycles. b) Test 2.7 from Table 6-1 at 21 million cycles. c) Test 2.7 from Table 6-1 at 25 million cycles. d) Test 2.8 from Table 6-1 at 2 million cycles. e) Test 2.8 from Table 6-1 at 7 million cycles. g) Test 2.8 from Table 6-1 at 13 million cycles. h) Test 2.9 from Table 6-1 at 1 million cycles. h) Test 2.9 from Table 6-1 at 2 million cycles. j) Test 2.9 from Table 6-1 at 7 million cycles.

a) P_{max}: 2 GPa, N: 1 Million, SRR: 2.0%, H: 62 HRC

b) P_{max}: 2 GPa, N: 18 Million, SRR: 2.0%, H: 62 HRC

c) P_{max}: 2.25 GPa, N: 34 Million, SRR: 2.0%, H: 62 HRC

Figure 6-5: Negligible delamination of coating on the 62 HRC hard roller with surface roughness of 0.2 µm against softer discs with hardness of 58 HRC and roughness of 0.2 µm.

6.6. Delamination of coating as contact stress increases incrementally

Test numbers 2.7 to 2.9 have been performed on a coated roller by incrementally increase the contact stress with |SRR|= 0.0% and 10.0%. It is noted that at each level of stress, a new set of discs was used to keep the initial λ ratio constant. At each level of contact stress, the test was stopped after 0.5 or 1 million cycles and then after 5 or 10 million cycles to study the rate of delamination during running-in and high number of cycles.

It is observed that the rate of random delamination is higher in running-in period (first 0.5 or 1 million cycle for each new set of discs). In most cases, during the high cycle number period (5 or 10 million cycles) either delamination stops or the rate of delamination decreases dramatically. Therefore, it can be speculated that random delamination of the coating is more of a stochastic phenomenon rather than a degradation or fatigue process.

6.7. Failure of coating and substrate hardness

Complete failure and collapse of the coating occurs at nominal contact stress of 2.5 GPa when there is no sliding and counterpart's hardness is 62 HRC. A decrease in substrate's hardness can increase the life of coating and failure threshold contact stress. Comparing the results of tests number 2.7, 2.9 and 2.10 from Table 6-1 suggests that a decrease in the hardness of the disc or roller; coated or uncoated, can increase the number of cycles required to delaminate the coating. Coating on the roller from test 2.7 in still in a partial delamination regime after 20 million cycles at 2.55 GPa contact stress with the roller hardness of 57 HRC. But in the test 2.9, the roller with a hardness of 62 HRC is already in a complete delamination state after only 2 million cycles at 2.55 GPa.

It pointed out that, although a decrease in the hardness of the coated roller might be beneficial regarding wear and surface failures of roller and disc, a softer roller has a reduced contact fatigue limit (Figure 6-4c). Meanwhile, a decrease in hardness of the uncoated part will increases its rate of wear. Therefore, an optimization may be desired for the hardness configuration of the components in an actual application.

6.8. Mechanism of random delamination

In most of the cases, delamination or degradation of the coating occurs around surface asperities and imperfections. TEM was performed on sections of the WC/a-C:H coated roller prepared by focused ion beam milling in an attempt to elucidate the mechanism of delamination. Two samples, one from an untested area of the coating and another from a tested region (wear track of a roller after 40 million cycles in contact stresses ranging from 2 to 2.5 GPa) are examined. Figure 6-6 displays the results of XEDS on the TEM samples. XEDS was performed to clarify that if tribo-mechanical and

shear stresses due to contact pressure and sliding in presence of oil are able to graphitize the sp^3 bonded carbon and eventually degrade the coating chemically. There is almost no change in the chemical composition of coating before and after running up to 2.5 GPa for more than 40 million cycles.

Microstructures and diffraction patterns of the samples are shown in Figure 6-7. No discernable differences are evident in the diffraction patterns of the untested and tested coating samples. This observation implies that the large number of cycles and high contact stresses caused no measurable alteration of the microstructure of the WC/a-C:H coating. However, evidence is presented in Figure 6-7b that the stress cycles have generated a crack in the coating that has originated at the surface of the coating and propagated in a random direction to the chromium interface. The characteristics of this crack are consistent with that of brittle fracture and not with fatigue or corrosion cracking, which are typically branched. An imperfection on the surface of the substrate or trapped voids between the coating layers causes inhomogeneity in stress careering elements through the layers of coating and eventually brittle cracking can happen due to excessive strains around the voids and surface imperfections. This phenomenon is stochastic and depends upon the surface roughness of both counterparts. The coating is able to polish the 52100 steel since its hardness is almost as twice that of steel. Therefore, superfinishing of the parts prior to coating is tremendously important to control rate of abrasive wear in the polishing mode or the rate of delamination.

As previously mentioned, a coated super-finished roller shows the best performance regarding delamination. Applying the coating on rollers with a surface

roughness less than 0.2 μm keeps the wear mode of uncoated discs in the polishing regime.

6.9. Conclusions

The objectives of this chapter are to evaluate the delamination behavior of WC/a-C:H coating, that was specifically optimized for bearing steels, mapping the coating delamination contact stresses, and investigating the mechanism of delamination. Combinations of several features such as surface roughness, hardness of substrate, contact stress and slide to rolling ratio are found to affect delamination.

Based upon the experimental results conducted here, the following observations and conclusions can be made:

- The roughness of the coated component plays a crucial role in flaking, delamination of coating and the rate of wear on the uncoated counterpart.
- Flaking happens only for a coating on rough surfaces with surface roughness (Ra) of 0.4 μm and above. Decreasing the surface roughness to 0.2 μm ceases the flaking of the coating and decreases the rate of delamination considerably. Also, the coating on a Ra = 0.2 μm roller only removes the asperities and polishes the surfaces of the uncoated discs. This has an important consequence that the λ value of the contact becomes larger and the macro and micropiting fatigue lives will increase significantly.
- Delamination due to edge stresses happens only when the coating is applied to the discs. The generation of hydrostatic pressure inside the smaller part (Roller in MPR) due to contact stress causes a recession on the disc and consequently a sharp

change from compression to tension at the edge of the contact on the surface of disc. This phenomenon causes an early stage delamination of the coating at a medium value of contact stresses.

- The coating on a super-finished roller can withstand contact stresses as high as 2.5 GPa with no delamination in a pure rolling condition. Sliding decreases the delamination resistance of the coating as it increases the coefficient of friction and shear stress by almost a factor of two.

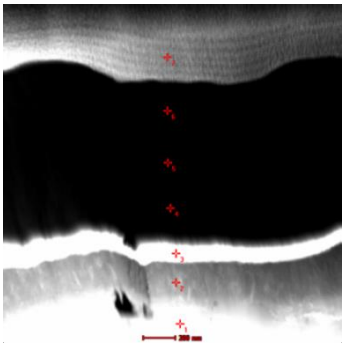

(a) Position of XDES points in the un-tested coating

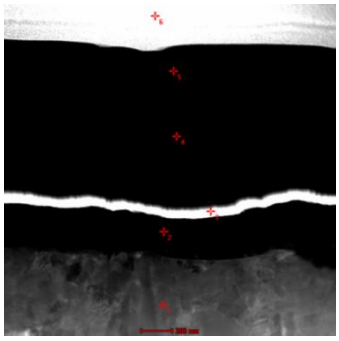

(b) Position of XDES points in the tested coating

Point 4			
Element	Wt %	Atomic %	Uncert. %
C(K)	39.89	90.33	0.54
Cr(K)	0.35	0.18	0.02
Fe(K)	1.89	0.92	0.07
W(L)	57.84	8.55	0.47

Point 5			
Element	Wt %	Atomic %	Uncert. %
C(K)	38.12	89.33	0.6
Cr(K)	0	0	100
Fe(K)	3.41	1.71	0.1
W(L)	58.46	8.94	0.49

Point 6			
Element	Wt %	Atomic %	Uncert. %
C(K)	30.26	85.61	0.61
Cr(K)	0.23	0.15	0.03
Fe(K)	3.28	1.99	0.13
W(L)	66.21	12.23	0.67

(c) Composition of elements at points 4, 5 and 6 in Fig.10a

Point 4			
Element	Wt %	Atomic %	Uncert. %
C(K)	41.3	91.1	0.41
Cr(K)	0	0	100
Fe(K)	1.3	0.61	0.04
W(L)	57.39	8.27	0.4

Point 5			
Element	Wt %	Atomic %	Uncert. %
C(K)	26.39	83.62	0.38
Cr(K)	0	0	100
Fe(K)	2.39	1.63	0.06
W(L)	71.21	14.74	0.49

(d) Composition of elements at points 4 and 5 in Fig.10b

Figure 6-6 a Bright field TEM photo of samples on WC/a-C:H coating before micropitting test (Original coating) and b after running for more than 40 million cycles at 2, 2.25 and 2.5 GPa contact stresses. c and d composition of labeled points in a and b. There is almost no change in chemical composition of WC/a-C:H coating before and after running. The chemical degradation of coating through chemical reaction is negligible.

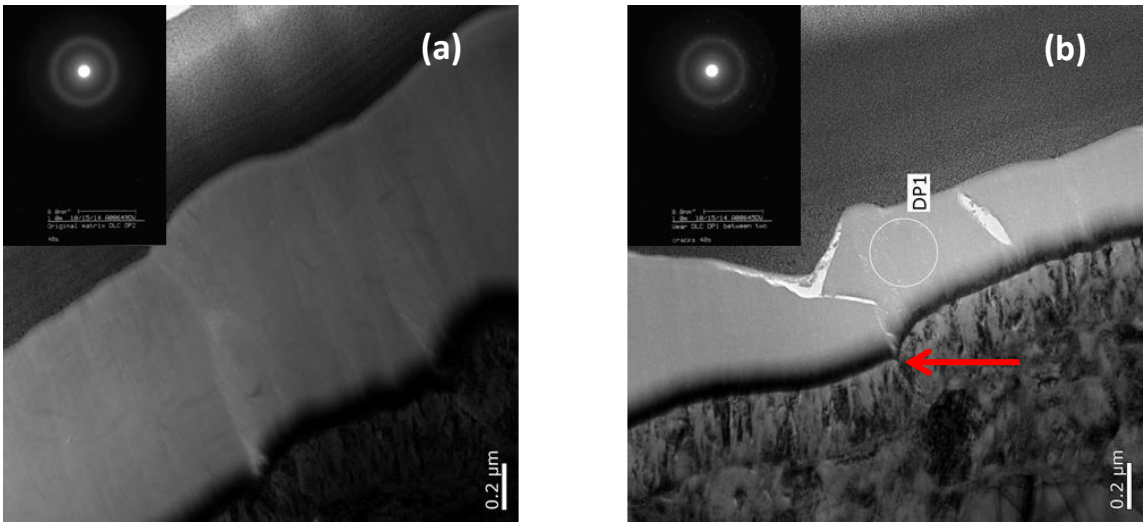

(a) Diffraction pattern of un-tested coating (b) Diffraction pattern after 40 million cycles

Figure 6-7: a Diffraction pattern of WC/a-C:H coating before micropitting test (Original coating) and b after running for more than 25 million cycles at 1.7, 2.0 and 2.25 GPa contact stresses at the delaminated area. It shows essentially there is no microstructural change or recrystallization in the coating during micropitting test at 2-2.25 GPa contact stress. It confirms there is no microstructural degradation in the coating. Red arrow shows the submicron imperfection on the surface may cause brittle fracture and crack propagation laterally in the coating.

CHAPTER VII

NUMERICAL MODELLING AND PLASTICITY INDEX

7.1. Overview

Micropitting is influenced by numerous factors such as contact stress, physical and mechanical properties of the relative contacts, lubricant properties, environmental parameters such as temperature, entrainment velocity, slide to roll ratio, etc. Several of the aforementioned parameters are independent while others are not. Moreover, the micropitting behavior on the variables is not necessarily linear, and in some cases curve fitting of only one variable can be complicated. For example, a small change in the slide to roll ratio can completely alter the wear mode from micropitting to abrasion. Therefore, one possible method for the numerical modeling of micropitting would be non-linear multiple variable regression.

Although the number of parameters that influence micropitting is so high that it is unrealistic to extensively test all parameters, it is possible to combine some of these parameters. For example, it is possible to combine oil temperature, viscosity, entrainment velocity, and surface roughness into one parameter λ. However, the reduction in the number of parameters may be at a cost of precision in the modeling. For example, the micropitting progression rate of two rough surfaces is considerably higher than two smooth surfaces with the same λ ratio.

It is essential to define a micropitting cut off criterion when performing numerical modeling on the effect of several factors on the progression rate of micropitting. One criterion could be a limit on the peak-to-peak acceleration (Accel P/P) measurement performed by the micropitting rig. Changes in entrainment velocity, surface roughness, and oil viscosity all influence the Accel P/P.

7.2. Image processing

Another criterion could be the ratio between the micropitted areas to the total area with the number of cycles [5, 24]. Image processing has been done on images captured by an optical profilometer in order to measure the progression rate of micropitting. The commercially available software, ImageJ was used for image processing.

Figure 7-1 shows a sequence of images processed from a micropitted sample.

In order to compare the micropitting rate of different samples properly, a certain number of cycles have to be chosen as a cut off limit. Since progression of micropitting depends upon many factors, the cut off limit should be chosen based upon the testing conditions and mechanical properties of components. One million cycles was chosen as the cycle limit in the MPR testing. In some tests, images of micropitted surfaces were available at exactly one million cycles while in others extrapolation was used to approximate the percentage of micropitted area at one million stress cycles.

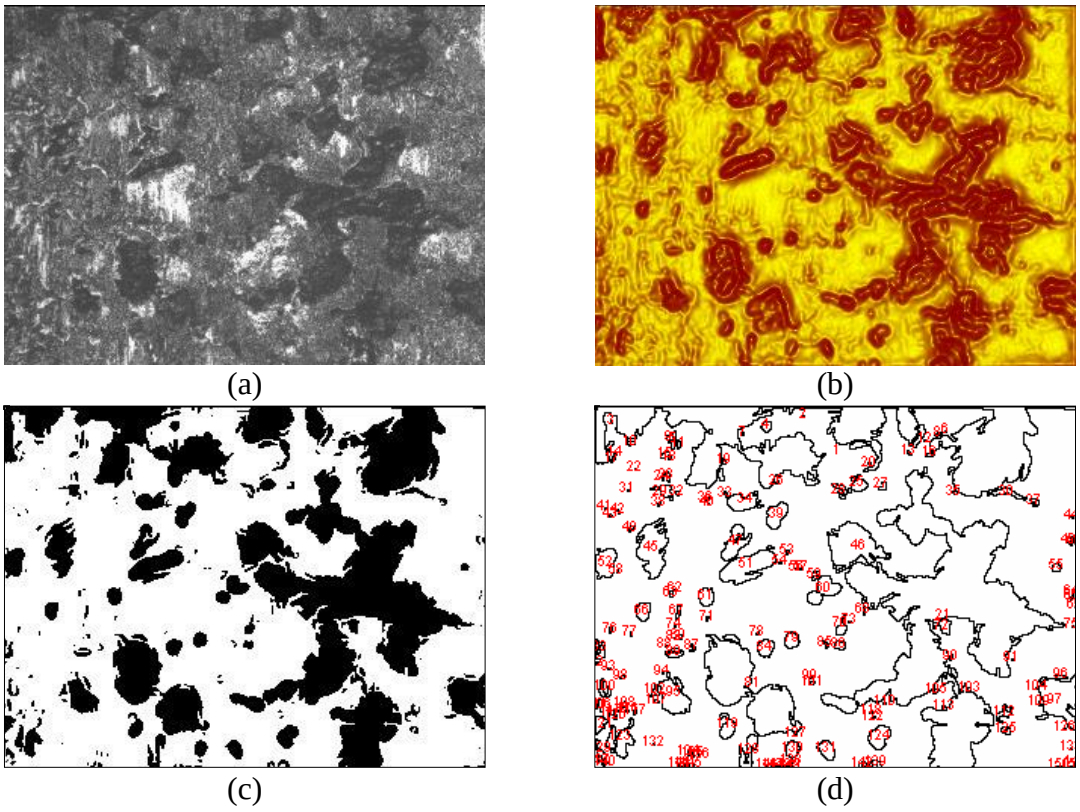

Figure 7-1: Image processing of the micropitted samples. (a). Surface of micropitted roller by 3D profilometer. (b) Solid plot of micropitted roller by 3D profilometer. (c) Surface contour image after processing by ImageJ. (d) Analyzed image; pits are counted, labeled and their area is measured. 151 micropits and 32.61% of total area are micropitted.

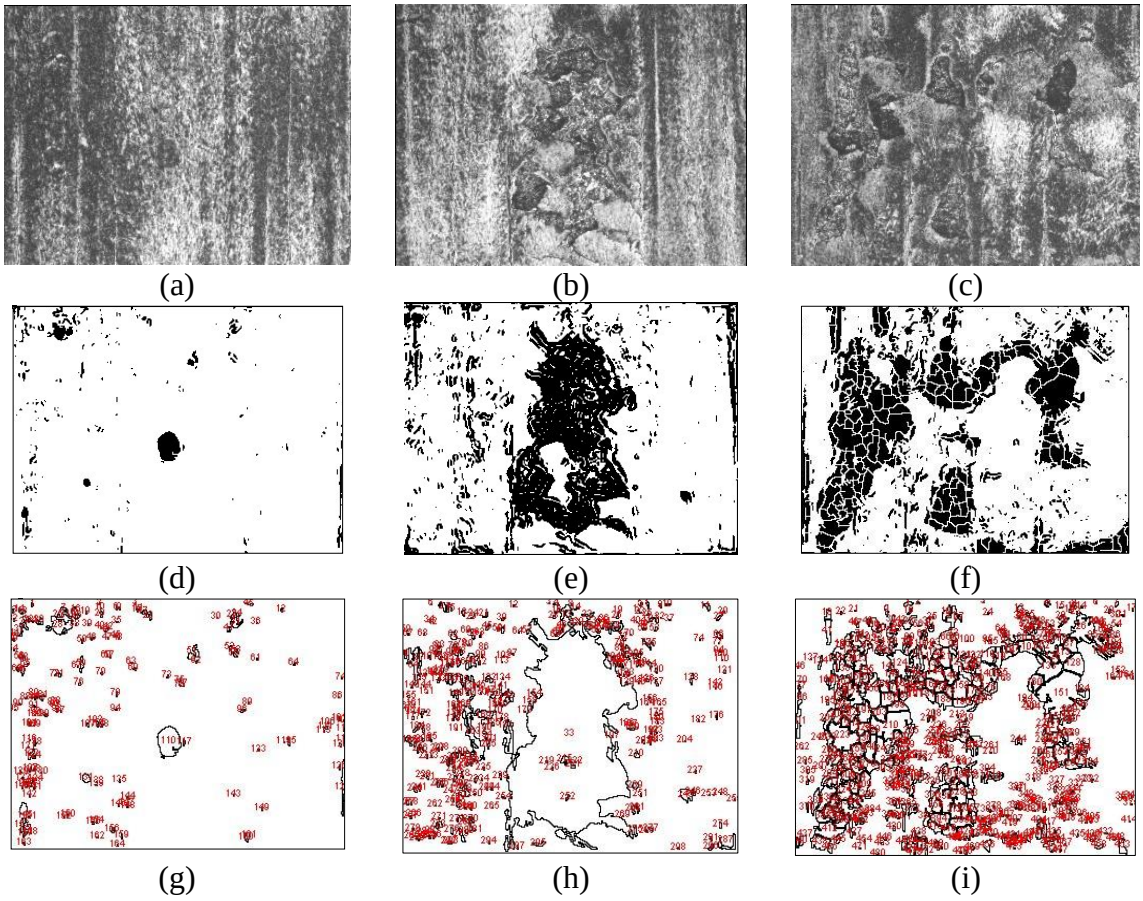

Figure 7-2: Micropitting image processing of micropitted sample. Optical image of surface after (a) 0.6 million cycle, (b) 1.8 million cycles and (c) 2.1 million cycles. Surface contour image of sample after (d) 0.6 million cycles, (e) 1.8 million cycles and (f) 2.1 million cycles. Analyzed image after (g) 0.6 million cycles, (h) 1.8 million cycles and (i) 2.1 million cycles.

Figure 7-2 shows the image processing of a sample at several stress cycles of 0.6, 1.8 and 2.1 million cycles. This particular sample is an uncoated roller running against WC/a-C:H coated discs, test 3.2 from Table 4-4. Figure 7-3 shows the analysis of the image processing of same sample from 0.3 million to 2.1 million cycles. It is speculated that the micropitting progress on this particular sample is following the power law shown in Figure 7-3.

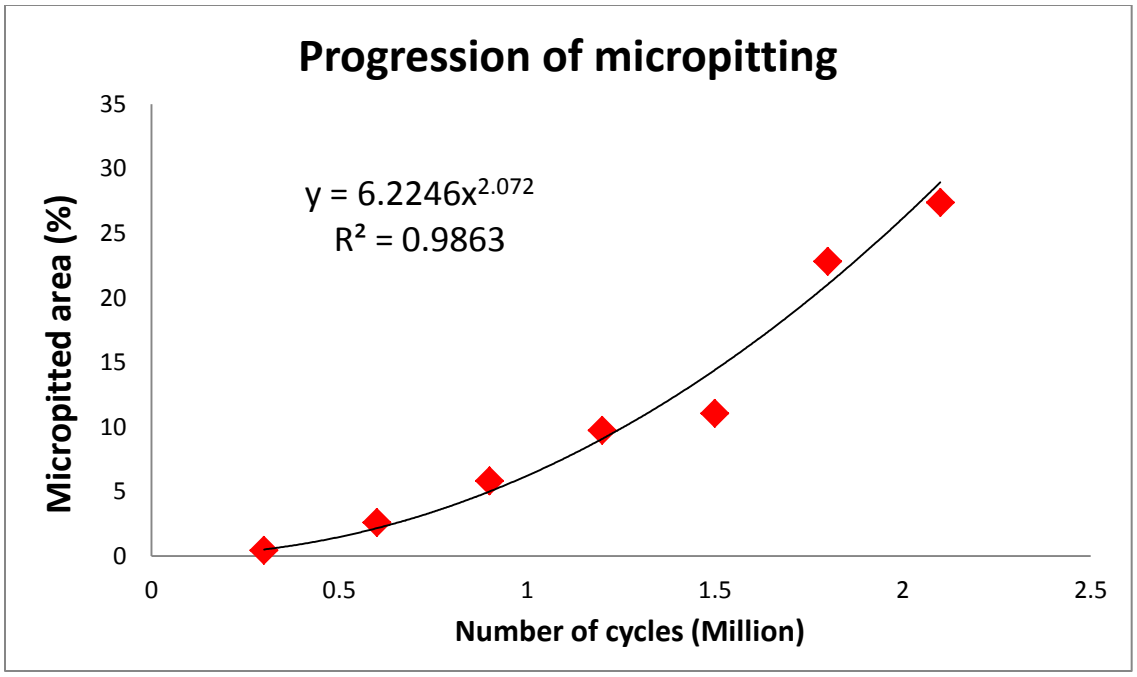

Figure 7-3: Progression of micropitting by increase in the number of cycles based on image processing of micropitted sample.

Table 7-1

Table 7-1 shows the result of the image processing of several samples after one million cycles for different testing parameters.

Table 7-1: The percentage of micropitted area based on testing parameters

	Contact	Contact Stress			Hardness (GPa)				
No.	Discs/Roller	Pmax (GPa)	SRR	λ	Disc	Roller	Roller Hardness / Contact Stress	H Disc-H Roller	% micropitted area at 1 million cycles
1-1	Steel/Steel	2.25	0	0.13	7.32	7.3	3.3	0.0	33.96
1-2	Steel/Steel	2.0	10	0.14	7.32	6.0	3.0	1.3	2.10
1-3	Steel/Steel	2.00	-10	0.13	7.32	6.0	3.0	1.3	5.33
1-4	Steel/Steel	2.00	0	0.14	7.32	6.0	3.0	1.3	15.43
1-5	Steel/Steel	1.50	2	0.12	7.32	5.5	3.6	1.8	0.00
1-6	Steel/Steel	2.00	2	0.13	7.32	6.0	3.6	1.3	11.63
1-7	Steel/Steel	1.70	2	0.07	7.32	6.2	3.6	1.1	0.00
1-8	Steel/Steel	1.50	0	0.09	7.32	6.2	4.1	1.1	0.00
1-9	Steel/Steel	1.50	2	0.09	7.32	6.2	4.1	1.1	0.00
1-10	Steel/Steel	1.50	2	0.11	7.32	7.3	4.8	0.0	0.00
1-11	Steel/Steel	2.20	2	0.17	6.41	7.3	3.3	-0.9	0.00
1-12	Steel/Steel	2.00	2	0.12	5.49	7.3	3.6	-1.8	0.00
1-13	Steel/Steel	2.00	2	0.17	7.32	6.0	3.0	1.3	22.18
2-1	WC/a-C:H/Steel	1.50	0	0.11	12.0	6.2	4.1	5.7	4.50
2-2	WC/a-C:H/Steel	1.50	2	0.12	12.0	6.2	4.1	5.7	10.17
2-3	WC/a-C:H/Steel	2.00	2	0.13	12.0	7.3	3.6	4.6	46.32
3-1	Steel/WC/a-C:H	2.00	2	0.14	7.32	12	6.0	-4.6	0.00
3-2	Steel/WC/a-C:H	2.55	10	0.19	7.32	12	4.7	-4.6	0.00
3-3	Steel/WC/a-C:H	2.55	-10	0.13	7.32	12	4.7	-4.6	0.00
3-4	Steel/WC/a-C:H	2.00	2	0.13	7.32	12	6.0	-4.6	0.00
3-5	Steel/WC/a-C:H	1.50	2	0.12	7.32	12	8.0	-4.6	0.00

7.3. Non-linear multivariable regression

Abstractly, Equation (7-1) is followed for the regression of variables and factors affecting micropitting. Notice that at this stage with limited number of tests, it is no possible to accurately drive an equation for prediction of micropitting behavior.

$$\boldsymbol{Mp = \alpha X^A Y^B Z^C W^D} \quad (7\text{-}1)$$

X, Y, Z and W are variables or parameters affecting micropitting and A, B, C and D are powers that influence each parameter. α is a constant that accounts for other parameters not considered.

Numerically modelling of equation (7-1) could be complicated and needs considerably large number of data. However, applying natural log converts equation (7-1) to equation (7-2) which then is a linear multivariable regression.

$$\boldsymbol{Ln(Mp) = Ln(\alpha) + Aln(X) + Bln(Y) + Cln(Z) + Dln(W)} \quad (7\text{-}2)$$

7.4. Selection of parameters influencing micropitting

It is possible to combine some of parameters to create a new parameter such as the lubricant film ratio (λ), which is the combination of oil temperature, viscosity, surface roughness, and entrainment velocity. At the other hand, there are parameters that each of them individually has a considerable influence on the micropitting behavior. For instance, by scanning the data presented in

Table 7-1, it is observed that softer discs cannot generate micropitting on harder rollers. (In cases that the roller substrate is harder or the roller is coated with the WC/a-C:H coating which is significantly harder than 52100 steel.) Therefore, either hardness or the difference in hardness between the disc and roller was considered as one independent factor.

Another independent factor is slide to roll ratio. Notice that, only four SRR values (-10, 0, 2 and 10%) were utilized in these study. Experimental results show that higher SRR (±10%) causes wear (Figure 5-1 shows the comparison of ±10% with 0.0% SRR) but if SRR increases slightly (2%), a higher rate of micropitting exists than when there is no sliding (SRR = 0.0%). Figure 7-4 shows the initiation of micropitting on the surface of an uncoated roller running against smooth WC/a-C:H coated discs. The large difference between the hardness of WC/a-C:H and steel provided an opportunity to study micropitting in more depth. As shown in Figure 7-4, introducing 2.0% SRR (i.e., more shear stress on the roller) yielded a higher rate of micropitting wear.

Five factors were considered in the numerical modeling: Hertzian contact stress (P_{max}), slide to roll ratio (SRR), lubricant film thickness parameter (λ), ratio of the roller hardness to the contact stress (H_r/p_{max}), and the hardness difference between the discs and roller ($H_d - H_r$). All variables were initially assigned arbitrary values between 0 and 1 and then converted to their natural logarithm values. Processed micropitting data is shown in Table 7-2. Linear regression was performed on the micropitting data shown in Table 2, and the results are presented in Table 7-3.

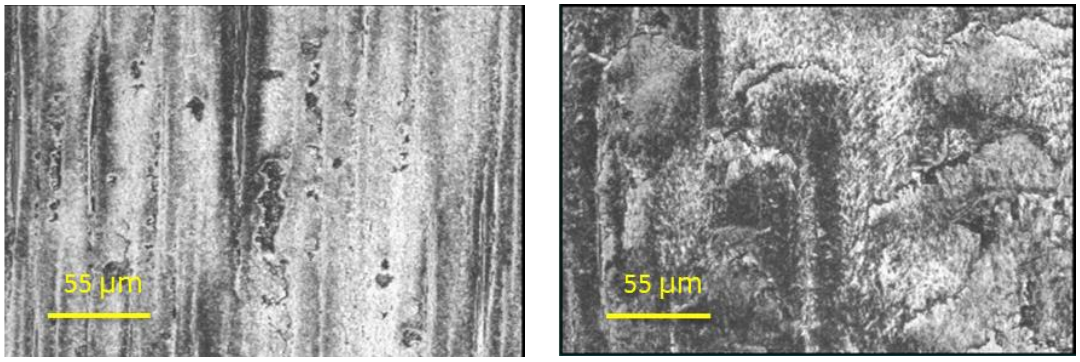

(a) (b)

Figure 7-4: Effect of 2.0% slide to roll ratio on increase in the micropitting progression rate. (a). Surface of uncoated roller after running against smooth WC/a-C:H coated discs with 0.0% slide to roll ratio at 1.5 GPa contact stress. (b). Surface of uncoated roller after running against smooth WC/a-C:H coated discs with 2.0% slide to roll ratio at 1.5 GPa contact stress.

Table 7-2: Processed micropitting data of non-linear multi variable regression

No.	Discs/Roller	CONV Ph(GPa)	CONV SRR	λ	Roller Hardness / Contact Stress	CONV HD-HR	% micropitted area at 1 million cycles
1-1	Steel/Steel	-0.29	-0.69	-2.04	-1.10	-0.69	-0.39
1-2	Steel/Steel	-0.41	0.00	-1.97	-1.20	-0.57	-3.17
1-3	Steel/Steel	-0.41	-6.91	-2.04	-1.20	-0.57	-2.24
1-4	Steel/Steel	-0.41	-0.69	-1.97	-1.20	-0.57	-1.18
1-5	Steel/Steel	-0.69	-0.51	-2.12	-1.01	-0.53	-10.82
1-6	Steel/Steel	-0.41	-0.51	-2.04	-1.01	-0.57	-1.46
1-7	Steel/Steel	-0.57	-0.51	-2.66	-1.01	-0.59	-10.82
1-8	Steel/Steel	-0.69	-0.69	-2.41	-0.88	-0.59	-10.82
1-9	Steel/Steel	-0.69	-0.51	-2.41	-0.88	-0.59	-10.82
1-10	Steel/Steel	-0.69	-0.51	-2.21	-0.72	-0.69	-10.82
1-11	Steel/Steel	-0.31	-0.51	-1.77	-1.10	-0.79	-10.82
1-12	Steel/Steel	-0.41	-0.51	-2.12	-1.01	-0.89	-10.82
1-13	Steel/Steel	-0.41	-0.51	-1.77	-1.20	-0.57	-0.81
2-1	WC/a-C:H/Steel	-0.69	-0.69	-2.21	-0.88	-0.24	-2.41
2-2	WC/a-C:H/Steel	-0.69	-0.51	-2.12	-0.88	-0.24	-1.59
2-3	WC/a-C:H/Steel	-0.41	-0.51	-2.04	-1.01	-0.31	-0.08
3-1	Steel/WC/a-C:H	-0.41	-0.51	-1.97	-0.51	-1.32	-10.82
3-2	Steel/WC/a-C:H	-0.16	-0.01	-1.66	-0.75	-1.32	-10.82
3-3	Steel/WC/a-C:H	-0.16	-6.91	-2.04	-0.75	-1.32	-10.82
3-4	Steel/WC/a-C:H	-0.41	-0.51	-2.04	-0.51	-1.32	-10.82
3-5	Steel/WC/a-C:H	-0.69	-0.51	-2.12	-0.22	-1.32	-10.82

Table 7-3: The multivariable regression of processed variables.

Regression Statistics	
Multiple R	0.847
R Square	0.717
Adjusted R Square	0.623
Standard Error	2.934
Observations	21.000

ANOVA

	df	SS	MS	F	Significance F
Regression	5.000	327.529	65.506	7.611	0.001
Residual	15.000	129.104	8.607		
Total	20.000	456.633			

	Coefficients	Standard Error	t Stat	P-value	Lower 95%	Upper 95%	Lower 95.0%	Upper 95.0%
Intercept	37.341	12.432	3.004	0.009	10.843	63.839	10.843	63.839
Pmax	17.041	8.005	2.129	0.050	-0.022	34.103	-0.022	34.103
SRR	-0.224	0.372	-0.603	0.555	-1.017	0.568	-1.017	0.568
λ	6.544	4.085	1.602	0.130	-2.164	15.251	-2.164	15.251
Hr/Pmax	10.107	5.724	1.766	0.098	-2.093	22.307	-2.093	22.307
Hd-Hr	18.183	4.414	4.119	0.001	8.774	27.592	8.774	27.592

Table 7-3 reveals that maximum contact stress, hardness difference between disc and roller, and hardness of the roller over contact stress have the largest influence on micropitting. Interpretation of the data presented in Table 7-3 shows that the regression is acceptable: R^2 is 0.71 and the significance is 0.001. The probability of variables (P-value) shows strong evidence that hardness difference between discs and roller and maximum

contact stress are the most significant factors affecting micropitting. The ratio between the hardness of the roller and the maximum contact stress is of secondary importance. The result of regression does not indicate a strong linkage between specific lubricant film thickness, and also slide to roll ratio to micropitting. Because the purpose of experiments is evaluating the effects of WC/a-C:H on the micropitting behavior of bearing steel and not λ or SRR. Therefore, experiments were designed to maintain a nearly same lubricant film thickness in order to avoid effect of lubrication quality on micropitting. On the other hand, only four SRR values were tested, and since SRR has a nonlinear relationship with the micropitting, the range of SRR values used in these experiments is too narrow to unravel how exactly SRR affects the micropitting of bearing steels.

Numerical modeling of micropitting data indicates that the hardness difference between discs and the roller is the most dominant factor affecting micropitting, followed by maximum contact stress. In 1986, Spikes et al. performed similar tests on a three contact rolling/sliding contact machine that is similar to the PCS MPR only with larger discs and roller [111]. The authors tested rollers and discs with different hardness values and the result showed that harder discs and softer rollers had higher wear rate than softer discs against harder rollers as shown in Figure 7-5. Nano-indentation of the WC/a-C:H coating and 52100 reported by Evans et al. indicates that WC/a-C:H is almost 3 GPa harder than 52100 [112]. Figure 7-5 (from Spike et al) shows the wear rate relative to hardness difference between a roller and discs. Applying the relative hardness values of 52100 and WC/a-C:H into Figure 7-5 indicates that the wear rate would be considerably higher when the coating is applied to discs (cD/uR). On the other hand, little if any wear is expected when the coated roller is mated with uncoated discs (uD/cR).

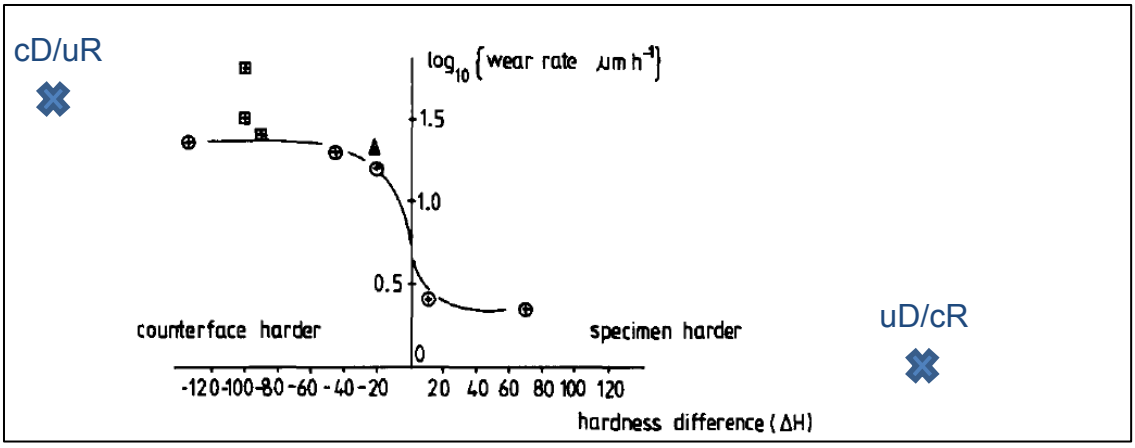

Figure 7-5: The effect of the hardness difference on the wear with different sliding to rolling ratios [111]. cD/uR represents Coated Discs against Uncoated Roller.

7.5. Wear Analysis

7.5.1. Effect of roughness

In the following paragraphs, the effect of roughness of the coated part, slide to roll ratio and hardness of substrate on the wear of the discs and roller are compared and reported.

As previously noted, application of the coating on a rough disc or roller surface caused a high rate of wear on the uncoated counterpart.

Figure 7-6 shows the total wear rate (micrometers/million cycles) of the disc as a function of coated roller roughness. Two values of surface roughness; smooth (Rq: 26 μm) and rough (Rq: 56 μm) were examined. The contact stress was 1.5 GPa and the lubricant film thickness was in boundary lubrication condition and close to 0.1. An increase in the lubricant film thickness decreases the rate of wear. However, since the lubricant film thickness is much less than the surface roughness values, surface roughness had a greater effect on wear than lubricant film thickness. It was observed that the rate of

wear decreased considerably after the profile of the counterpart changed and reduced the level of contact stress to below 1 GPa.

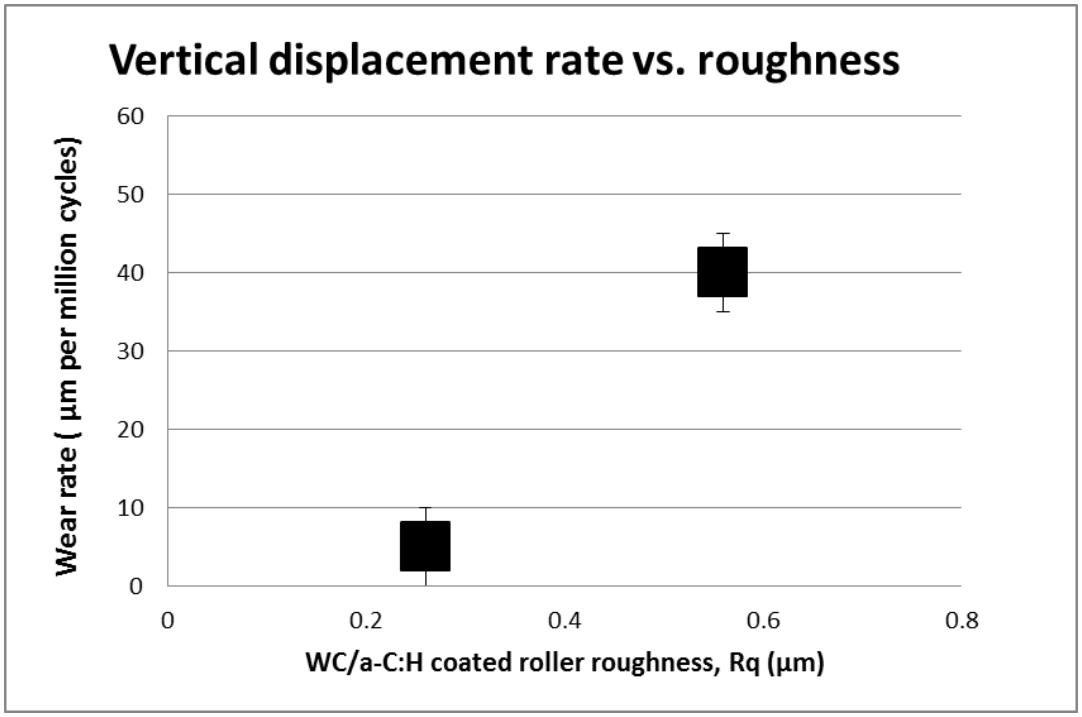

Figure 7-6: Effect of roughness of WC/a-C:H coated roller on the wear rate of discs and roller at Pmax= 1.5 GPa.

7.5.2. Effect of slide to roll ratio on wear of WC/a-C:H coating

An increase in sliding caused an increase in the rate of wear of the WC/a-C:H. Negative sliding ($u_r - u_d < 0$) produced greater wear than positive sliding. Wear of the coating was characterized as fracture or delamination in these experiments. Shear due to negative sliding should generate tensile stress in the coating at the outlet position of the contact where the lubricant film thickness is at a minimum.

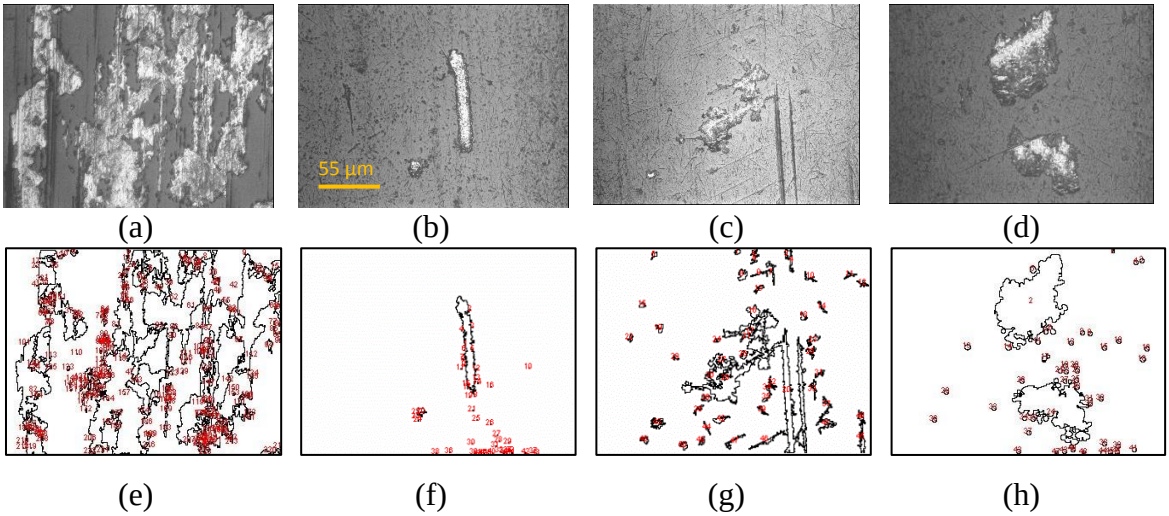

Figure 7-7: Image analysis of worn spots on the coated roller with different rolling to sliding ratios. (a) Surface of WC/a-C:H coated roller after 2 million cycles with -10.0% slide to roll ratio at 2 GPa contact stress and specific lubricant film thickness around 0.1. (b) Surface of WC/a-C:H coated roller after 2 million cycles with 0.0% slide to roll ratio at 2 GPa contact stress and specific lubricant film thickness around 0.1. (c) Surface of WC/a-C:H coated roller after 2 million cycles with 2.0% slide to roll ratio at 2 GPa contact stress and specific lubricant film thickness around 0.1. (d) Surface of WC/a-C:H coated roller after 2 million cycles with 10.0% slide to roll ratio at 2 GPa contact stress and specific lubricant film thickness around 0.1. (e) Analysis of worn area of image presented in (a) with 25.3% worn area. (f) Analysis of worn area of image presented in (b) with 5.9% worn area. (g) Analysis of worn area of image presented in (c) with 10.2% worn area. (h) Analysis of worn area of image presented in (d) with 19.1% worn area.

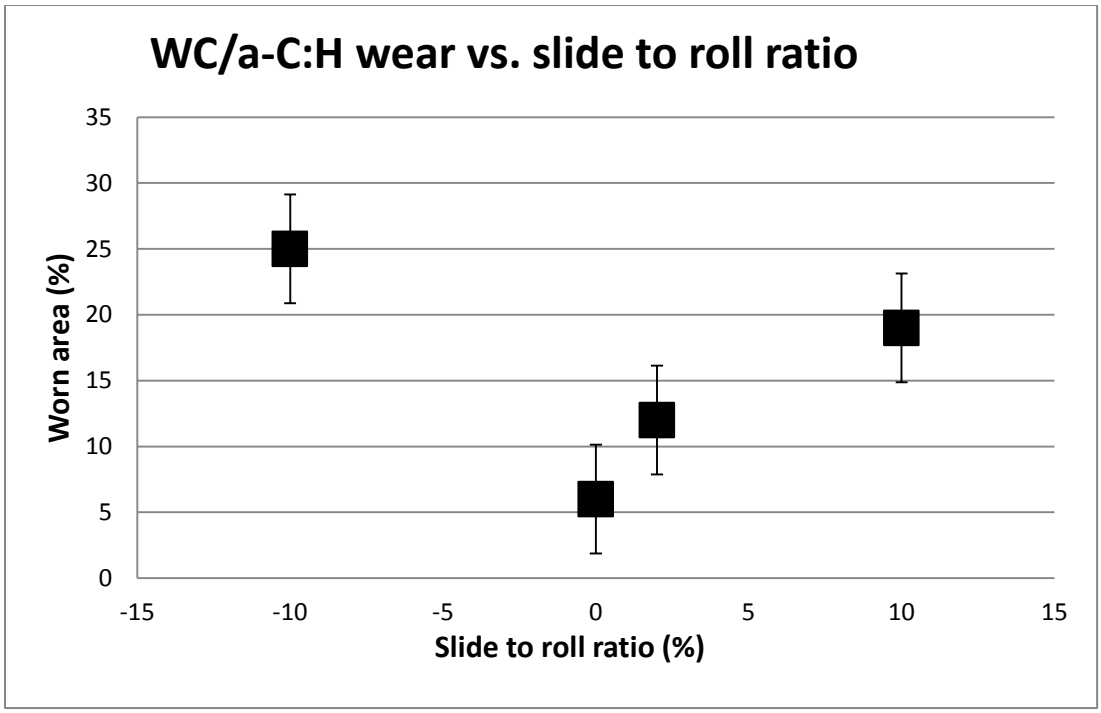

Figure 7-8: Result of image analysis of worn or delaminated area on the coated roller in different sliding to rolling ratios. Experiments have been done at 2 GPa contact stress and lubricant film thickness of about 0.1.

Minimum lubricant film thickness and central film thickness equations were discussed in Chapter 1. Calculation of minimum and central lubricant film thickness for the +10.0% and -10.0% SRR under 2GPa contact stress shows that the minimum lubricant film thickness is almost 30% thinner than the central film thickness. The MPR measured friction coefficients are almost 30% higher for -10.0% SRR than for +10% SRR. This tribological phenomenon has been observed in steel/steel contact as well as black oxide coated roller and discs contact. Additionally, the rate of wear and occurrence of delamination of the coating is higher in negative SRR than in positive SRR. Figure 7-8 shows the percentage of wear on the coated rollers with several SRRs and Figure 7-9 shows the surface of rollers after positive and negative 10.0% SRR. An increase in SRR

generates more heat. Higher temperatures reduce lubricant viscosity and consequently lubricant film thickness. Therefore, an increase in the rate of coating wear with increasing SRR is expected. However, negative SRR appears to have a tribo-mechanical effect on the wear rate of the roller. Figure 7-9.(a) shows a crack oriented perpendicular to the rolling direction followed by trailing edge of the crack in direction of sliding (arrow) for a roller tested under +10.0% SRR. Figure 7-9.(b) shows three parallel cracks formed perpendicular to the rolling direction on the surface of roller tested under -10% SRR. The trailing edges of the cracks are still aligned with the sliding direction. However, in the case of negative SRR, rolling and sliding are in opposite directions. Measurements performed on the lengths of cracks produced during the tests are 210 to 220 μm for +10% SRR and about 300 μm for -10% SRR. That is, cracks produced in the coating are about 30% larger for tests conducted at -10% SRR than for +10% SRR.

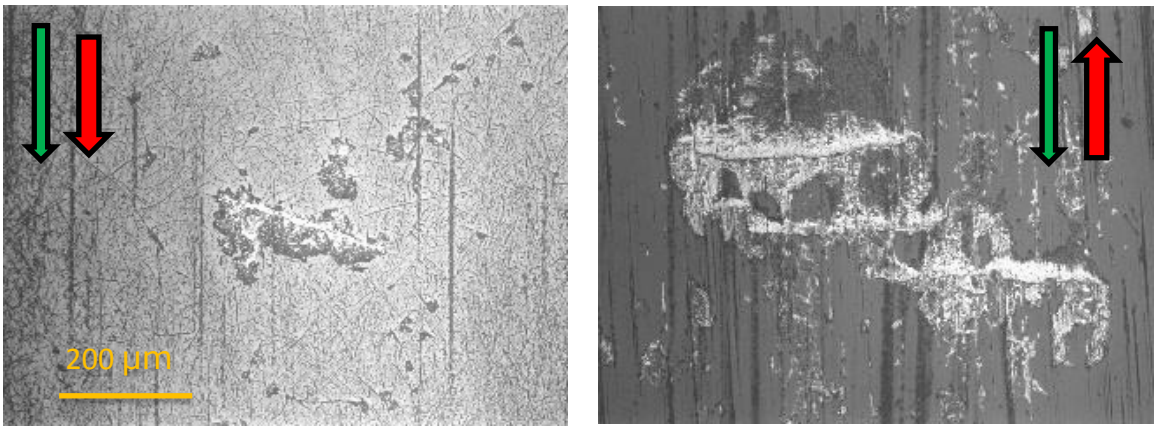

(a) (b)

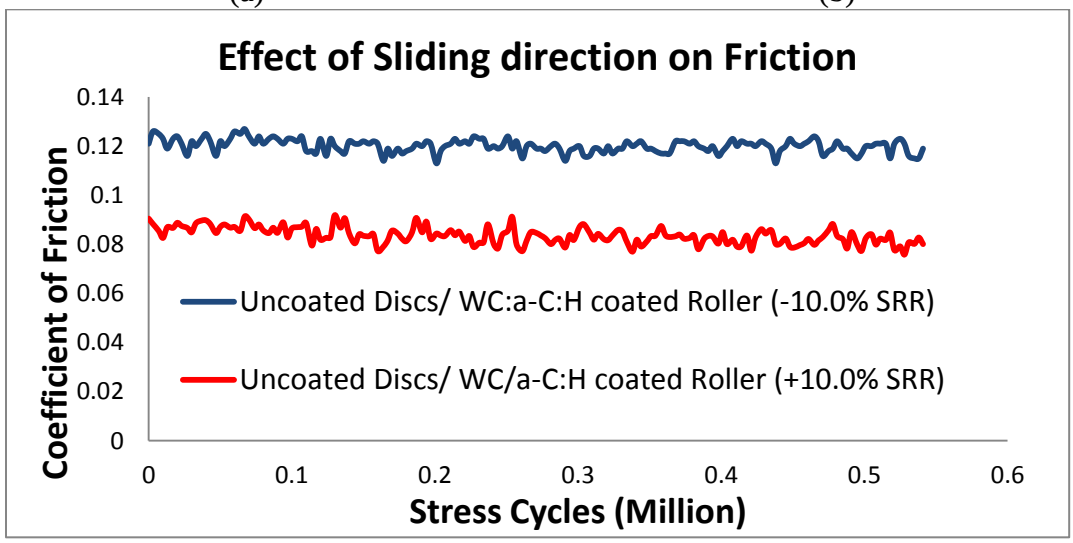

(c)

Figure 7-9: Effect of positive and negative sliding to rolling ratio on friction coefficient and coating delamination on the roller. (a). Surface of coated roller under positive SRR on the roller shows less coating delamination. (b). Surface of coated roller with negative SRR on the roller showing higher delamination and wear rate on the roller. (c). friction coefficient of samples with positive and negative 10.0% . Maximum contact stress is 2GPa and λ=0.11. Green flash shows the rolling direction and red flash shows sliding direction on the roller.

It appears that there may be a relationship between rolling/sliding coefficient of friction, and wear damage on the coating with positive and negative SRR, and consequently, central and minimum lubricant film thickness. Although the rate of wear and crack initiation appears to be higher in the negative SRR tests, this condition does not

necessary lead to a higher rate of crack propagation. Most literature studies have been performed using zero and positive slide to roll ratios that cause a higher progression rate of micropitting due a phenomenon known as hydraulic pressure crack propagation. That is, a crack generated on a surface through traction forces ahead of the rolling contact becomes filled with lubricant that becomes pressurized when traction forces work to close the crack at the trailing edge of the contact [113]. However, with negative SRR, the tensile stresses that are responsible for crack opening occur at the outlet location of the contact and hydraulic pressure crack propagation does not occur. Therefore, the rate of crack propagation is less in negative SRR than in positive or zero SRR in elastohydrodynamic lubrication.

7.6. Contact of rough surfaces and plasticity index

In general, there are two types of asperity micro-contact models: statistical and deterministic. Whereas the deterministic approach utilizes the actual surface profile to obtain film thickness and asperity pressure, surface parameters are employed to define the surface roughness in the statistical approach. Greenwood and Williamson [114] pioneered micro-contact modeling based upon the assumption of a rough surface contacting a flat surface.

In most statistical models, the mechanical behavior of each individual asperity is considered separately from the mechanical behavior of all other asperities. The cumulative effect is the sum of the behavior of all the individual asperities [115]. On the other hand, fully-coupled contact problems of rough surfaces are more mathematically complicated because the equations of elasticity must be solved for the entire body simultaneously [115].

In statistical modeling, a probability function defines the height of asperities relative to a reference plane where asperity contact can occur when their height lies above this plane.

In the elastic contact of a single sphere with an elastic half-space, the contact area varies as the two-thirds power of the applied force. However, when the asperities have an exponential distribution of heights, the real area of contact varies linearly with the applied force [115]. For a Gaussian asperity distribution, the force is nearly proportional to the real contact area over several orders of magnitude variation of the applied load. This near constant elastic contact pressure can be thought of as an "elastic hardness" in which P/A does not change with increasing approach [115].

For the case of WC/a-C:H and steel contact application of asperity contact would not yield to robust results since the materials properties of steel and WC/a-C:H are substantially different. Greenwood and Williamson also define a plasticity index as below

$$\boldsymbol{\psi} = \frac{\boldsymbol{E}^*}{\boldsymbol{H}} \sqrt{\frac{\boldsymbol{\sigma}}{\boldsymbol{R}}} \tag{7-3}$$

where ψ is plasticity index, E* is reduced modulus, H is the hardness of softer contact, σ is the r.m.s surface roughness and R is radius of asperities. Interestingly, it is the plasticity index, and not the load, which dominates the behavior of the contact [115]. Elastic behavior is observed when plasticity index is below 0.6 and any load is sufficient to cause some plastic deformation when the plasticity index is above 1.0.

Micropitting arises from the cyclic plastic deformation of asperities. Therefore, the rate of micropitting increases as opportunities for plastic deformation increase. The

plasticity index may be used to examine micropitting behavior of different surfaces to some extent. Figure 7-10 shows the overall result of coating performance on the micropitting behavior of the rollers. The best performance was achieved when WC/a-C:H was applied to a roller that ran against uncoated discs. Conversely, the worst performance was observed when black oxide coated rollers ran against black oxide coated discs. Indentation hardness and modulus values of the WC/a-C:H and the 52100 steel were reported by Evans [112] and listed in Table 7-4.

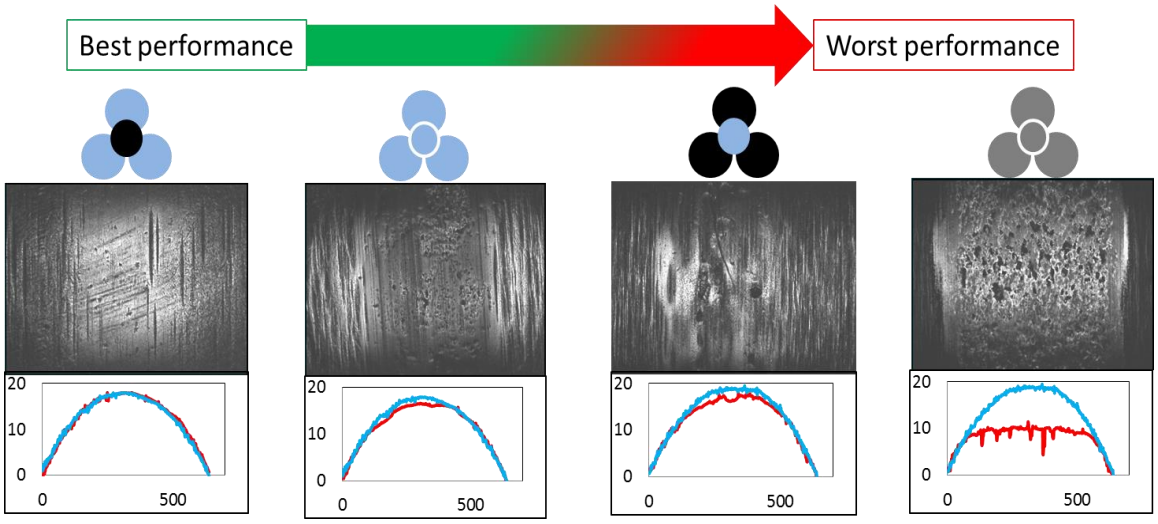

Figure 7-10: The overall performance of different combination of tribological coatings regarding micropitting resistance of the roller. From left to right: Uncoated discs/ coated roller, steel/steel contact, coated discs/uncoated roller and, black oxide/black oxide contact.

Table 7-4: Mechanical properties of WC/a-C:H coating, Black oxide coating and 52100 steel [112].

Sample	Average Hardness (GPa)	SD Hardness (GPa)	Depth Range for Average Hardness (nm)	Average Elastic Modulus (GPa)	SD Elastic Modulus (GPa)	Depth Range for Average Modulus (nm)
Untreated AISI 52100 steel	10.6	0.5	100–200	230	10	100–200
Double-bath black oxide	2.6	0.3	200–300	61	5	80–100
WC/a-C:H coating	13.1	1.5	175–225	112	25	40–60

Assuming the surface roughness and radius of asperities are the same for all samples, differences in E*/H is representative of differences in the plasticity index. Using the hardness and modulus values from Table 7-4 into equation 7-3 yields to the results presented in Table 7-5. The minimum E*/H is associated with the uncoated discs/ WC/a-C:H roller which has least rate of micropitting. The largest E*/H corresponds to the black oxide/black oxide coating that suffers the greatest amount of micropitting. Larger values of E*/H have a greater opportunity to experience plastic deformation of asperities and are therefore more prone to exhibit micropitting. The exception to this trend is the case of the WC/a-C:H coated discs running against an uncoated roller, where the large hardness difference (i.e., $H_d - H_r$) between specimens dominates. In reality, the elements under the radical in the plasticity index equation are neither equivalent for the materials pairs nor constant throughout the testing. Since the magnitude of E*/H dominates differences between the materials pairs and dynamic changes in σ/R associated with these experiments, the ratio of E*/H appears to be a promising gauge that can be used to estimate the proclivity of materials pairs to exhibit micropitting in a tribological contact.

Table 7-5: E*/H based on plasticity index for four tested contact combination.

	E^*/H
Steel/ WC/a-C:H (uncoated discs/coated roller)	6.26
Steel/Steel	11.88
WC/a-C:H/steel (coated discs/uncoated roller)	7.73
Black Oxide/Black Oxide	12.69

However, coated discs/uncoated roller has smaller plasticity index than steel/steel contact but it shows higher rate of micropitting on the roller.

CHAPTER VIII

THERMAL EFFECT OF THE COATING ON TRIBOLOGICAL BEHAVIOR OF THE CONTACT

8.1. Overview

One of the open questions from this study is why the onset of micropitting occurs earlier on DLC coating discs/uncoated roller experiments that with uncoated discs/uncoated roller experiments. In the next section, an argument will be made that the thermal properties of the DLC may be one possible reason for this.

Micropitting is a complex phenomenon influenced by mechanical issues such as vibration and sudden changes in loading, tribological issues such as sliding and lubricant film thickness, chemical issues and additives or moisture in the oil and thermal effects due to friction. Therefore micropitting is a thermo-chemical-mechanical phenomenon. Although the plasticity index can provide a perspective on the mechanical side of micropitting, thermal properties of the contact can also have a huge impact on micropitting. In the next sections, an introduction to the thermal effects of occurring in a tribological contact and their influence on micropitting will be presented.

8.2. Viscosity of oil vs. Temperature

A calculation of the lubricant film parameter (λ) is dependent on the viscosity of the oil that in turn is highly dependent on the temperature. Even small changes in

temperature cause a measurable change in lubricant film thickness. Increases in temperature reduce lubricant density and the temperature-pressure coefficient of the lubricant.

The density of a lubricant at any temperature can be approximated according to Equation (8-1) [2].

$$\boldsymbol{\rho_\theta = \rho_{15}\left(1 - 0.7\ \frac{(\theta+273)-289}{\rho_{15}}\right)} \tag{8-1}$$

Where $\boldsymbol{\rho_{15}}$ is density of lubricant at 15 ˚C and $\boldsymbol{\theta}$ is also in ˚C. $\boldsymbol{\rho_{15}}$ in return can be calculated according to equation (8-2).

$$\boldsymbol{\rho_{15} = 43.37\, log\, \nu_{40} + 805.5} \tag{8-2}$$

Where $\boldsymbol{\nu_{40}}$ is the kinematic viscosity of the lubricant at 40˚C expressed in mm/s^2.

Now it is possible to calculate the dynamic viscosity based on the kinematic viscosity and density by equation (8-3).

$$\boldsymbol{\eta_\theta = 10^{-6}\, \nu_\theta\, \rho_\theta} \tag{8-3}$$

where $\boldsymbol{\eta_\theta}$ is the dynamic viscosity of lubricant expressed in N.s/m^2 at any temperature compatible for calculation of lubricant film thickness in Hambrock-Dowson equation.

Kinematic viscosity between 40 and 100˚C can be modeled based on equation (8-4) to (8-7).

$$\boldsymbol{Log(log\, \nu_\theta + 0.7) = A.log(\theta + 273) + B} \tag{8-4}$$

Where

$$\boldsymbol{A} = \frac{\boldsymbol{Log(log\, \nu_{40} + 0.7)/Log(log\, \nu_{100} + 0.7)}}{\boldsymbol{log(\frac{313}{373})}} \tag{8-5}$$

$$\boldsymbol{B = Log(log\, \nu_{40} + 0.7) - A.log(313)} \tag{8-6}$$

where $\boldsymbol{\nu_{40}}$ is the kinematic viscosity of the lubricant at 40˚C and $\boldsymbol{\nu_{100}}$ is the kinematic viscosity of the lubricant at 100˚C expressed in mm/s^2.

Temperature changes not only effects viscosity but also influences temperature-pressure coefficient according to equation (8-7).

$$\boldsymbol{\alpha_\theta = \alpha_{38}(1 + 516(\frac{1}{\theta + 273} - \frac{1}{313}))} \tag{8-7}$$

$\boldsymbol{\alpha_{38}}$ is the pressure-viscosity coefficient of the lubricant at 38˚C.

The dynamic viscosity (η) and temperature-pressure coefficient (α) are two main properties of a lubricant that have great influence on the lubricant film thickness parameter used in the Hamrock-Dowson equation. η and α are calculable according to equations (2) to (8).

What is difficult to measure and calculate is the heat generation and temperature rise inside the contact (the flash temperature) and the heat flow and its dissipation through the oil and contacting elements.

8.3. Flash temperature

Flash temperature in elastohydrodynamic lubrication (EHL) contact is the transient temperature distributions of a lubricant and adjacent solid surfaces in the area of an EHL lubrication conjunction [116].

The heat generates from asperity contact, viscous shear of lubricant, and compressive stress due to EHL pressure. The heat dissipates through the oil and substrates. A substantial increase in temperature can significantly reduce lubricant viscosity, diminishing the thickness of the lubricant film and amplify asperity interactions.

The flash temperature is difficult to measure since it is transient and only resides in the small area of contact. However, in some cases, the flash temperature is large enough to cause tribo-chemical reactions even in low-speed sliding [117].

8.4. History of scientific work on flash temperature

There are several available models which predict the flash temperature between two rubbing parts. One of the pioneering works on frictional heating belongs to Blok in 1937 [118]. Many models are still using the fundamentals of Blok's model. Blok developed the concept of "thermal skin", the depth under the surface where the local temperature drops by 90%. Blok rationalized since the heat generation time is very short (10^{-3} to 10^{-5} S), the penetration depth of the flow of heat from the flash temperature volume has to be shallow. Eventually, Blok came up with the idea of "thermal rod model". In this model, a long rod moving against flat surface and the resulting thermal field in the rod would be one dimensional which simplifies an analytical solution.

In 1942 Jaeger [119] modified Blok's heat partition factor by equating the average temperature on both surfaces. Jaeger considered the effects of moving sources that simultaneously vary their shape, velocity and distribution of heat fluxes as a given function of time or position [116].

Archard [120] in 1959 expanded the flash temperature calculation by taking into account the size of the contact, applied load, and asperity deformation. Flash temperature calculation and modeling were continued by Kuhlmann-Wilsdorf (1987), Greenwood (1991), Tian and Kennedy (1994), and Bos and Moes (1994) [121, 122, 123, 124].

8.5. Mathematics and calculation of flash temperature

General and fundamental equations for calculation of flash temperature are presented here. For further information and details of mathematical calculations readers are suggested to study [125], [116] and [126].

When two bodies is rubbing against each other either in sliding or rolling/sliding contact mode, heat generates at the boundary and contact area between the two according to equation (8-8).

$$\boldsymbol{q_{total} = \mu p U} \tag{8-8}$$

where μ is the coefficient of friction

p is the contact pressure (which may vary within the contact area)

U is the relative sliding velocity =V2 – V1

Fourier's law for heat conduction in an isotropic solid which is moving with velocity V may be written

$$\boldsymbol{\nabla . k \nabla T + Q = \rho C \frac{DT}{Dt} = \rho C [\frac{\partial T}{\partial t} + V . \nabla T]} \tag{8-9}$$

where Q is internal heat generation rate per unit volume, k is thermal conductivity, ρ is density, and C is specific heat. If there is no internal heat generation and if k is uniform and constant:

$$\boldsymbol{k \nabla^2 T = \rho C [\frac{\partial T}{\partial t} + V . \nabla T]} \tag{8-10}$$

or

$$\boldsymbol{\nabla^2 T = \frac{1}{k} \frac{DT}{Dt}} \tag{8-11}$$

where $\boldsymbol{K = \frac{k}{\rho C}}$ is thermal diffusivity.

Analytically solving equation 8-9 and applying error function leads to equation 8-12 which is one of the major fundamental equations for calculating flash temperature. The other fundamental equation is equation (8-13).

$$\boldsymbol{\Delta T = \frac{Q/\rho C}{2\pi K r} = \frac{Q}{2\pi k r}} \tag{8-12}$$

Equation (8-12) is valid for flash temperature rise due to stationary heat source on a stationary body and for stationary heat source on moving body (or moving heat source on stationary body) equation (8-13) is applicable:

$$\boldsymbol{\Delta T = \frac{Q}{2\pi k R} e^{-V(R-x)/2K}} \tag{8-13}$$

where $\boldsymbol{R = x^2 + y^2 + z^2}$

Shape and speed of moving contact become important in the head penetration profile under the contact. There is non-dimensional term so called Peclet number (Pe) which determines depth of heat penetration in the contact bodies.

$$\boldsymbol{Pe = \frac{Vb}{2K}} \tag{8-14}$$

Low Peclet numbers (below 0.1) means stationary or low speed moving contact and high Peclet number means high speed sliding contact as it shown in Figure 8-1.

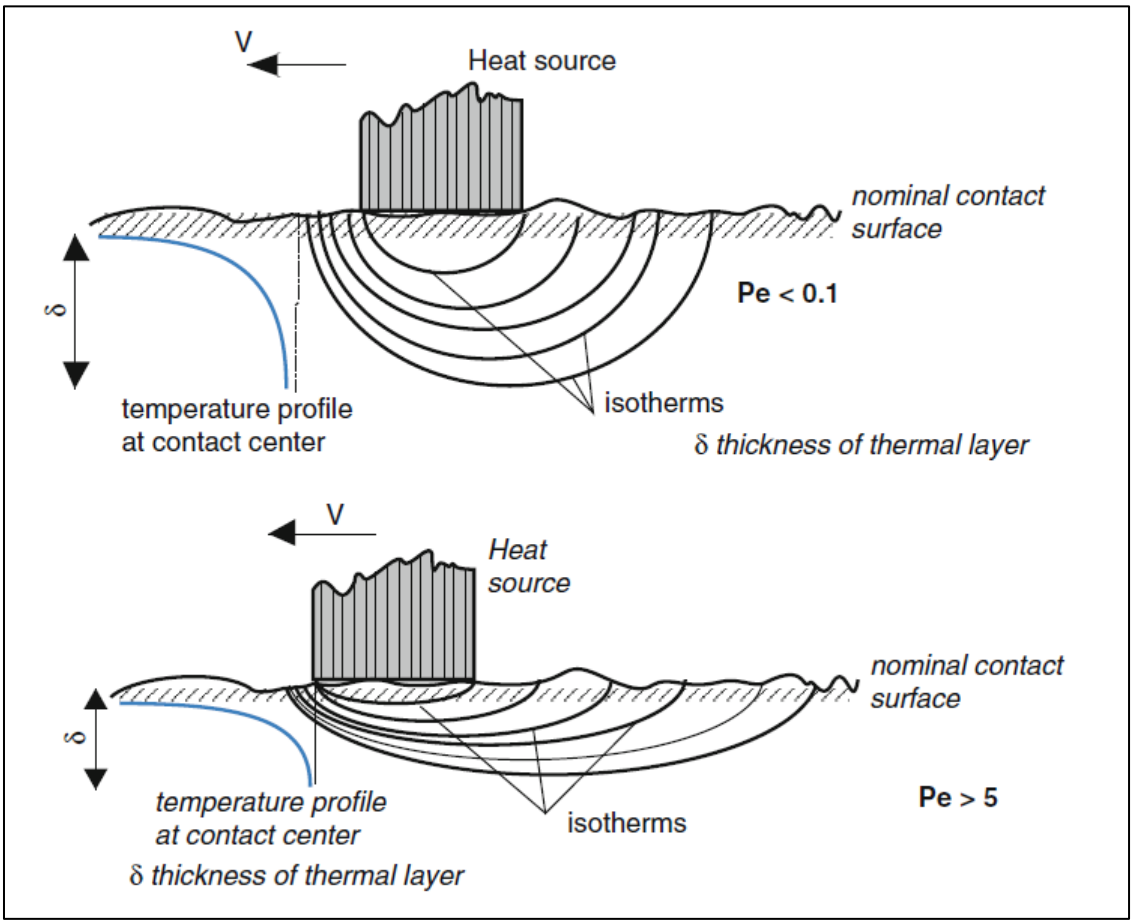

Figure 8-1: Schematic of the flash temperature thermally affected zone at low and high sliding speeds (Peclet numbers) [126].

Combination of heat source and contact shape is shown in Figure 8-2. Summary of solutions for maximum flash temperature with head source of various shapes is presented in Table 8-1. It is noted that contacting asperities that are plastically deformed have a contact pressure distribution that is approximately uniform, giving a uniform heat

flux, whereas elastic contacts have a Hertzian contact pressure distribution that results in a parabolic or semi-ellipsoidal heat flux distribution [125].

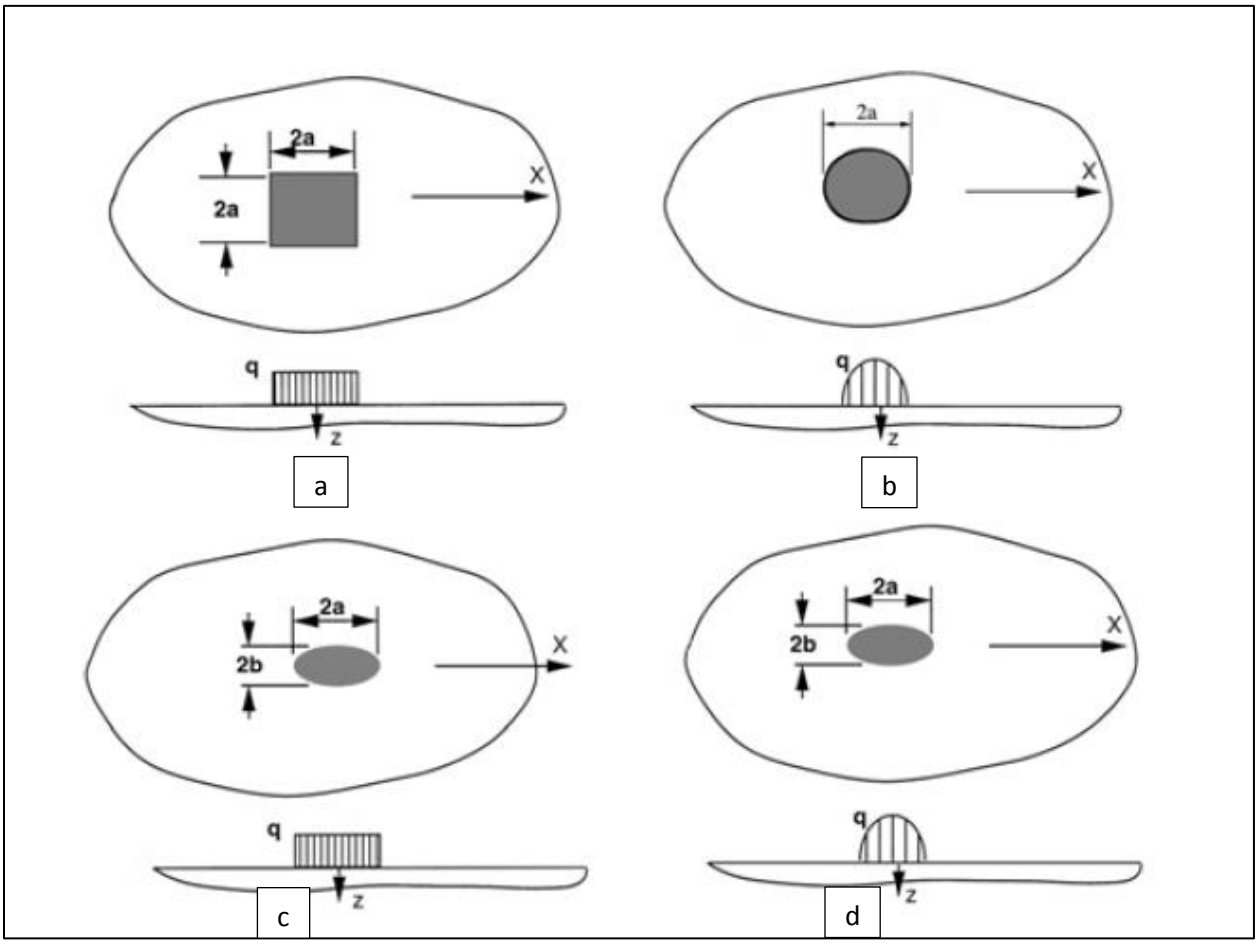

Figure 8-2: Diagrams of heat sources used in Table 6. (a) Square heat source with uniform heat flux distribution. (b) Circular heat source with parabolic heat flux distribution. (c) Elliptical heat source with uniform heat flux distribution. (d) Elliptical heat source with semi-ellipsoidal heat flux distribution [125].

Table 8-1: Expressions for Maximum Flash Temperature Rise for Various Heat Source Distributions [125]

Shape of Heat Source	Heat Flux Distribution	Figure No.	Maximum Flash Temperature Rise (Steady State)		
			Stationary or Low Speed Pe < 0.1	High Speed Pe > 10	Approximate Expression for All Velocities
Band	Uniform	12a	$\frac{2qb}{k\sqrt{\pi}}$	$\frac{2qb}{k\sqrt{\pi Pe}}$	$\frac{2qb}{k\sqrt{\pi(1+Pe)}}$
Square	Uniform	12a	$\frac{1.122qb}{k}$	$\frac{2qb}{k\sqrt{\pi Pe}}$	$\frac{2qb}{k\sqrt{\pi(1.011+Pe)}}$
Circular	Uniform	12a	$\frac{qa}{k}$	$\frac{2qa}{k\sqrt{\pi Pe}}$	$\frac{2qa}{k\sqrt{\pi(1.273+Pe)}}$
Circular	Parabolic	12b	$\frac{3\pi\bar{q}a}{8k}$	$\frac{2.32\bar{q}a}{k\sqrt{\pi Pe}}$	$\frac{2.32\bar{q}a}{k\sqrt{\pi(1.234+Pe)}}$
Elliptical	Uniform	12c	$\frac{qa}{k\sqrt{Se}}$	$\frac{2qa}{k\sqrt{\pi Pe}}$	$\frac{2qa}{k\sqrt{\pi(1.273Se+Pe)}}$
Elliptical	Semi-ellipsoidal	12d	$\frac{3\pi\bar{q}a}{8k\sqrt{Se}}$	$\frac{2.32\bar{q}a}{k\sqrt{\pi Pe}}$	$\frac{2.32\bar{q}a}{k\sqrt{\pi(1.234Se+Pe)}}$

Where $\boldsymbol{Se} = \frac{\mathbf{16}e^{\mathbf{1.75}}}{(\mathbf{3}+e^{\mathbf{0.75}})(\mathbf{1}+\mathbf{3}e^{\mathbf{0.75}})}$ and e=b/a is the aspect ratio of the elliptical source.

8.6. Partition of frictional heat

In order to determine the surface temperature of each contact, it is essential to distinguish the heat flux that is absorbed by each contact. Therefore, (neglecting the thermal functionality of the lubricant) a part of generated heat goes to body 1 that moves with velocity of V_1 and the rest goes to the body 2 which moves with velocity of V_2 relative to the contact. Therefore from equation (8-8):

$$\boldsymbol{q_1 + q_2 = q_{total} = \mu p U} \tag{8-15}$$

Let us define heat partitioning factor α:

$$\boldsymbol{q_1 = \alpha \mu p U} \text{ and } \boldsymbol{q_2 = (1 - \alpha) \mu p U} \tag{8-16}$$

8.7. General contact case

In general, it is possible to approximate partitioning factor (α) by using equations available in Table 8-1 and assuming the maximum flash temperature is equal for the two surfaces, giving [125]:

$$\boldsymbol{T_{cmax1} = T_{b1} + \Delta T_{nom1} + \Delta T_{fmax1} = T_{cmax2}} \tag{8-17}$$
$$\boldsymbol{= T_{b2} + \Delta T_{nom2} + \Delta T_{fmax2}}$$

where $\Delta T_{nom1}$is the nominal temperature rise and $\Delta T_{fmax1}$is the maximum flash temperature rise for body 1 and can be found as a linear function of an unknown heat flux q_i entering the surface and by using equations available in Table 8-1 for maximum flash temperature.

The nominal heat is the heat accumulation due to repeated and frequent heat generation due to friction. This will give an expression of the form $\Delta T_{nomi} = A_i q_i$. where A_i is the surface of the contact (in the case of rolling contact it can be assumed as contact width in circumference of the ball or roller). $\Delta T_{fmaxi} = B_i q_i$. A_i and B_i are influence coefficients that depend upon contact geometry, sliding velocity and thermal properties.

For example, the contact is circular and the pressure distribution is uniform in Table 8-1 [125]:

$$B_i = \frac{2a}{K_i\sqrt{\pi(1.273 + P_{ei})}} \tag{8-18}$$

and α can be expressed as:

$$\alpha = \frac{(T_{b2} - T_{b1}) + q_{total}(A_2 + B_2)}{q_{total}(A_1 + A_2 + B_1 + B_2)} \tag{8-19}$$

It is possible to perform the flash temperature calculation by taking into account the combined radius of curvatures and reduced modulus of the contact between two surfaces with different thermal and mechanical properties. The general solution is given by [127] as:

$$T_{fmax} = \frac{\sqrt{\pi}}{2}\frac{\mu PU}{B_{M1}\sqrt{V_1} + B_{M2}\sqrt{V_2}}\sqrt{8R^*\frac{P}{E^*}} \tag{8-20}$$

Where

$U = |V_1 - V_2|$

$B_{Mi} = \sqrt{\rho_{Mi} C_{Mi} k_{Mi}}$

U	is the local sliding velocity (m/s)
B_{Mi}	is the thermal contact coefficient of contact i
μ	is the coefficient of friction
P	is the Hertzian contact stress (MPa)

V_i is the local tangential velocity of contact i (m/s)

R^* is reduced contact radius $\frac{1}{R^*} = \frac{1}{R_1} + \frac{1}{R_2}$ (m)

E^* is effective young modulus $\frac{1}{E^*} = \frac{1}{E_1} + \frac{1}{E_2}$ (MPa)

Material properties of steel can easily be found in many references, however, material properties of DLC coatings in general are difficult to find. Moreover, the thermal properties of the coating used in this study is unknown. Table 8-2 displays some physical and thermal properties of several DLC coatings. Diamond-like carbon is a family of thin film materials possessing various amounts of C–C sp^3 bonds. Hydrogen-free DLCs, also called tetrahedrally bonded amorphous carbon (ta-C), can have the highest C-C sp^3 content (~85 %). Hydrogenated amorphous carbons (a-C:H) can be classified into four groups: 1) polymer-like a-C:H (PLCH), with 35 to 60 at. % H and up to 70% sp^3 bonds; 2) diamond-like a-C:H (DLCH), with 20–35% H and sp^3 content between 20% and 60%; 3) hydrogenated tetrahedral amorphous carbon (ta-C:H), with 70% sp^3 and 25–30 at. % H and 4) graphite-like a- C:H (GLCH), with less than 20% C-C sp^3 [128].

Table 8-2: Material and thermal properties of DLC coatings [128].

Film	Density (g/cm^3)	H (at. %)	E (GPa)	K (W/mK) at RT	θ_D (K)
PLCH	1.55	36	16	0.277	310
DLCH	1.76	28	95	0.69	584
DLCH	1.86	30	150	0.566	550
GLCH	1.8	18	···	0.374	412
GLCH	2	24	···	0.248	379
ta-C:H	2.2	30	250	0.77	···
ta-C:H	2.4	28	300	1.3	···
ta-C HCA	2.59	0	396.8	1.41	1217
ta-C single	3	0	700	2.7	···
ta-C Sbend	3	0	700	2.2	···
ta-C Sbend	3.26	0	760	3.5	···

The coating in this study is WC/a-C:H with E = 120 GPa which should have thermal properties residing between PLCH group 1 and DLCH group 2 in Table 8-2. For DLC coatings containing about 30 at% of hydrogen, the specific heat capacity (C) value was measured to be 0.97 J g^{-1} K^{-1} [129]. The mass density of DLC (ρ) is usually in the range of 1.9–3.0 g/cm^3 [129]. As a result, the thermal conductivity of DLC coatings would be about 3Wm^{-1} K^{-1}, assuming that the mass density is 2.5 g/cm^3. It has been reported that the thermal conductivity of DLC coatings was in the range of 0.7–7 W m^{-1} K^{-1}, depending on the film composition and structure [129].

Table 8-3 shows thermal properties of steel and DLC which is based on [129, 130] and used as data for calculation of the thermal contact coefficient of WC/a-C:H coating and steel.

Table 8-3: thermal properties of steel and DLC used for calculation of flash temperature.

Material	Density ρ (kg/m3)	Specific heat capacity c (J/kg.K)	Specific heat conductivity k (W/m.K)
steel	7800	440	45
DLC	2500	850	1.5

As it mentioned and it shown in Figure 8-3 , the presence of a DLC coating on one of the contact surfaces causes an increase in the flash temperature over a steel/steel contact. Although this increase in temperature happens instantly (and dissipates quickly) it should cause a decrease in the viscosity of the lubricant and a concomitant decrease in the specific lubricant film thickness in the duration of the contact. Figure 8-4 shows the dynamic viscosity of PAO ISO-10 as a function of temperature. In order to clarify the change in the specific lubricant film thickness caused by flash temperature, an example is given in next paragraph. One of the experimental tests performed in this study used a bulk or oil temperature of 40 ˚C, a maximum contact pressure of 2 GPa, and a SRR of 10.0%. Under these conditions and based upon the flash temperature calculation, the flash temperature for steel/steel contact would be around 59 ˚C and for steel/DLC contact would be 79 ˚C. The dynamic viscosity of ISO10 at 60 and 80 ˚C would be around 0.004688 and 0.002975 $N.s/m^2$ respectively. Applying these viscosities and assuming the change in the pressure-viscosity coefficient of ISO10 is negligible over this small temperature range, the decrease in specific lubricant film thickness based upon the Hamrock-Dowson equation for an entrainment mean velocity of 2 m/s, for roller and discs with surface roughness of 0.26 and 0.56 μm, would be about 25%. In other words, the use of a DLC coating on either discs or the roller could cause a 25% decrease in the specific lubricant film thickness (λ) compared with a steel/steel contact. This 25% is

hypothetical and based on mathematical calculations containing heat flow assumptions and "best guess" physical and thermal values for WC/a-C:H, but could possibly be experimentally determined with the proper tribological test equipment. Nevertheless, the estimation of the flash temperature suggests for the first time that the lubricant film thickness may actually be smaller in a DLC/steel tribological contact than in a steel/steel contact. Although the calculations suggest a decrease in the lubricant film thickness; 25% may be too large since the thermal diffusivity of oil (0.07-0.09 mm^2/s) is very low compared with steel (11-14 mm^2/s) and DLC (0.5-1 mm^2/s).

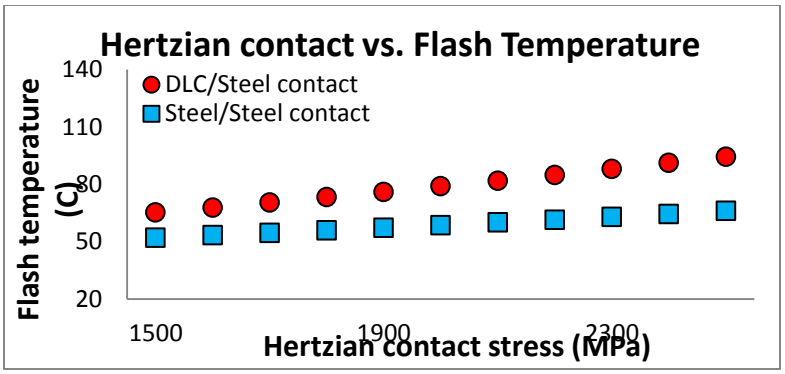

(a)

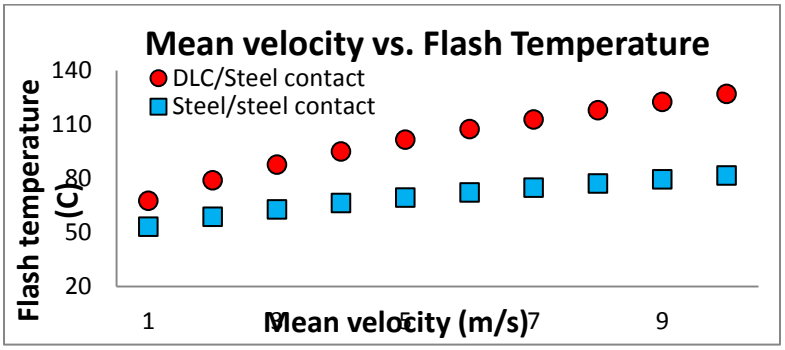

(b)

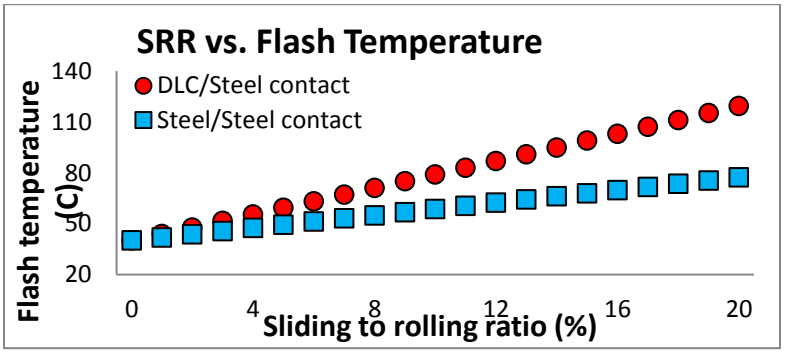

(c)

Figure 8-3: Effect of several parameters on flash temperature: (a). Effect of Hertzian contact stress on maximum flash temperature when sliding to rolling ratio is 10.0% and mean entrainment velocity is 2 m/s. (b). Effect of mean entrainment velocity on maximum flash temperature when sliding to rolling ratio is 10.0% and Hertzian contact stress is 2 GPa. (c). Effect of sliding to rolling ratio on maximum flash temperature when mean entrainment velocity is 2 m/s and Hertzian contact stress is 2 GPa.

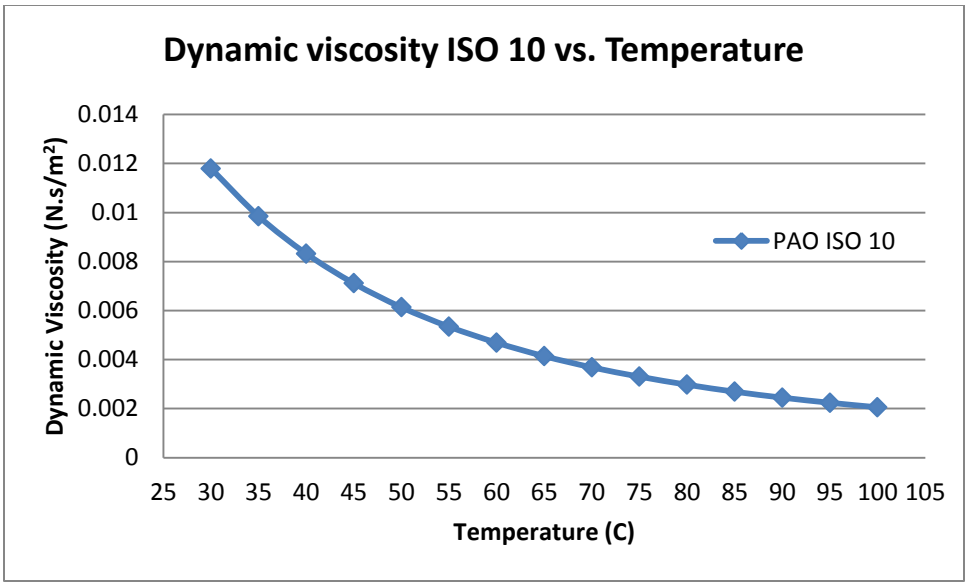

Figure 8-4: behavior of dynamic viscosity of PAO ISO 10 by increase in temperature

8.8. Partition of frictional heat (case study: Micropitting rig)

Assuming a maximum Hertzian contact stress of 2GPa, SRR = 10.0%, mean entrainment velocity of 2 m/s, and mean friction coefficient of 0.1, it is possible to estimate the partition of frictional heating based on equation (19) and the last equation in Table 8-1 for steel/steel and DLC/steel contacts. The calculation shows that whereas the heat dissipates equally between the two counter parts in steel/steel contact, almost 88% of the heat is absorbed by the steel in the DLC/steel contact.

8.9. Thermal diffusivity of steel and DLC

Up to this point, how the DLC coating causes an increase in flash temperature and a decrease in specific lubricant film thickness has been examined. The consequence of a thinner lubricant film thickness in a DLC/steel contact is that more asperities interact in the contact zone, which leads to higher rate of wear or micropitting on the steel counter-face. The occurrence of wear or micropitting depends upon several factors such as

plasticity index, roughness, or slide to roll ratio. Besides the mechanical and rheological effects that the DLC has on the lubricant, DLC also has a thermal diffusivity effect on the coated substrate as well.

Thermal conductivity, thermal diffusivity and specific heat capacity define a material's ability to store and transfer heat. Thermal diffusivity ($K = \frac{k}{\rho C}$) is a thermo-physical term which shows the ability of a material to conduct thermal energy relative to its ability to store thermal energy. In a substance with a high thermal diffusivity, heat moves rapidly through the material because the substance conducts heat quickly relative to its volumetric heat capacity or 'thermal bulk'. Based upon the information provided in Table 8-3, the thermal diffusivity of steel is close to 13.11 mm^2/s, DLC is about 0.7 mm^2/s, and oil is about 0.08 mm^2/s.

In this study, the lubricant film thickness compared to the surface roughness is small and the occurrence of micropitting has been studied in boundary lubrication regime ($0.1 < \lambda < 0.2$). Therefore, the convective heat flow by the oil would be negligible compared to conduction of heat by the oil and the contacting surfaces. On the other hand, both the thermal conductance and thermal diffusivity values of the DLC are probably considerably smaller than steel. It is therefore expected that most of the frictional heating generated in the contact will flow through the steel counter-face when it is in contact with a DLC-coated substrate. Although the heat generation due to contact is transient and of very short duration, it could still affect phase changes on the surface of steel. Elevated local temperatures could promote a rapid diffusion of carbon from the martensite matrix

of the steel, resulting in the creation of a heterogeneous surface region containing ferrite and cementite or other FeC phases.

In the design of the MPR test rig, a surface element on the roller experience a Hertizan contact every 12.5 mm since the roller has three contact points with the discs in each revolution. On the other hand, a surface element on a disc would experience a Hertizan contact every 170 mm. At a rotational speed of 2 m/s, elements of surface areas would experience thermal shocks every 6.25 ms and 85 ms on the roller and disc, respectively.

Apart from the time interval between the thermal shocks, the respective volumes of the disc and roller have an impact on the amount of heat that can be absorbed and dissipated through the components. Moreover, during operation, two of the three discs are partially submerged in the oil sump, but the roller, which is in the middle of three discs, is relatively thermally isolated from the sump. Therefore when discs are coated with the DLC the amount of frictionally-produced-heat that flows into the uncoated roller should be considerably larger than the amount of heat that is dissipated in uncoated discs when the roller is coated with the DLC. The results of this qualitative thermal analysis are consistent with the observations that DLC coated discs causes an earlier onset of micropitting on an uncoated roller than when uncoated discs are tested against uncoated rollers with the same test rig parameters. Conversely, when the DLC is applied to the roller, the discs do not exhibit micropitting but can experience an amount of abrasive wear that is consistent with the surface roughness of and hardness difference between the DLC coated roller and the uncoated 52100 steel.

Results of this analysis supports application testing results that find that bearings with WC/a-C:H coated rolling elements and uncoated raceways exhibit superior performance to bearings with uncoated rollers and raceways. Furthermore, these results also provide insight into why bearings with DLC coated raceways and uncoated rollers exhibit inferior performance to bearings with uncoated rollers and raceways. That is, the coating on the raceways restrict the flow of generated heat to the housing and shaft through the outer and inner bearing rings respectively, resulting in a higher temperature rise in the thermally (relatively) isolated rolling elements. Elevated temperatures in the rolling elements should increase the kinetics of C diffusion from the martensite matrix, and along with high pressures in the contact, driving phase changes in the near-surface region that can accelerate the onset of surface fatigue mechanisms responsible for micropitting and macropitting.

CHAPTER IX

SUMMARY AND CONCLUSION

The objective of this study was to evaluate the ability of a WC/a-C:H coating specifically optimized for rolling contact durability to mitigate micropitting wear on bearing steels. Through the pursuit of this study, tribological conditions in the MPR test rig were varied in order to determine the combination of parameters that produce micropitting in uncoated steel specimens and the combination of parameters where abrasive wear dominates. Hardness difference between the discs and rollers was found to greatly influence the amount of micropitting and abrasive wear in both regimes. But samples with rougher surfaces only experienced abrasive wear.

Tests conducted with the coating applied on rough surface (Rq = 0.56 μm) specimens increased the rate of abrasive wear dramatically on the uncoated counterpart. On the other hand, tests conducted with the coating on smooth surface specimens produced a rate of wear on the uncoated counterfaces that was comparable to that realized with uncoated steel contacts.

Decrease in the roughness of contacting surfaces depends on the relative hardness of counterparts. Generally, there is considerably less change in the roughness of WC/a-C:H coated surface and considerably higher change in the roughness of the uncoated counterpart, especially in cases where the coated component has a rough surface with

sharp asperities. Applying the coating on isotropically finished surfaces decreases rate of wear or change in roughness of uncoated part substantially to the steel/steel contact level.

Compared to steel/steel contact, applying the coating on smooth-finished-discs leads to an increase in the rate of micropitting of the uncoated roller. However, when the coating is applied to the smooth rollers, micropitting damage on both the roller and uncoated disc samples was mitigated.

Results of friction studies of this coating shows there is almost no adhesive wear between the coating and steel counterpart which attributed in a low chemical affinity between steel and DLC. Therefore, unlike steel/steel contact, there is almost no increase in friction coefficient between DLC and steel when the entrainment velocity decreases gradually to zero and in boundary lubrication regime.

The overall result of micropitting testing in this study shows that micropitting is much more pronounced when discs have rougher and sharper asperities in steel/steel contact. Applying the coating on the roller can wear the asperities on the surface of discs and smoothen the surface of a disc, increase the real contact area and decreases the Hertzian contact stress and eventually increase the surface fatigue life of the system.

Although rate of abrasive wear of the uncoated counterpart decreases substantially by applying the coating on the smooth surface, the uncoated counterpart still undergoes an infinitesimal abrasive wear rate. This small amount of material removal from the surface appears to impede the accumulation of plastically deformed layers and therefore fatigue initiation sites on the surface of uncoated counterpart.

The contact stress and number of stress cycles that initiated wear of a WC/a-C:H coating are found to depend upon the finishing quality of the roller prior to the application of the coating, the lambda value, and the slide-to-roll ratio.

Severe wear of the coating was found to occur only when the substrate surface roughness was high (i.e., R_q= 0.56 μm). When the roller surface roughness was lower (R_q = 0.26 μm), the coating was found to be able to withstand more than 30 million cycles in boundary lubrication conditions when the contact stress was less than 2 GPa. In experiments performed with 0% SRR and R_a = 0.2 μm rollers, coating wear did not occur at contact stresses less than 2 GPa. Roller wear was found to initiate with boundary lubrication conditions at contact stresses around 2 GPa when a negative slide-to-roll ratio of 10% was used.

The most important differences in the tribological behavior of steel/DLC contact and steel/steel contact are hardness difference and the thermal effect of the coating. One of the most important questions of this research was why the coated disc causes higher rate of micropitting on the roller but coated roller cannot generate surface fatigue on discs. The answer derived in this research is believed to be associated with the different thermal properties of DLC and steel. DLC is thermally isolating material compared to steel and when these two materials come into contact, most of the heat generated at the contact should be absorbed by the steel counterpart. In case of coated discs/uncoated roller, the heat capacity of system (only the roller) is not sufficient to dissipate the heat without causing phase changes on the surface of roller. On the other hand, in uncoated discs/coated roller testing, much more generated heat should dissipate through the discs decreasing the local temperature that could drive phase changes on the surface of rollers.

This hypothesis is consistent with application testing results that find that bearings with WC/a-C:H coated rolling elements and uncoated raceways exhibit superior performance to bearings with uncoated rollers and coated raceways [131] Furthermore, these results also provide insight into why bearings with DLC coated raceways and uncoated rollers exhibit inferior performance to bearings with uncoated rollers and raceways [131]. That is, the coating on the raceways restricts the flow of generated heat to the housing and shaft through the outer and inner bearing rings respectively, resulting in a higher temperature rise in the thermally (relatively) isolated rolling elements. Elevated temperatures in the rolling elements should increase the kinetics of C diffusion from the martensite matrix, and along with high pressures in the contact, driving phase changes in the near-surface region that can accelerate the onset of surface fatigue mechanisms responsible for micropitting and macropitting.

Based upon the results of this research project, it is concluded that a WC/a-C:H coating deposited by CFUMS on the rollers of bearings provides an effective, and possibly unparalleled means of mitigating micropitting wear of raceways. Importantly, the tests in this research were conducted in synthetic base oils without extreme pressure or anti-wear additives. Positive or negative synergies between the WC/a-C:H material and sulfur-based additives are the focus of another study, but will undoubtedly influence the micropitting mitigation capabilities of bearings with WC/a-C:H coated rollers.

Although the microstructural architecture of the WC/a-C:H coating was optimized for cyclic Hertzian contact, it was revealed in this research that the coating can experience a stress/cycle fatigue limit. This limit was found to greatly depend upon the slide/roll ratio. While rolling element bearings generally have small slide/roll ratios,

gears do not. One implication of this research is that the onset of crack initiation and propagation in WC/a-C:H should occur more rapidly in gears than in bearings, and the wear rate of the WC/a-C:H should be greater in the dedendum of a gear tooth (Figure 9-1) where a negative slide/roll ratio exists.

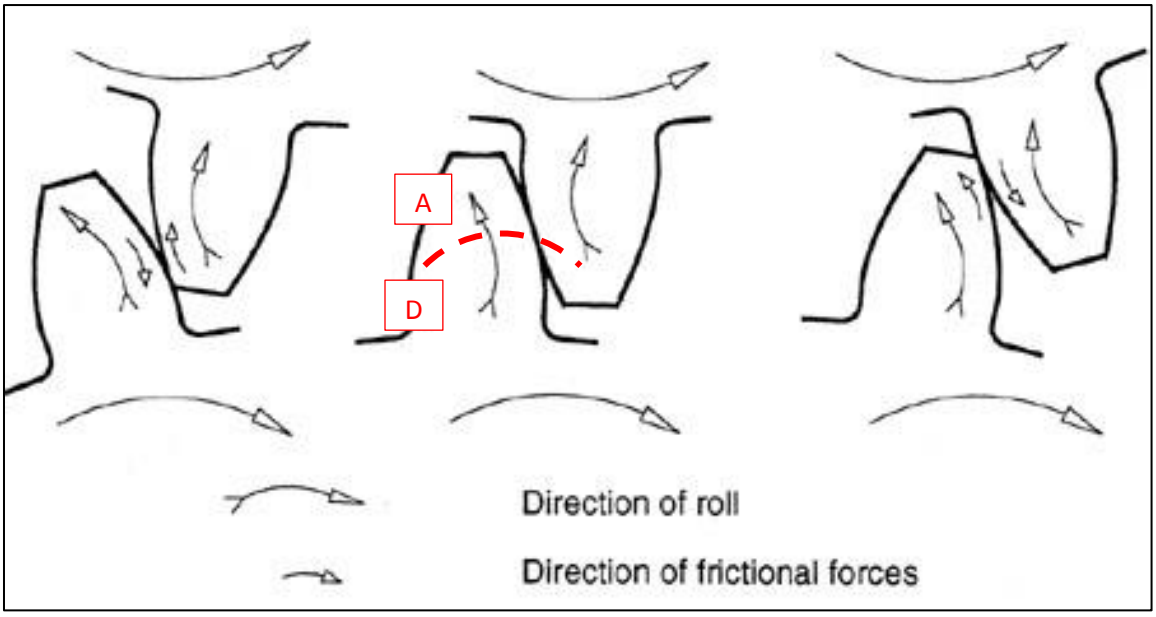

Figure 9-1: Graphical representation of the pitch line and dedendum on a gear tooth. A is represented addendum an D is represented of dedendum where negative SRR occurs [132]

REFERENCES

[1] B. 7848, "Wear and damage to gear teeth - Terminology.," London: British, Feb 1996.

[2] 2. ISO/TR 15144-1, "Calculation of micropitting load capacity of cylendrical spur and helical gears. part 1: Introduction and basic principles," Switzerland, 2010.

[3] Oila,A., Shaw, B. A., Aylott, C. A., and Bull, S. J., "Martensite decay in micropitted gears," Proceedings of the Institution of Mechanical Engineers, Part J: Journal of Engineering Tribology, vol. 219, pp. 77-83, 2005.

[4] OILA, A., BULL J. S., "Phase transformations associated with micropitting in rolling/sliding contacts," JOURNAL OF MATERIALS SCIENCE, vol. 40, pp. 4767-4774, 2005.

[5] Oila, A., Bull, S. J., "Assessment of the factors influencing micropitting in rolling/sliding contacts," wear, vol. 258, pp. 1510-1524, 2005.

[6] Zafosnik, B.,Glodez, S., Ulbin, M., Flasker,J., "A fracture mechanics model for the analysis of micro-pitting in regard to lubricated rolling–sliding contact problems," International Journal of Fatigue, vol. 29, p. 1950–1958, 2007.

[7] Fabre, A., Barrallier, L., Desvignes, M. Evans, H. P. and Alanou, M. P. , "Microgeometrical influences on micropitting fatigue damage: multi-scale analysis," Proceedings of the Institution of Mechanical Engineers, Part J: Journal of Engineering Tribology, vol. 225, pp. 419-427, 2011.

[8] Winter, H. , Weiss, T. , "Some Factors Influencing the Pitting, Micro-Pitting (Frosted Areas) and Slow Speed Wear of Surface Hardened Gears," J. Mech. Des., vol. 103, no. 2, pp. 499-505, 1981.

[9] Muroga, A., Hiroyasu, S., "Analysis of rolling contact fatigued microstructure using focused ion beam sputtering and transmission electron microscopy observation," Scripta Metallurgica et Materialia, vol. 33, no. 1, pp. 151-156,

1995.

[10] Li, S.,Kahraman, A., "A micro-pitting model for spur gear contacts," International Journal of Fatigue, vol. 59, pp. 224-233, 2014.

[11] Li, S., Kahraman, A., "A physics-based model to predict micro-pitting lives of lubricated point contacts," International Journal of Fatigue, vol. 47, pp. 205-215, 2013.

[12] Martins, R., Seabra, J., Magalhaes, L., "Austempered ductile iron (ADI) gears: Power loss, pitting and micropitting," wear, vol. 264, pp. 838-849, 2008.

[13] Cardoso, N.F.R., Martins, R.C., Seabra, J.H.O., Igartua, A., Rodrıguez, J.C., Luther, R., "Micropitting performance of nitrided steel gears lubricated with mineral and ester oils," Tribology International, vol. 42, pp. 77-87, 2009.

[14] S. Way, "Pitting due to Rolling Contact," J. of Appl. Mech., vol. 57, pp. A49-A58, 1935.

[15] T. E. Tallian, "On competing failure modes in rolling contact," ASLE TRANACTIONS, vol. 10, pp. 418-439, 1967.

[16] Tokuda, M., Nagafuchi, M., Tsushima, N. and Muro, H., "Observations of the peeling mode of failure and surface-originated flaking from a ring to ring rolling contact fatigue tet rig," in Rolling contact fatigue testing of bearing steel, Phoenix, Arizona: ASTM SPECIAL TECHNICAL PUBLICATION 771, May 1981, pp. 150-165.

[17] K. L. Johnson, "The strength of surfaces in rolling contact," Proceedings of the Institution of Mechanical Engineers, Part C: Journal of Mechanical Engineering Science, vol. 203, pp. 151-163, 1989.

[18] Y. Akamatsu, "Peeling damage due to rolling contact fatigue," Society of Automotive Engineers (SAE technical paper series), 1989.

[19] P.J.L. Fernandes, C. McDuling, "Surface contact fatigue failures in gears," Engineering Failure Analysis, vol. 4, no. 2, p. 99–107, 1997.

[20] P. Fernandes, "Contact fatigue in rolling-element bearings," Engineering Failure Analysis, vol. 4, no. 2, p. 155–160, 1997.

[21] Nelias, D., Dumont, M. L., Champiot, F., Vincent, A., Girodin, D., Fougeres, R.,

Flamand, L., "Role of Inclusions, Surface Roughness and Operating Conditions on Rolling Contact Fatigue," Journal of Tribology, vol. 121, pp. 240-251, 1999.

[22] Graham, R. C., Olver, A., Macpherson, P. B., "An Investigation into the mechanism of pitting in high-hardness carburized steels," in ASME Conference, Century 2 International Power Transmissions & Gearing, San Francisco, 1981.

[23] Webster, M. N. & Norbart, C. J. J., "An Experimental Investigation of Micropitting Using a Roller Disk Machine," Tribology Transaction, vol. 38, no. 4, pp. 883-89, 1995.

[24] Morales-Espejel, G. E. and Brizmer, V. , "Micropitting Modelling in Rolling–Sliding Contacts:Application to Rolling Bearings," Tribology Transactions, vol. 54, pp. 625-643, 2011.

[25] Berthe, D., Flamand, L., Foucher D. and Godet, M., "Micropitting in Hertzian Contacts," Journal of Tribology, vol. 102, no. 4, pp. 478-489, 1980.

[26] Zhou, R. S., Cheng, H. S., Mura, T., "Micropitting in Rolling and Sliding Contact Under Mixed Lubrication," Journal of Tribology, vol. 111, pp. 605-613, 1989.

[27] K. L. Johnson, Contact Mechanics, Cambridge: Cambridge University Press, 1987.

[28] V. Popov, Contact Mechanics and Friction, Verlag Berlin Heidelberg: Springer, 2010.

[29] L. Houpert, "An Engineering Approach to Hertzian Contact Elasticity—Part I," Journal of Tribology, vol. 123, no. 3, pp. 582-588, 2000.

[30] L. Houpert, "An Engineering Approach to Non-Hertzian Contact Elasticity- Part-II," Journal of Tribology, vol. 123, pp. 589-594, 2001.

[31] A. Minato-ku, JIS B 0601: Geometrical Product Specificaions (GPS)-Surface texture: Profile method- Terms, definitions and surface texture parameters, Japanese Standards Association, 2013.

[32] "Roughness (2D) parameter," Olympus, [Online]. Available: http://www.olympus-ims.com/en/knowledge/metrology/roughness/2d_parameter/.

[33] B. Bhushan, "Surface Roughness Analysis and Measurement Techniques," in

Modern Tribology Handbook, New York, CRC Press LLC, 2001.

[34] Abbott, E.J. and Firestone, F.A., "Specifying surface quality," Mechanical Engineerng, vol. 55, pp. 569-572, 1933.

[35] B. Bhushan, "Contact mechanics of rough surfaces in tribology: multiple asperity contact," Tribology Letters, vol. 4, pp. 1-35, 1998.

[36] Woo, K.L. and Thomas, T.R., "Contact of rough surfaces: A review of experimental work," Wear, vol. 58, no. 2, pp. 331-340, 1980.

[37] P. Jost, " "Lubrication (tribology)." London: Her Majesty's Stationary Office (1966)".

[38] Taylor, R. and Wang, Y. Y., "Lubrication regimes and Tribological Properties of Fire-Resistance Hydraulic Fluids," Lubrication Engineering, vol. 40, no. 1, pp. 44-50, 1983.

[39] C. Barus, "Isothermals, isopiestics, and isometrics relative to viscosity," American Journal of Science, vol. 45, no. 3, pp. 87-96, 1893.

[40] R. Larsson, "EHL Film Thickness Behavior," in Encyclopedia of Tribology, New York, Springer, 2013, pp. 817-827.

[41] H. M. Martin, "Lubrication of gear teeth," Engineering, vol. 102, pp. 119-121, 1916.

[42] A. N. Grubin, "Fundamentalso f the hydrodynamict heory of lubrication of heavily loaded cylindrical surface," In K. F. Ketova (ed.) Investigation of the Contact of Machine Components, Central Scientific Research Institute for Technology and Mechanical Engineering, Moscow, Book 30,DSIR Translation 337, pp. 115-16, 1949.

[43] Hamrock, B. J. and Dowson, D., "Isothermal Elastohydrodynamic Lubrication of Point Contacts: Part 1—Theoretical Formulation," Journal of Tribology, vol. 98, no. 2, pp. 223-228, 1976.

[44] Hamrock, B. J. and Dowson, D., "Isothermal Elastohydrodynamic Lubrication of Point Contacts: Part III—Fully Flooded Results," Journal of Tribology, vol. 99, no. 2, pp. 264-275, 1977.

[45] Hamrock, B. J. and Dowson, D., "Isothermal Elastohydrodynamic Lubrication of

Point Contacts: Part II—Ellipticity Parameter Results," Journal of Tribology, vol. 98, no. 3, pp. 375-381, 1976.

[46] Hamrock, B. J. and Dowson, D., "Isothermal Elastohydrodynamic Lubrication of Point Contacts: Part IV—Starvation Results," Journal of Tribology, vol. 99, no. 1, pp. 15-23, 1977.

[47] Dowson, D. & Higginson, G. R, "A numerical solution to the elastohydrodynamic problem," Journal of Mechanical Engineering Science, vol. 1, no. 1, pp. 6-15, 1959.

[48] B. Hamrock, Fundamentals of Fluid Film Lubrication, New York: McGraw-Hill, 1994.

[49] Cann, P.,Ioannides, E., Jacobson, B., Lubrecht, A.A., "The lambda ratio – a critical re-examination," Wear, vol. 175, pp. 177-188, 1994.

[50] B. Jacobson, "Thin film lubrication of real surfaces," Tribology International, vol. 33, no. 3-4, pp. 205-210, 2000.

[51] Lubrecht, A. A.,Venner, C. H. and Colin, F., "Film thickness calculation in elasto-hydrodynamic lubricated line and elliptical contacts: The Dowson, Higginson, Hamrock contribution," Proceedings of the Institution of Mechanical Engineers, Part J: Journal of Engineering Tribology, vol. 223, p. 223: 511, 2009.

[52] J. Vetter, "60 years of DLC coatings: Historical highlights and technical review of cathodic arc processes to synthesize various DLC types, and their evolution for industrial applications," Surface & Coatings Technology, vol. 257, p. 213–240, 2014.

[53] A. E. Christophe Donnet, Tribology of Diamond-Like Carbon Films: Fundamentals and Applications, Springer, 2008.

[54] G. L. Doll, "Improving the Performance of Rolling Element Bearings with Nanocomposite Tribological Coatings," SAE Technical Paper, 2006.

[55] Holmberg, k. and Matthews, A., Coatings Tribology: Properties, Mechanisms, Techniques and Applications in Surface Engineering (Tribology and interface engineering series, v56), Elsevier, 2009.

[56] Franklin, S. E., Baranowska, J., "Conditions affecting the sliding tribological performance of selected coatings for high vacuum bearing applications," Wear,

vol. 263, p. 1300–1305, 2007.

[57] Vanhulsel, A., Velasco, F., Jacobs, R., Eersels, L., Havermans, D., Roberts, E.W., Sherrington, I., Anderson, M.J., Gaillard, L., "DLC solid lubricant coatings on ball bearings for space applications," Tribology International, vol. 40, p. 1186–1194, 2007.

[58] Jiang. J. C., Meng, W. J., Evans A. G., Cooper C. V., "Structure and mechanics ofW-DLC coated spur gears," Surface and Coating Technology, vol. 176, pp. 50-56, 2003.

[59] Kalin, M., Vižintin, J., "The tribological performance of DLC-coated gears lubricated with biodegradable oil in various pinion/gear material combinations," Wear, vol. 259, pp. 1270-1280, 2005.

[60] Kano, M., Tanimoto, I., "Wear mechanism of high wear-resistant materials for automotive valve trains," Wear, vol. 151, pp. 229-243, 1991.

[61] Cruz, R., Rao, J., Rose, T., Lawson, K., Nicholls, J. R., "DLC-ceramic multilayers for automotive applications," Diamond and Related Materials, vol. 15, p. 2055–2060, 2006.

[62] Tung, S.C., Gao, H., "Tribological characteristics and surface interaction between piston ring coatings and a blend of energy-conserving oils and ethanol fuels," Wear, vol. 255, pp. 1276-1285, 2003.

[63] Etsion, I., Halperin, G., Becker, E., "The effect of various surface treatments on piston pin scuffing resistance," Wear, vol. 261, pp. 785-791, 2006.

[64] M. Kano, "Super low friction of DLC applied to engine cam follower lubricated with ester-containing oil," Tribology International, vol. 39, p. 1682–1685, 2006.

[65] Hershberger, J., Ozturk, O., Ajayi, J. B., Woodford, J. B., Erdemir, A., Erck, R. A., Fenske, G. R., "Evaluation of DLC coatings for spark-ignited direct-injected fuel systems," Surface and Coating Technology, vol. 179, p. 237–244, 2004.

[66] Dai, M., Zhou, K., Yuan, Z., Ding, Q., Fu, Z., "The cutting performance of diamond and DLC-coated cutting tools," Diamond and Related Materials, vol. 9, pp. 1753-1757, 2000.

[67] Sato, T., Besshi, T., Tsutsui, I., Morimoto, T., "Anti-galling property of a diamond-like carbon coated tool in aluminium sheet forming," Journal of

Materials Processing Technology, vol. 104, pp. 21-24, 2000.

[68] Shi, B., Ajayi, O. O., Fenske, G., Erdemir, A., Liang, H., "Tribological performance of some alternative bearing materials for artificial joints," Wear, vol. 255, p. 1015–1021, 2003.

[69] Sheeja, D., Tay, B. K., Nung, L. N., "Feasibility of diamondlike carbon coatings for orthopaedic applications," Diamond and Related Materials, vol. 13, pp. 184-190, 2004.

[70] A. H. Tan, "Corrosion and tribological properties of ultra-thin DLC films with different nitrogen contents in magnetic recording media," Diamond and Related Materials, vol. 16, pp. 467-472, 2007.

[71] Zhao, X., Bhushan, B., "Comparison studies on degradation mechanisms of perfluoropolyether lubricants and model lubricants," Tribology Intenational, vol. 9, pp. 187-197, 2000.

[72] Gatzen, H. H. and Beck, M., "Tribological investigations on micromachined silicon sliders," Tribology International, vol. 36, p. 279–283, 2003.

[73] Numata, T., Nanao, H., Mori, S., Miyake, S., "Chemical analysis of wear tracks on magnetic disks by TOF-SIMS," Tribology International, vol. 36, pp. 305-309, 2003.

[74] Kodali, P.,Walter, K. C.,Nastasi, M., "Investigation of mechanical and tribological properties of amorphous diamond-like carbon coatings," Tribology International, vol. 30, no. 8, pp. 591-598, 1997.

[75] Evans, R. D.,Doll, G. L., Morrison Jr, P. W., Bentley, J., More, K. L., Glass, J. T., "The effects of structure, composition, and chemical bonding on the mechanical properties of Si-aC: H thin films," Surface and Coatings Technology, vol. 157, no. 2-3, pp. 197-206, 2002.

[76] Meng, W. J., Gillispie, B. A. , "Mechanical properties of Ti-containing and W-containing diamond-like carbon coatings," Journal of applied physics, vol. 84, no. 8, pp. 4314-4321, 1998.

[77] Wang, R., Mercer, C.,Evans, A.G.,Cooper, C.V.,Yoon, H.K., "Delamination and spalling of diamond-like-carbon tribological surfaces," Diamond and Related Materials, vol. 11, pp. 1797-1803, 2002.

[78] Podgornik, B.,Jacobson, S., Hogmark, S., "LC coating of boundary lubricated components—advantages of coating one of the contact surfaces rather than both or none," Tribology International, vol. 36, no. 11, p. 843–849, 2002.

[79] B. Podgornik,Vizintin, J., Jacobson, S., Hogmark, S., "Tribological behaviour of WCyC coatings operating under different lubrication regimes," Surface and coating technology, Vols. 177-178, p. 558–565, 2004.

[80] Manier, C.A., Theiler, G.,Spaltmann, D.,Woydt, M.,Ziegele, H., "Benchmark of thin film coatings for lubricated slip-rolling contacts," Wear, vol. 268, no. 10-11, p. 1442–1454, 2010.

[81] Dimofte, F. and Krantz, T.L., "Tests of bearings and gears with PVD coatings for aerospace transmissions; results and problems," in Proceedings of the 3rd International Conference on Manufacturing Engineering (ICMEN), Chalkidiki, Greece, 2008.

[82] Kalin,M., Vizintin, J., "Differences in the tribological mechanisms when using non-doped, metal-doped (Ti, WC), and non-metal-doped (Si) diamond-like carbon against steel under boundary lubrication, with and without oil additives," Thin solid films, vol. 515, p. 2734–2747, 2006.

[83] Kalin, M., Vizintin, J., "A comparison of the tribological behaviour of steel/steel, steel/DLC and DLC/DLC contacts when lubricated with mineral and biodegradable oils," Wear, vol. 261, pp. 22-31, 2005.

[84] Dearnley, P. A., Elwafi, A. M., Chittenden, R. J., Barton, D. C., "Wear and friction of diamondlike-carbon coated and uncoated steel roller bearings under high contact pressure oil lubricated rolling/sliding conditions," Journal of Tribology, pp. 021101-1-11, April 2014.

[85] Moorthy, V. and Shaw, B. A., "An observation on the initiation of micro-pitting damage in as-ground and coated gears during contact fatigue," Wear, vol. 297, pp. 878-884, 2013.

[86] Moorthy, V., Shaw, B. A., "Effect of as-ground surface and the BALINIT C and Nb–S coatings on contact fatigue damage in gears," Tribology International, vol. 51, p. 61–70, 2012.

[87] A. Oliva, "Historical Overview on the Fundamentals of Sputtering," Materials Modification by High-fluence Ion Beams, vol. 155, pp. 31-81, 1989.

[88] Kelly, P. J., Arnell, R.D. , "Magnetron sputtering: a review of recent developments and applications," Vacuum, vol. 56, pp. 159-172, 2000.

[89] O'Brien, J., Arnel,l R. D., "The production and characterisation of chemically reactive porous coatings of zirconium via unbalanced magnetron sputtering," Surface and Coatings Technology, Vols. 86-87, part 1, pp. 200-206, 1996.

[90] Kelly, P.J., Arnell, R. D., "The influence of magnetron configuration on ion current density and deposition rate in a dual unbalanced magnetron sputtering system," Surface and Coatings Technology, Vols. 108-109, p. 317–322, 1998.

[91] Monaghan, D. P., Teer, D. G., Laing, K. C., Efeoglu, I., Arnell, R. D., "Deposition of graded alloy nitride films by closed field unbalanced magnetron sputtering," Surface and Coatings Technology, vol. 59, no. 1-3, pp. 21-25, 1993.

[92] Fox, V., Hampshire, J., Teer, D. G., "MoS2/metal composite coatings deposited by closed-field unbalanced magnetron sputtering: tribological properties and industrial uses," Surface and Coatings Technology, vol. 112, no. 1-3, p. 118–122, 1999.

[93] Eckels, M., Kotzalas, M.N., Doll, G.L., "Attaining high levels of bearing performance with a nanocomposite diamond-like carbon coating.," Tribology Transactions, vol. 56, no. 3, pp. 410-416, 2013.

[94] Evans, R.D., Shiller, P.J., Howe, J.Y., "Adhesion of tungsten carbide reinforced amorphous hydrocarbon thin films (WC/aC: H) to steel substrates for tribological applications," Journal of Applied Physics, vol. 109, no. 2, p. 023518, 2011.

[95] Scharf, T. W., Romanes, M. C., Mahdak, K. C., Hwang, J. Y., Banerjee, R., Evans, R. D. Doll, G. L., "Atomic-scale structure and composition of tungsten carbide reinforced diamondlike carbon films," Applied Physics Letters, vol. 93, no. 15, pp. 151909-151909-3, 2008.

[96] C. Strondl, G.J. van der Kolk, T. Hurkmans, W. Fleischer, T. Trinh,N.M. Carvalho, J.Th.M. de Hosson, "Properties and characterization of multilayers of carbides and diamond-like carbon," Surface and Coatings Technology, Vols. 142-144, pp. 707-713, 2001.

[97] "MPR (Micro Pitting Rig)," PCS Instruments, [Online]. Available: http://www.pcs-instruments.com/mpr/mpr.shtml#page=page-2.

[98] S. Woods, "Understanding scanning white light interferometry," December 2009. [Online]. Available: http://www.micromanufacturing.com/content/understanding-scanning-white-light-interferometry.

[99] D. Manning, "The mikronite process," Gear solutions, 2005.

[100] Klein, C., Hurlbut C. S., Manual of Mineralogy, John Wiley & Sons Inc, 1998.

[101] Evans, R.D., Barr, T.A., Houpert, L., Boyd, S.V., "Prevention of smearing damage in cylindrical roller bearings," Tribology Transactions, vol. 56, pp. 703-716, 2013.

[102] Casagrande, A., Cammarota, G.P., Micele, L.,, "Relationship between fatigue limit and Vickers hardness in steels.," Materials Science and Engineering A, vol. 528, p. 3468–3473, 2011.

[103] D. Tabor, Hardness of Metals, Oxford: Clarendon Press, 1951.

[104] Y. P. Chiu, "The mehanism of bearing surface faigue: experiments and theories," TRIBOLOGY TRANSACTIONS, vol. 40, no. 4, pp. 658-666, 1997.

[105] Akamatsu, Y., Tsushima, N., Goto, T. and Hibi, K. , "Influence of surface roughness skewness on rolling contact fatigue life," Tribology Transactions, vol. 35, no. 4, pp. 745-750, 1992.

[106] Zhai, X., Chang, L., Hoeprich, M.R. and Nixon, H.P., "On mechanisms of fatigue life enhancement by surface dents in heavily loaded rolling line contacts.," Tribology Transaction, vol. 40, no. 4, pp. 708-714, 1997.

[107] A. Grill, "Tribology of diamond-like carbon and related materials: An updated review.," Surface and Coatings Technology, vol. 94, pp. 507-513, 1997.

[108] Ciulli, E., Stadler, K., Draexl, T., "The influence of the slide-to-roll ratio on the friction coefficient and film thickness of EHD point contacts under steady state and transient conditions," Tribology International, vol. 42, no. 4, p. 526–534, 2009.

[109] Yonekura, D., Chittenden, R. J., Dearnley, P. A., "Wear mechanisms of steel roller bearings protected by thin, hard and low friction coatings," Wear, vol. 259, p. 779–788, 2005.

[110] Hoppel, C. P. R., Bogetti, A. T., Gillespie, Jr. J. W., "Effect of hydrostatic

pressure on the mechanical behavior of composite materials," Army Research Laboratory, 1995.

[111] Spikes, H. A.,Olver, A. V., Macpherson, P. B., "Wear in rolling contacts," Wear, vol. 112, pp. 121 - 144, 1986.

[112] Evans,R. D., Hager Jr., C. H., Kung,Y. S., Doll, G., "Comparison of Black Oxide and Tungsten Carbide–Reinforced Diamond-Like Carbon (WC/a-C:H) Surface Treatments for Rolling Element Bearings," Tribology Transactions, vol. 58, p. 444–453, 2015.

[113] Stachowiak and Batchelor, in Engineering Tribology, Amsterdam, 3rd Edition, Elsevier, 2005, p. 611.

[114] Greenwood, J. A., and Williamson, J. B., "Contact of Nominally Flat surfaces," Proc. R. Soc. London, Ser. A, vol. 295, no. 1442, p. 300–319, 1966.

[115] R. W. Bruce, Handbook of Lubrication and Tribology, Boca Raton: CRC, 2010.

[116] Y. Liu, "Flash temperature in EHL contacts," in encyclopedia of tribology, Springer, 2013, pp. 1172-1193.

[117] M. Kalin, "Influence of flash temoeratures on the tribological behaviour in low-speed sliding: a review," Materials science and engineering A, vol. 374, pp. 390-397, 2004.

[118] H. Blok, "Theoretical study of temperature rise at surfaces of actual contact under oiliness lubricating conditions," Proc. General Discussion on Lubrication and Lubricants, I.Mech.E., London,, pp. 222-235, 1937.

[119] Carslaw, H.S. and Jaeger, J.C., Conduction of Heat in Solids, vol. 76, Oxford: Clarendon Press, 1959, p. 203–224.

[120] J. Archard, " The temperature of rubbing surfaces," Wear, vol. 2, pp. 438-455, 1958/59.

[121] Bos, J. and Moes, H. , " Frictional heating of tribological contacts," ASME J. Tribol., vol. 117, pp. 171-177, 1995.

[122] J. Greenwood, "An interpolation formula for flash temperatures,," Wear, vol. 150, pp. 153-158, 1991.

[123] D. Kuhlmann-Wilsdorf, "Temperatures at interfacial contact spots: dependence on velocity and on role reversal of two materials in sliding contact," ASME J. Tribol., vol. 109, pp. 321-329, 1987.

[124] Tian, X. and Kennedy, F.E., "Contact surface temperature models for finite bodies in dry and boundary lubricated sliding," ASME J. Tribol., vol. 115, pp. 411-418, 1993.

[125] E. F. Kennedy, "Frictional Heating and contact temperature," in Modern Tribology Handbook, Danvers, CRC Press LLC, 2001, pp. 235-259.

[126] Wang, Q. J., Chung, Y. W., Encyclopedia of Tribology, Springer, 2013.

[127] "ISO/TR 15144-1:2014 Calculation of micropitting load capacity of cylindrical spur and helical gears -- Part 1: Introduction and basic principles," ISO, Switzerland, 2014.

[128] Shamsa, M., Liu, W. L., Balandin, A. A.,Casiraghi, C.,Milne, W. I.,Ferrari, A. C., "Thermal conductivity of diamond-like carbon films," APPLIED PHYSICS LETTERS, vol. 89, p. 161921, 2006.

[129] Zhou, Z.F., Li, K.Y., Bello, I.,Lee, C.S., Lee, S.T., "Study of tribological performance of ECR–CVD diamond-like carbon coatings on steel substrates Part 2. The analysis of wear mechanism," Wear, vol. 258, p. 1589–1599, 2005.

[130] Hakovirta, M., Vuorinen, J. E., He,X. M.,Nastasi, M.,Schwarz, R. B., "Heat capacity of hydrogenated diamond-like carbon films," Applied physics letters, vol. 77, no. 15, pp. 2340-2342, 2000.

[131] "Doll, private communication".

[132] [Online]. Available: http://www.ewp.rpi.edu/hartford/~ernesto/F2012/FWM/Pics/Contact/Gears/gear meshing.jpg.